Department of Materials Science and Rock Engineering
Laboratory of Mechanical Process- and Recycling Technology
Espoo 2003

INVESTIGATION OF PARTICLE-BUBBLE INTERACTIONS WITH A NEW EXPERIMENTAL SETUP

Nóra Schreithofer

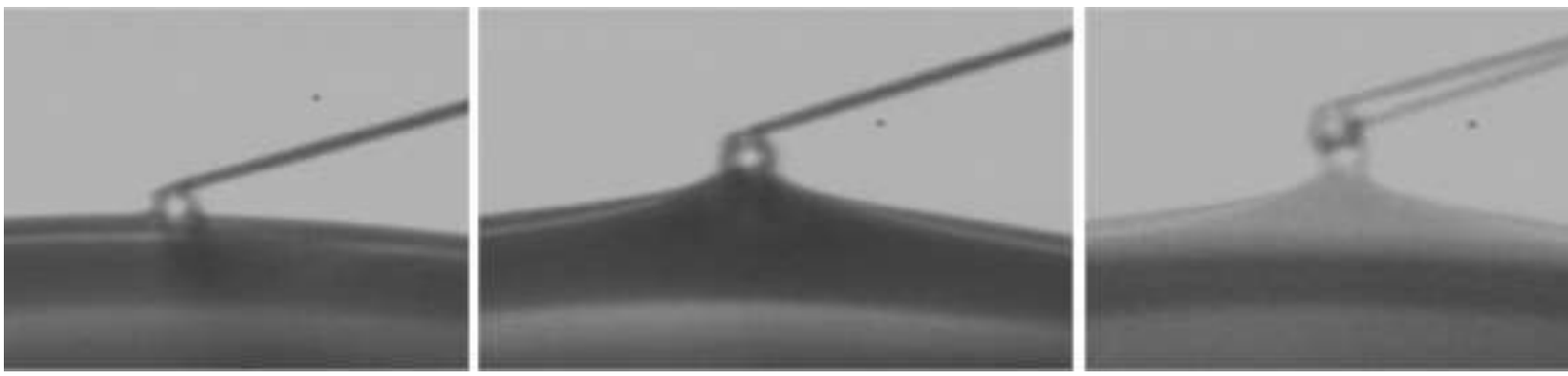

TEKNILLINEN KORKEAKOULU
TEKNISKA HÖGSKOLAN
HELSINKI UNIVERSITY OF TECHNOLOGY
TECHNISCHE UNIVERSITÄT HELSINKI
UNIVERSITE DE TECHNOLOGIE D'HELSINKI

HELSINKI UNIVERSITY OF TECHNOLOGY
Department of Materials Science and Rock Engineering
Laboratory of Mechanical Process- and Recycling Technology

INVESTIGATION OF PARTICLE-BUBBLE INTERACTIONS WITH A NEW EXPERIMENTAL SETUP

Nóra Schreithofer

Dissertation for the degree of Doctor of Science in Technology to be presented with due permission of the Department of Materials Science and Rock Engineering, Helsinki University of Technology for public examination and debate in Auditorium 1 at Helsinki University of Technology (Espoo, Finland) on the 28th of November, 2003, at 12 o'clock noon.

ESPOO 2003

ISBN 951-22-6749-7 (printed version)
ISBN 951-22-6750-0 (electronic version)

Szüleimnek

Life is not easy for any of us. But what of that? We must have perseverance and above all confidence in ourselves. We must believe that we are gifted for something and that this thing must be attained.

Marie Curie

ABSTRACT

Flotation is one of the most widely used processes in mineral beneficiation industry. Research on flotation circuit modelling and optimisation has for long time been of major importance. Flotation is mainly driven by surface chemical properties of the particles attaching to air bubbles. Earlier flotation models are based solely on dynamic consideration, but in the recent years serious research effort has been focused on finding surface chemical parameters, which may improve the existing flotation models. Parameters were mainly obtained from measurements performed with surface force apparatus, thin film balance techniques and atomic force microscopy.

This thesis work aimed to design and develop a new experimental apparatus, suitable for in-depth study of particle-bubble interactions. The experimental results of this work provide additional data for the improvement of existing, and development of new flotation models.

The new experimental setup named **C**olloidal **I**nteraction **F**orce **M**easurement **A**pparatus (CIFMA) is based on AFM force measurement principle. The apparatus eliminates the limitations caused by the small measurement range of commercial instruments and provides several new features that facilitate the in-depth investigation of particle-bubble interactions. In connection with the instrument design, the errors and problems associated with the technique are reviewed.

The experiments conducted with CIFMA were focused on ultrapure, electrolyte containing and gas saturated aqueous systems. In addition the effects of approach velocity, applied load and contact time on the particle-bubble adhesion were studied.

The results among others revealed, that the particle-bubble interaction process is time dependent, highly dynamic phenomena. The jump-in force and the adhesion decrease with time. Increased load and contact time enhance the adhesion of the particle to the air bubble even if no three-phase contact is formed. The nanometer-sized roughness of the particle surfaces has a significant effect on the particle-bubble adhesion. In ultrapure system a very long-range jump of the bubble towards the particle occurred, that was detected by optical means. With increasing electrolyte concentration this effect disappeared.

These results emphasize the importance of reassessment of existing flotation models and development of new ones by taking into consideration the observed effects.

Key words: particle-bubble interactions, CIFMA, adhesion, applied load, contact time, time dependent effect

PREFACE

The research work presented in this thesis was carried out at Helsinki University of Technology (HUT), Laboratory of Mechanical Process and Recycling Technology during years 1998-2003.

Foremost, I would like to express my sincere gratitude to Professor Kari Heiskanen for the possibility to work and study in this laboratory and for the support during the research. His vision and belief in this project gave me confidence and helped me over the difficulties and low-points encountered.

I wish to gratefully acknowledge Professor emeritus Janusz S. Laskowski for the very stimulating discussions and very useful comments and suggestions on the manuscript. His boundless enthusiasm and dedication to science and research will always be exemplary to me.

I wish to thank Professor Hans-Jürgen Butt for the possibility to visit his laboratory and for reviewing the manuscript.

I would also like to thank my friends and colleagues at HUT for their help and interest during the work as well as for the staff of the mechanical workshop for making the parts for the experimental setup.

I thank Prof. J.M. Cases for the invitation to visit and do research at L.E.M. in Nancy, and for all the people in that laboratory for their help during my stay.

Financial support from Academy of Finland and Outokumpu Oy Foundation is also acknowledged.

My warmest thanks belong to my parents and my brother for all their support and patience during these years I spent away from home, and for Zoltán for the love, encouragement and help.

Espoo, October 2003

Nóra Schreithofer

CONTENTS

LIST OF SYMBOLS AND ABBREVIATIONS

β	material dependent London constant
ψ	Stern potential
ψ_i	surface potential
κ	inverse Debye length
θ	contact angle
ρ_1	atomic number density (concentration of atoms per unit volume)
ε_i	permittivity, static dielectric constants
A	Hamaker constant
AFM	atomic force microscope
C, C^*	force constant
C_b	cantilever deflection per unit sample translation when pushed against the bubble
C_h	cantilever deflection per unit sample translation when pushed against hard surface
c_i	ionic concentration
D	distance, actual separation
D_0	decay length
d_c	cantilever deflection
D_c	contact value of separation
d_{cont}	contact value of cantilever deflection
F	force
F_c	capillary force
$F_{hydrophob}$	hydrophobic force
f_d	detector calibration coefficient
h	Planck constant
I	ionic strength of the solution
K_b	bubble spring constant
k_B	Bolzmann constant
K_c	cantilever spring constant
K_m	measured stiffness
K_{123}	hydrophobic force constant
M	mole/liter

n_i	refractive indices of different phases
r	inter-centre distance of particles
R_1, R_2	radius of particles R_1 and R_2 (in some cases bubble radius)
S_d	detector signal
T	absolute temperature in Kelvin
v_e	plasma frequency of the free electron gas
V_{EDL}	electric double layer interaction energy
V_T	total interaction energy
V_{VdW}	Van der Waals interaction energy
x_ζ	distance from the particle surface to the slipping plane
z	valency
z_c	contact value of piezo position
Z_p	piezo position
TPC	three phase contact
SFA	Surface Force Apparatus

CHAPTER 1 INTRODUCTION

Knowing is not understanding. There is a great difference between knowing and understanding: you can know a lot about something and not really understand it.

Charles F. Kettering

The colloidal interactions are crucial to in-depth understanding of the phenomena undergoing in industrial applications such as flotation, paper de-inking, sewage water treatment, etc. The study of colloidal interactions therefore got in the centre of interest of several research groups in the past few years.

In the last 30 years several direct force-measuring techniques have been developed which allow interaction measurements between two surfaces with angstrom resolution. Several published studies mainly deal with the forces measured between two surfaces in controlled liquid or vapour environment using Surface Force Apparatus (ISRAELACHVILI AND ADAMS, 1978; ISRAELACHVILI AND PASHLEY, 1982).

The invention and improvement of Atomic Force Microscopy (AFM) has opened the possibility to measure directly interaction forces between colloidal particles and solid surfaces in air or liquid. Several papers are available on the forces between colloidal particles (silica, gold) and planar surfaces (glass, silica, mica, gold, PTFE, etc.) measured either in air and/or aqueous media (DUCKER ET AL. 1991; WEISENHORN ET AL. 1992; LARSON, ET AL. 1995; MILLING, ET AL. 1996; YOON ET AL. 1997).

Results of measurements of the interactions between particles and deformable surfaces such as particles and liquid droplets and particles and air bubbles have also been published (MULVANEY ET AL. 1996; DUCKER ET AL. 1994; FIELDEN, ET AL. 1996). This made obvious that the commercial atomic force microscopes are not ideal for such measurements for several reasons that will be described in this thesis. Therefore BUTT (1994) and PREUSS AND BUTT (1999) constructed an instrument based on AFM force measurement principle, for measuring colloidal interactions between particles and deformable surfaces. Nevertheless, this instrument had still some technical limitations restricting the range of particle-air bubble force measurements. As part of this thesis, a new instrument was

designed and built which eliminates the limitations of the available commercial and non-commercial units, and meets the requirements of particle-bubble attachment and detachment studies.

Despite the extensive research work and large amount of papers published, the interpretation of the AFM force curve obtained for particle-bubble interaction measurements is still not clear. There is no established method for the determination of the absolute separation between the colloidal probe and the air bubble and the interpretation of the results of particle-bubble interaction force measurements is difficult due to the factors, which will also be discussed in this thesis.

1.1 STRUCTURE OF THE THESIS

The thesis is organized into three main units. Chapter 2 briefly surveys the AFM force measurements as a technique for studying colloidal interactions, the different modifications of the commercial instruments and the obtained results. It also reviews the publications describing the structure of silica surfaces and the effect of surface treatment procedures on the surface properties of silica.

Chapter 3 presents the design considerations and the development work of a new, unique experimental setup, and also the bottlenecks of using AFM force measurement technique for particle-bubble interactions.

Chapter 4 presents the hypothesis and objectives of the experimental work. Chapter 5 describes the materials and methods used in the experimental work. Chapter 6 deals with the stability problem of AFM cantilevers. Chapter 7 presents the results of the contact angle measurements and AFM imaging. Chapters 8 and 9 show the results of experiments on the silica particle-bubble interactions obtained with the new instrument. The variables included gas type, electrolyte concentration, hydrophobicity, loading force, contact time and approach velocity.

Chapter 10 gives a discussion on the obtained results, while Chapter 11 summarizes the conclusions of the experimental results. Recommendation for further research concludes the thesis.

1.2 BACKGROUND AND AIM OF THE RESEARCH

Flotation is the most widely used separation process in mineral processing. The estimated amount of ores and coal processed by flotation exceeds two billion tons per year, which represents about 85 % of the ores mined annually. In addition to mineral processing applications, flotation is used in wastewater treatment, paper de-inking, food industry and separation of secondary raw materials.

Although the first flotation applications date back to 1910-1915, there are still many un-clarified questions concerning the basic interactions in the flotation process. Traditionally, the flotation research has been conducted along two main lines during the last decades: the surface chemical research and the kinetic studies and modelling. Only recently has there been any work to really combine the two research lines in a scientifically rigorous way. This is highly important for further improvement of flotation models (see chapter 10.4). The idea of force balance (SCHULZE 1984) can be used in conjunction with the kinetic models. A fundamental point is that the particle size effects can only be taken into account by the force model.

This research project was undertaken in order to provide a deeper understanding of the solid-gas interactions in flotation processes from the surface chemistry perspective. The primary objective was to develop and build an experimental setup suitable for extensive study of the particle-bubble interactions. The secondary aim was to provide additional data for the improvement of existing, and development of new flotation models; model development itself was outside the scope of this thesis.

1.3 CONTRIBUTION OF THE THESIS

This thesis focuses on experimental studies of the colloidal interactions, and in particular on the measurement of the force between particles and air bubbles, the topic of outstanding importance for improvement of flotation models. The main contribution of this work includes the following:

- Development of a new experimental setup which eliminates the limitations inherent in the commercial atomic force microscopes;
- Presents a new approach to design of scientific instruments in order to facilitate easy archive data access;

- Presents results of force measurements between particles and air bubbles in different gas environments and with particles having different degree of hydrophobicity;
- Shows aspects of colloidal interactions not discussed so far, which are of interest in modelling flotation processes, such as time dependent effects, dynamic behaviour, etc.;
- Emphasizes the main reasons for errors and misunderstandings in the AFM force measurement technique;

References chapter 1

Butt, H.-J., 1994. A Technique for Measuring the Force between a Colloidal Particle in Water and a Bubble, *J. Colloid Interface Sci*., **166**, (1), 109-117.

Ducker, W. A., Senden, T. J., Pashley, R. M., 1991. Direct measurement of colloidal forces using atomic force microscope, *Nature,* **353**, (6341), 239-241.

Ducker, W.A., Xu, Z., Israelachvili, J.N., 1994. Measurement of Hydrophobic and DLVO Forces in Bubble-Surface Interactions in Aqueous Solutions, *Langmuir,* **10**, (9), 3279-3289.

Fielden, M.L., Hayes, R.A., Ralston, J., 1996. Surface and Capillary Force Affecting Air Bubble-Particle Interactions in Aqueous Electrolyte, *Langmuir,* **12**, (15), 3721-3727.

Israelachvili, J. N., Adams, G. E., 1978. Measurement of Forces between Two Mica Surfaces in Aqueous Electrolyte Solutions in the Range 0-100 nm, *J. Chem. Soc. Faraday Trans*. **I**, (4), 975-1001.

Israelachvili, J. N., Pashley, R., 1982. The hydrophobic interaction is long range, decaying exponentially with distance, *Nature* **300**, 341-342.

Larson, I., Drummond, C. J., Chan, D. Y.C., Grieser, F., 1995. Direct Force Measurement between Dissimilar Metal Oxides, *J. Phys. Chem.* **99**, (7), 2114-2118.

Milling, A., Mulvaney, P., Larson, I., 1996. Direct Measurement of Repulsive van der Waals Interactions using an Atomic Force Microscope, *J. Colloid Interface Sci.* **180**, (2), 460-465.

Mulvaney, P., Perera, J.M., Biggs, S., Grieser, F., Stevens, G.W., 1996. The Direct Measurement of the Forces of Interaction between a Colloidal Particle and an Oil Droplet, *J. Coll. Interf. Sci.,* **183**, (2), 614-616.

Preuss, M., Butt, H.-J., 1999. Direct measurement of forces between particles and bubbles, *Int. J. Miner. Process*, **56,** (1), 99-115.

Schulze, H.-J., 1984. Physico-chemical Elementary Processes in Flotation, *Elsevier, Amsterdam.*

Weisenhorn, A. L., Maivald, P. Butt, H.-J., Hansma, P. K., 1992. Measuring adhesion, attraction, and repulsion between surfaces in liquids with atomic-force microscope, *Physical Review* B, **45**, (19), 11226-11232.

Yoon, R.-H., Flinn, D. H., Rabinovich, Y. I., 1997. Hydrophobic Interactions between Dissimilar Surfaces, *J. Colloid Interface Sci.,* **185**, (2), 363-370.

CHAPTER 2 REVIEW OF EXISTING THEORIES

Learn from yesterday, live for today, hope for tomorrow. The important thing is not to stop questioning.

Albert Einstein

This chapter presents a review of the main theoretical issues related to the experimental part. Theories describing particle-bubble interactions are reviewed first, then the properties and interactions of silica with water and silanes, important for the interpretation of the experimental results, while the last part surveys the topics related to the Atomic Force Microscopy (AFM) as a tool for colloidal force measurements.

2.1 THEORIES OF PARTICLE-BUBBLE INTERACTIONS

The forces experienced by particles and bubbles in industrial and certain experimental systems are the hydrodynamic forces, surface forces and non-surface forces. These play a key role in the flotation process. Therefore their incorporation into the flotation models have been in the centre of interest since the early 1960's. The sub-chapter below summarizes the most important forces that play a role in particle-bubble interactions in systems where no flow field is present, such as experimental systems used in AFM related techniques. These forces can be categorized in two groups: surface forces playing a role before the three-phase contact line formation and the non-surface forces acting after the three-phase contact line formation.

2.1.1 Surface forces acting before three-phase contact formation

The surface forces are categorized into two large groups: DLVO and non-DLVO forces.

2.1.1.1 DLVO theory for particle-particle and particle-bubble interactions

The DLVO (Derjaguin-Landau-Verwey-Overbeek) theory, developed independently by DERJAGUIN AND LANDAU (1941) in the former Soviet Union and VERWEY AND OVERBEEK (1948) in the Netherlands, formulates the basis for understanding colloid stability. The

theory assumes, that the colloidal stability is determined by the balance of two forces: the van der Waals force and the electric double-layer force. This is expressed in terms of interaction energies as follows:

$$V_T = V_{VdW} + V_{EDL} \tag{1}$$

where V_T is the total interaction energy, V_{VdW} the van der Waals interaction energy and V_{EDL} the electric double layer interaction (Figure 1).

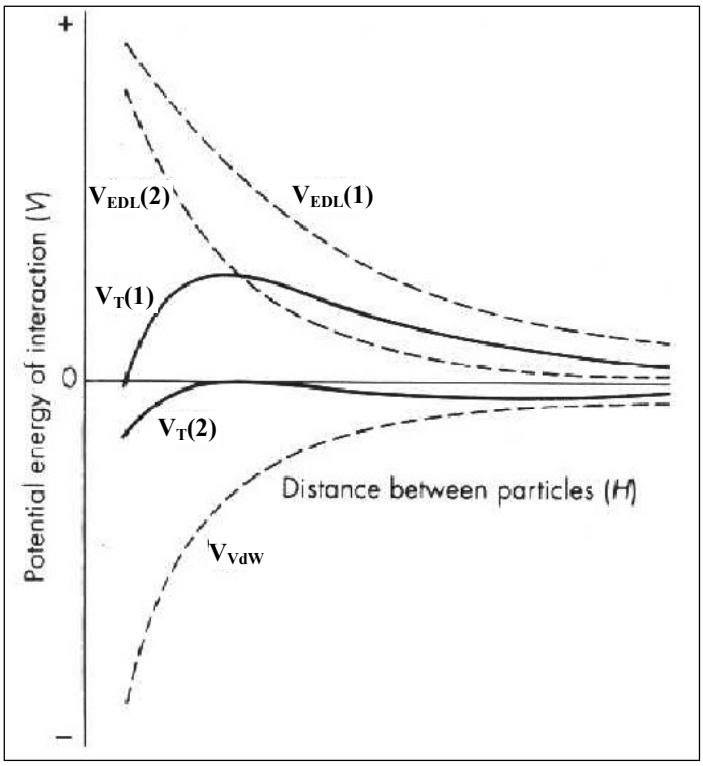

Figure 1 Total interaction energy curves $V_T(1)$ and $V_T(2)$, obtained by the summation of the attractive V_{VdW} curve with different repulsive $V_{EDL}(1)$ and $V_{EDL}(2)$ curves

2.1.1.1.1 The van der Waals force

The van der Waals interaction acts between molecules and macroscopic bodies. It has three main components: the *dispersion* (London) interaction between two induced dipoles, the *induction* (Debye) interaction between a rotating dipole and an induced dipole, and the orientation (Keesom) interaction between permanent rotating dipoles. The dispersion interaction, which is long range, gives probably the most important contribution to the van der Waals force (ISRAELACHVILI 1991).

In the literature the van der Waals force is usually given in terms of interaction energy. For macroscopic bodies the interaction energy can be calculated with two different approaches. The *microscopic* approach developed by HAMAKER (1937) calculates the V_{VdW} interaction energy by summing the interactions between molecule pairs of the two interacting spherical particles as follows:

$$V_{VdW} = -\frac{A}{6}\left[\frac{2R_1R_2}{r^2-(R_1+R_2)^2}+\frac{2R_1R_2}{r^2-(R_1-R_2)^2}+\ln\frac{r^2-(R_1+R_2)^2}{r^2-(R_1-R_2)^2}\right] \tag{2}$$

where r is the inter-centre distance of particles with radius R_1 and R_2 and A the material dependent Hamaker constant. At very close separations for spherical particles equation 2 reduces to the following formula:

$$V_{VdW} = -\frac{A}{6D}\frac{R_1R_2}{R_1+R_2} \tag{3}$$

for D<<R, where D is the inter-particle separation. The above formulas do not take into consideration the retardation effect, which arises due to finite propagation time of the electromagnetic interaction. The retardation leads to a weakened interaction at separations larger than 5 nm. It also neglects the entropic contributions and assumes that the interactions are additive and that the media of the interaction is vacuum. This approach is quite simplistic, and the estimation of the interaction energies with these assumptions is not very accurate. In spite of these drawbacks still many scientists use this approach, probably because its simplicity and because for certain systems it works as a first iteration. The forces acting between the surfaces can be obtained by differentiating the interaction energies with respect to the distance.

It should be highlighted, that the interaction energies are dependent on the Hamaker constant, which is an expression of material properties. Combining relations are widely used to approximate the unknown Hamaker constants in terms of known ones as follows (ISRAELACHVILI 1972):

$$A_{123} \approx \pm\sqrt{A_{131}A_{232}} \tag{4}$$

$$A_{131} \approx A_{313} \approx A_{11}+A_{33}-2A_{13} \approx \left(\sqrt{A_{11}}-\sqrt{A_{33}}\right)^2 \tag{5}$$

where A_{123} is the non-retarded Hamaker constant for particles 1 and 2 interacting across medium 3. A_{12} is for particles 1 and 2 interacting across vacuum and A_{11} and A_{22} are the Hamaker constants of the individual media, which are expressed by means of β_{11} the material dependent London constant, and ρ_1 the number density of the material, as follows:

$$A_{11} = \pi^2 \beta_{11} \rho_1^2 \tag{6}$$

By combining equations 4 and 5 the following relation is obtained:

$$A_{123} \approx \left(\sqrt{A_{11}} - \sqrt{A_{33}}\right)\left(\sqrt{A_{22}} - \sqrt{A_{33}}\right) \tag{7}$$

For identical entities interacting in a medium the above-described equation gives a positive Hamaker constant, and a resulting attractive Van der Waals force. For different entities the Hamaker constant can be positive or negative resulting in attractive or repulsive Van der Waals force. If the Hamaker constants of the particles 1 and 2 and the medium 3 follow the order:

$$A_{11} > A_{33} > A_{22} \quad \text{or} \quad A_{11} < A_{33} < A_{22} \tag{8}$$

the Van der Waals force is repulsive. For example for the silica-air-water interaction the value of the Hamaker constant calculated with the combining rule is negative (A_{123} = -3.12 $\times$ 10^{-21} J) and therefore the Van der Waals force is repulsive (LASKOWSKI 1986). It has to be noted that this rule predicts well the Hamaker constants only in the case when dispersion forces dominate the interaction, but it fails in the case of medium with high dielectric constant such as water. Therefore the calculation of the Hamaker constants in these cases is not very appropriate and the value should be calculated using the macroscopic approach.

In the *macroscopic* Lifshitz approach (LIFSHITZ 1956, DZYALOSHINSKII ET AL. 1961) the interacting particles and the medium are treated as a continuum and the interactions originate from the interference between fluctuating electromagnetic fields extending beyond the surface of the particles. With this approach the problem of additivity is completely avoided. The interaction energies between two bodies are derived in terms of dielectric constants and refractive indices of the continuous phases. The original Lifshitz approach requires a deep understanding and working knowledge of quantum theory, and therefore it was not widely used by researchers until much simpler equations were derived.

Although the calculation of the interaction energies is not very simple, the Lifshitz theory has a very remarkable contribution, namely, that it provides a reliable prediction of the Hamaker constant even when the dielectric constant of the media is high. The approximate expression for the non-retarded Hamaker constant for two macroscopic phases 1 and 2 interacting across a medium 3 is given as follows (ISRAELACHVILI 1991).

$$A_{Total} = A_{v=0} + A_{v>0}$$
$$\approx \frac{3}{4}kT\left(\frac{\varepsilon_1-\varepsilon_3}{\varepsilon_1+\varepsilon_3}\right)\left(\frac{\varepsilon_2-\varepsilon_3}{\varepsilon_2+\varepsilon_3}\right)+\frac{3\mathrm{h}v_e}{8\sqrt{2}}\frac{\left(n_1^2-n_3^2\right)\left(n_2^2-n_3^2\right)}{\left(n_1^2+n_3^2\right)^{1/2}\left(n_2^2+n_3^2\right)^{1/2}\left\{\left(n_1^2+n_3^2\right)^{1/2}+\left(n_2^2+n_3^2\right)^{1/2}\right\}} \quad (9)$$

where ε_i the static dielectric constants and n_i the refractive indices of different phases *I,* while η is the Planck constant, v_e the plasma frequency of the free electron gas (typically 3-5 $\times$ 10^{15} s). Figure 2 shows the calculated values of Hamaker constants for bodies of different materials interacting in water as calculated according to the Lifshitz approach (Eq. 9).

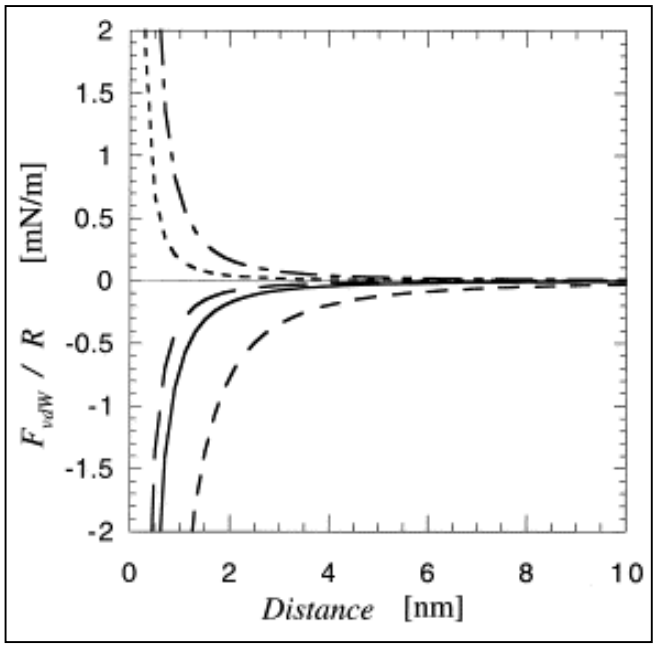

Figure 2 Calculated van der Waals forces between two spheres for different combinations of silica, water, air, and hydrocarbon (octane). The different curves correspond to the following combinations and Hamaker constants: (—) silica–water–silica A=0.83×10-20 J, (— —) hydrocarbon–water–hydrocarbon A=0.41×10-20 J, (– –) air–water–air A=3.7×10-20 J, (- -) air–water–hydrocarbon A=-0.20×10-20 J, and (— - —) air–water–silica A=-0.8×10-20 J. Note how a negative Hamaker constant results in a repulsive van der Waals force. (FRÖBERG ET AL. 1999)

It has to be emphasized that the Hamaker constant calculated with the Lifshitz approach in the case of silica-water-air system is also negative, which results in a repulsive Van der Waals force!

When the retardation effect is taken into consideration, the "Hamaker constant" will be dependent on the separation *h*, and therefore should be referred rather as Hamaker function $A_{123}(h)$. According to the calculations done by NGUYEN AND SCHULZE (2003), the quartz-water-air system can have both negative and positive values depending on the separation distance. At large separations (over 100 nm) the predicted values for the Hamaker function are positive, which results in an attractive Van der Waals force.

2.1.1.1.2 Electric double layer force

The second force included in the classic DLVO theory is the electric double layer force. The colloidal particles and air bubbles immersed in electrolyte acquire charge by one of the following mechanisms: acid-base equilibrium, desorption of lattice ions or adsorption of ionic surfactants or polymers. The surface charge is balanced by an equal, but oppositely charged region of counter-ions, some of which are bound to the surface in the so-called *Stern-layer,* while others form a "cloud" of ions close to the surface, in the so-called *diffuse layer*. The charged surface and the diffuse layer form the *electric double layer*.

Electrostatic double-layer force manifests when two charged surfaces come close enough and the electric double layers overlap. This force is of Coulombic nature and it is stronger and longer ranged than other surface forces. For similar particles the surface charge results in a repulsive *electric double-layer force*. As shown by PAULSON AND PUGH (1996) the interaction between particles and air bubbles is greatly influenced by electrostatic interactions. When the DLVO theory has to be applied for bubbles, the electrostatic interaction for bubble-particle V_{EDL} can be calculated using the equation suggested by HOGG ET AL. (1966):

$$V_{EDL} = \frac{\varepsilon R_1 R_2 \left(\psi_1^2 + \psi_2^2\right)}{4\left(R_1 + R_2\right)} \left[\frac{2\psi_1 \psi_2}{\psi_1^2 + \psi_2^2} \ln\left(\frac{1 + e^{-\kappa H}}{1 - e^{-\kappa H}} \right) + \ln\left(1 - e^{-2\kappa H}\right) \right] \tag{10}$$

where R_1 is the radius of the bubble, R_2 the radius of the particle, ε the dielectric constant of the medium, ψ_1 and ψ_2 are the Stern potentials of the bubble and the particle and $1/\kappa$ the Debye length. The Debye length $1/\kappa$ is described with the following equation:

$$1/\kappa = \left\{ \frac{\varepsilon\varepsilon_0 k_B T}{e^2 \sum n_i(\infty) z_i^2} \right\}^{1/2} \tag{11}$$

where e is the charge of the electron, $n_i(\infty)$ is the number per unit volume of the electrolyte ions of type i with valency z_i in the bulk solution far from the surface, k_B is the Bolzmann constant, T the absolute temperature in kelvin, ε_0 the permitivity of vacuum and ε the dielectric constant of the solution. The Debye length $1/\kappa$ [nm] can also be calculated from the solution ionic strength I, as follows:

$$I = \left(\sum c_i z_i^2 \right) / 2 \tag{12}$$

and for water at 25 °C:

$$\kappa = 3.288\sqrt{I} \tag{13}$$

where c_i is the ionic concentration in mol/l. Equation (10) assumes the bubble behaving as a rigid sphere, which is a very rough estimation, because of the bubble deformation and the mobility of surface charges on the bubble surface. It also has to be noted, that this equation only holds exactly for values of ψ_1 and ψ_2 less than 25 mV and under solution conditions where the double layer thickness is small compared with the particle size. Therefore when using this equation (10), one needs first to consider whether the calculation of DLVO interactions makes sense for bubbles and particles and also whether the calculation should be made for constant charge or constant potential conditions.

As a rough estimation, the surface potential of the particle and the bubble are often substituted with the ζ-potential. For a more precise approach, the surface potential has to be extrapolated from the ζ-potential with the following expression (NGUYEN AND SCHULZE 2003):

$$\psi_i = \frac{4k_B T}{ez} \operatorname{atanh}\left[\tanh\left(\frac{ez\zeta}{4k_B T} \right) \exp\left(\kappa x_\zeta \right) \right] \tag{14}$$

where i = 1 or 2 and x_ζ is the distance from the particle surface to the slipping plane.

As it has been shown by many authors (GRACIAA ET AL. 1995; LI AND SOMASUNDARAN 1991; MCSHEA AND CALLAGHAN 1983) the ζ-potential of air bubbles in indifferent

inorganic salt solutions such as KCl and NaCl is negative. The magnitude of the ζ-potential decreases with increased salt concentration. LASKOWSKI ET AL. (1989) showed that the ζ-potential of bubbles in strong electrolyte type surfactant is entirely determined by the type of surfactant, while for a weak electrolyte surfactant it dependent on the pH. However, there is very few data available on the ζ-potential of air bubbles, probably because of the difficulties encountered in the measurement techniques.

In surfactant-free silica-water-air systems the silica particles are negatively charged (LASKOWSKI AND KITCHENER 1969) and also the air bubbles bear a negative ζ-potential. Therefore the electric double layer force is expected to be repulsive in the pH range above 2.5.

2.1.1.2 Non-DLVO forces in particle-bubble interactions

For many solid surfaces the DLVO theory has been shown to be valid (ISRAELACHVILI 1976; PASHLEY, 1981). However experimental evidence shows that for some systems such as bacterial cell suspensions (CHANG AND CHANG 2002), systems involving polymers (MOLINA-BOLÍVAR ET AL. 1999) and interactions involving hydrophobic surfaces the classical DLVO theory breaks down because additional forces come into play. The additional non-DLVO forces are the *solvation forces* and the *steric forces*. The solvation forces are dependent on the properties of the intervening medium and the physico-chemical properties of the surfaces. In aqueous solutions they can be categorized as attractive *hydrophobic* and repulsive *hydration* forces. The steric forces are present in systems containing macromolecular reagents. The following chapter will focus on the hydrophobic force, which is likely to play an important role in the particle-bubble interactions.

2.1.1.2.1 Hydrophobic force

Probably one of the most researched but still the least understood surface force is the hydrophobic force. LASKOWSKI AND KITCHENER (1969) published the first paper discussing the existence of an additional attractive force not fitted in the conventional DLVO theory. They called this new force the *hydrophobic force*. ISRAELACHVILI AND PASHLEY (1982) were the first to measure the hydrophobic force between two mica surfaces in cethyltrimethylammonium bromide (CTAB) solution using Surface Force Apparatus (SFA). The results were fitted with a single exponential function as follows:

$$\frac{F_{hydrophob}}{R} = Ce^{-D/D_0} \tag{15}$$

where R is the mean radius of interacting surfaces, C=0.14±0.02 Nm^{-1}, D is the distance and D_0 is the decay length of 1.0±0.1 nm. Several research groups have confirmed the existence of the hydrophobic force since, using different measurement techniques such as AFM, SFA, Light Lever Instrument for Force Evaluation (LLIFE). The force was observed between different surfaces such as hydrophobized silica (RABINOVISH AND DERJAGUIN 1988), gold (EDERTH ET AL. 1998), polypropylene (MEAGHER AND CRAIG 1994), polystyrene (KARAMAN ET AL. 1993), etc.

Although there is a large amount of research data about the range and exact, functional form of the hydrophobic force, there is no agreement between researchers in these matters. The results of recent measurements showed that the experimental approximation function (Eq. 15) does not fit the experimental data therefore a double exponential function was found to be more suitable for these cases:

$$\frac{F_{hydrophob}}{R} = C\exp(-h/\lambda) + C^*\exp(-h/\lambda^*) \quad , \tag{16}$$

where the first term describes the short-range hydrophobic force with decay length of 1.2 nm while the second, the long-range hydrophobic force with decay length of 5.5 nm for the measurements in water and 4.5 nm for 0.01 M KBr solution (CLAESSON ET AL. 1986). A power law form similar to the van der Waals force was also proposed for the description of the hydrophobic force:

$$\frac{F_{hydroph}}{R} = -\frac{K_{123}}{h^2} \tag{17}$$

YOON ET AL. (1997) described the hydrophobic interaction constant K_{123} between surfaces 1 and 2 in medium 3 by the geometric mean which is dependent on the contact angles of the surfaces θ_1 and θ_2:

$$K_{123} = -\exp\left(a\frac{\cos\theta_1 + \cos\theta_2}{2} + b\right) = a(\cos\theta)_{avg} + b \tag{18}$$

The empirical constants *a* and *b* are obtained from the best fit of the experimental data. This approach is similar to the combining rule used for calculating the Van der Waals force in case of asymmetric interactions.

The origin of the hydrophobic force, and its functional form, is still a topic of debate between researchers. Experimental observations are contradictory with the theoretical assumptions. Hydrophobic force was shown to decrease (CHRISTENSON ET AL 1989; CHRISTENSON ET AL. 1990), increase slightly or remain constant (PARKER ET AL. 1994; MEAGHER AND CRAIG 1994) in presence of electrolyte. The effect of temperature on the hydrophobic force was also studied, and the results were again contradictory. TSAO ET AL. (1991) observed a decreased hydrophobic interaction at elevated (50 °C) temperature, while PARKER ET AL. (1994) observed the opposite effect: increasing strength of interaction with temperature (from room temperature to 41 °C). It has also been reported, that the hydrophobic force is strongly dependent on the method of preparation of the hydrophobic surfaces, surface roughness, amount and type of dissolved gas in the solution, etc. Several theoretical mechanisms have been proposed, but none of them has gained a general acceptance. The theories suggest: entropic origin (ISRAELACHVILI AND PASHLEY 1984; CLAESSON ET AL. 1986; ERIKSSON ET AL. (1989), electrostatic origin (ATTARD 1989; RABINOVICH ET AL. 1993), nucleation of sub-micron bubbles (CARAMBASIS ET AL. 1998), hydrodynamic correlations between fluctuations of the highly unstable water layer in the vicinity of the surface (RUCKENSTEIN AND CHURAEV 1991), etc.

Hydrophobic force is expected to participate in the bubble-particle interactions as well. DUCKER ET AL. (1994) and BUTT (1994) were the first to measure particle-bubble interaction forces with AFM. However, the AFM force measurement produces only semi-quantitative information because of the bubble deformation, which cannot be measured with this technique.

2.1.2 Non-surface forces acting after the three-phase contact formation

The non-surface forces stabilizing a particle-bubble aggregate are: the capillary force, the buoyancy, the gravity and the pressure force resulting from the hydrostatic pressure which acts over the effective area πr_{tpc}^2 enclosed by the three-phase contact line. In the

particle-bubble interaction studies carried out by AFM and related techniques, the most important non-surface force affecting the interactions is the capillary force.

2.1.2.1 Capillary force

The capillary force (F_c) acts along the tangent to the gas-liquid interface at the three-phase contact line (TPC) and pulls the particle into the gas phase. It can be expressed as a function of gas-liquid surface tension γ, particle radius R_P and receding contact angle θ_{rec} as follows:

$$F_c = 2\pi R_P \gamma \sin\alpha \sin(\theta_{rec} - \alpha) \tag{19}$$

The maximum capillary force, which provides the particle-meniscus stability, is equal to:

$$F_{c\max} = \pi R_P \gamma (1 - \cos\theta_{rec}) \tag{20}$$

The notations of Eq. 19 and 20 are shown in Figure 3:

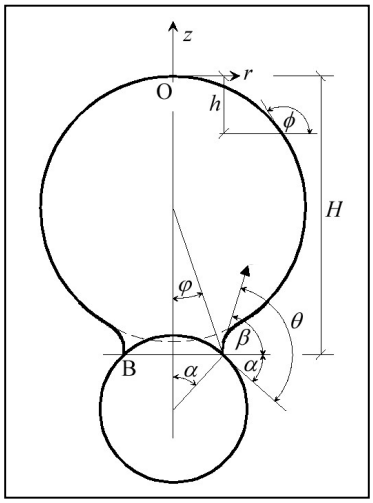

Figure 3 Geometry of particle-bubble interaction on detachment (NGUYEN AND SCHULZE 2003)

2.2 PROPERTIES OF SILICA, AND ITS INTERACTION WITH WATER AND SILANES

Amorphous silica is widely used in studies of wetting phenomena, colloidal interactions and flotation mechanisms as a model substrate, because it is considered to be one of the "simple" materials. Since it is possible to artificially produce pure silica samples, plates

and particles of required size, silica seems to be a simple material. However, due to its surface structure the behaviour of silica under different circumstances (pH, temperature, moisture, etc.) and following treatment conditions is very different, and therefore its "simple" nature is highly questionable.

This review concentrates mostly on the properties and interactions of amorphous silica because the experimental work presented in this thesis was carried out with this type of silica. It has also been shown (MEYER AND HACKERMAN 1966) that the particle size and radius of curvature of the surface may be more important variable than differences between amorphous and ordinary crystalline states of silica.

2.2.1 The properties of silica surfaces and their interaction with water

The properties of the amorphous silica depend on the chemistry of the solid surface. The most important characteristic of SiO_2 is that the so-called "residual valences" of the siloxane (SiOSi) groups composing the surfaces react with water at ordinary temperature, and the surface becomes covered with silanol (SiOH) groups (ILER 1979). The two main mechanisms by which silanol groups are formed on a silica surface are shown in Figure 4.

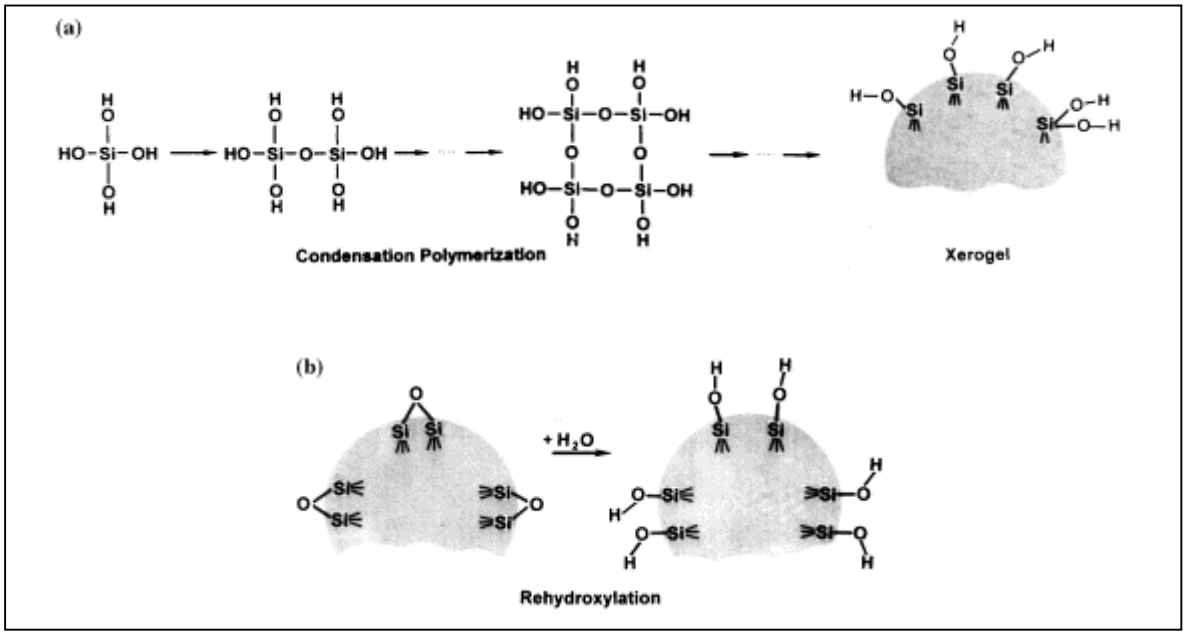

Figure 4 The formation of silanol groups on the silica surface: (a) Condensation polymerisation; (b) Rehydroxylation (ZHURAVLEV 2000)

In the first process, silanol groups are formed during the silica synthesis, e.g. condensation polymerisation of $Si(OH)_4$ (Figure 4a). In the second process, the OH groups

form on the silica surface as a result of rehydroxylation of dehydroxylated silica when it is treated with water or aqueous solutions (Figure 4b). In aqueous medium the free valence of surface silicon atoms becomes saturated with hydroxyl groups (ZHURAVLEV 2000).

By definition, the geometrical arrangement of silicon atoms on the surface of amorphous silica is not regular and therefore, the silicon atoms will not be exactly equidistant from each other. This means that also their behaviour in adsorption and chemical reactions will be different. Figure 5 shows the postulated types of hydroxyl groups on the surface of amorphous silica.

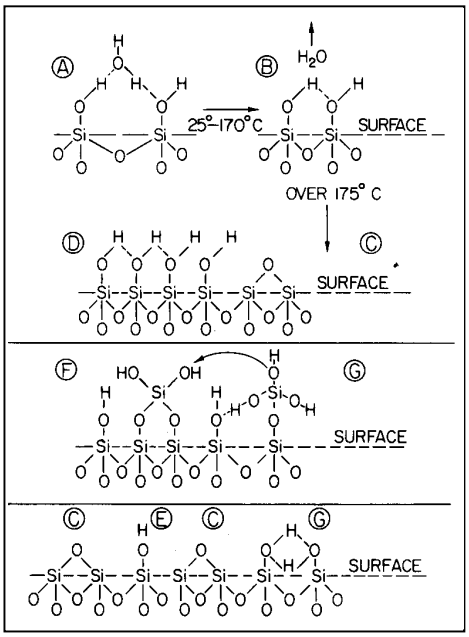

Figure 5 Postulated types of hydroxyl groups on the surface of amorphous silica. A, vicinal hydrated; B, vicinal anhydrous; C, siloxane-dehydrated; D, hydroxylated surface; E, isolated; F, geminal; G, vicinal, hydrogen bonded. Note: F and G probably do not actually exist on a dried surface (ILER 1979)

If the concentration of silanol groups on the silica surface is high enough, the surface becomes hydrophilic. The OH groups on the surface also act as centres of molecular adsorption when the silica substrate interacts with adsorbate capable of forming hydrogen bond with the OH group. The removal of hydroxyl groups from the surface of silica renders the surface more hydrophobic and less capable of adsorbing different molecules such as organosilanes or water. Therefore the conditions required to remove the physically adsorbed water and to dehydroxylate the silica surfaces is of key importance when working with silica.

ZHURAVLEV (2000) in his study summarized the results achieved over the last 50 years on the determination of boundary temperature for removing physically adsorbed water from the hydroxylated surface of amorphous silica. The results of the studies mostly done with IR spectroscopy show that physically adsorbed water can be removed at room temperature in vacuum. The opinion of different authors about the removal of water in atmosphere is different. The temperature shown to remove all physisorbed water molecules, ranges from 115 C° to 300 C° (FRIPIAT AND UYTTERHOEVEN 1962) in different experiments, depending on the drying time and pore size of the surfaces. LANGE (1965) states, that there are two types of adsorbed water on the hydroxylated silica surface. The "physically adsorbed", which desorbs between 25-105 C° and the "hydrogen bonded" desorbing at 105-180 C°. The physically adsorbed water requires an activation energy of 27.6-34.4 kJ mol^{-1} for removal, while the hydrogen bonded requires 41.8 kJ mol^{-1}. At rehydration, the hydrogen-bonded water follows the Langmuir isotherm, while the physically adsorbed water follows the type II isotherm, with monolayer coverage at p/p_0 = 0.18. According to ANDERSON AND WICKERSHEIM (1964), there are two types of H_2O and two types of SiOH on the hydroxylated silica surface. A monomeric H_2O molecule, which may be bonded to a single SiOH or a cluster of H_2O molecules may form hydrogen-bonded network. SiOH groups can be non-bonded or bonded to H_2O molecules.

The concentration, distribution and reactivity of surface hydroxyl groups determine the chemistry of the silica surface (GRIOT AND KITCHENER 1965). Therefore dehydroxylation and rehydroxylation of silica surface is of outstanding theoretical and practical importance. Authors agree that on fully hydroxylated, smooth, non-porous, heat stabilized amorphous silica surfaces there are 4-5 SiOH groups/nm^2 which remain even if the sample is heated to 120-150 C°. The data concerning the number of OH groups on the surface of silica determined by chemical methods such as esterification or chlorination is inconsistent with the data achieved by determination of active hydrogen or water loss. The chemical methods underestimate the number of OH groups on the surface (BOEHM 1966).

Hundreds of dehydration and rehydration studies have been performed over the last 50 years, but the data is not especially consistent in the estimation of the degree of dehydroxylation of silica surface with increasing temperature. This might be explained by very large differences in the structure of silica samples. The results of dehydroxylation studies of several authors summarized by ILER (1979) are shown in Figure 6.

The concentration of silanol groups on the silica surface decrease with increasing temperature. At 150 C° there are about 5 OH groups/nm^2. Above 170 C° the silanol groups start condensing and water is released. At 400 C° less than half of the OH groups are removed. Near complete dehydroxylation can be achieved by heating up to 1000 C° (ILER 1979).

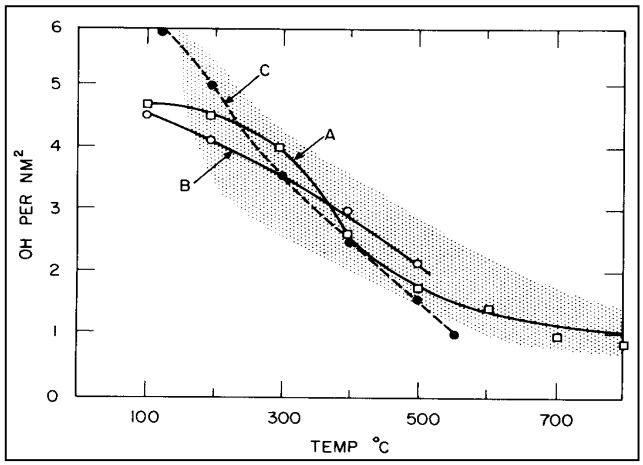

Figure 6 Dehydroxylation of silica versus temperature based on the data collected from several authors. Dehydration of annealed (700 C°) and rehydrated silica in A: air, B: vacuum. Broken line C: not annealed. (ILER, 1979)

Around 400 C° most of the hydroxyl groups are still adjacent and can adsorb water. Therefore the surfaces which were subjected to heat treatment below ~400 C° can be completely rehydroxylated. After heating to higher temperatures only partial rehydration takes place. Samples subjected to ~900 C° for example could be completely rehydroxylated only after 5 years of storage in water at room temperature. Boiling the dehydroxylated samples in water at 100 C° accelerate the rehydroxylation (YOUNG 1958; ZHURAVLEV, 1993) as well as changing the pH to alkaline region (GRIOT AND KITCHENER 1965). The changes in the number of surface silanol caused by heat treatment are summarized in Figure 7.

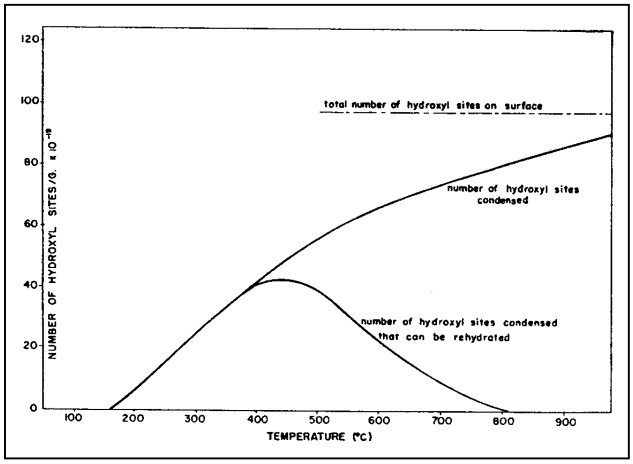

Figure 7 Change in surface silanol sites with sample heat treatment (YOUNG 1958)

ZHURAVLEV (2000) developed an advanced model for the description of the subsequent changes taking place on the surface of silica when the heat treatment temperature is changed. This is illustrated in Figure 8. The model describes the silica surface at different temperatures with six different states (stages).

In initial **stage 1** (25 C°, in vacuo), the surfaces are at a maximum state of hydroxylation and the surface is covered with multiple layers of physically adsorbed water (α_{OH}=4.60, Kiselev-Zhuravlev constant). All the different types of silanol groups (isolated singles, geminals, vicinals) are present on the surface. The surface OH groups and adsorbed water are permeated with H-bond network.

In the **transition from stage 1 to stage 2** (T_1=25 C°, in vacuo) (Figure 8a) the physically adsorbed water layers are completely removed. The process is completely reversible, if excess water is introduced.

In **stage 2 (**25-190 C°, in vacuo) the SiO_2 surface is in maximum state of hydroxylation, all the different types of silanol groups (isolated singles, geminals, vicinals) are present on the surface. The surface is covered with a complete or partially complete layer of adsorbed water, which disappears towards the end of stage 2. Surface silanol groups and adsorbed water molecules mainly bound via H-bonds.

In the **transition from stage 2 to stage 3 (**T_2= T_B=190 C° in vacuo) (Figure 8b) the H_2O monolayer is completely removed and the surface is in a state of maximum hydration. The process is completely reversible, if excess water is introduced.

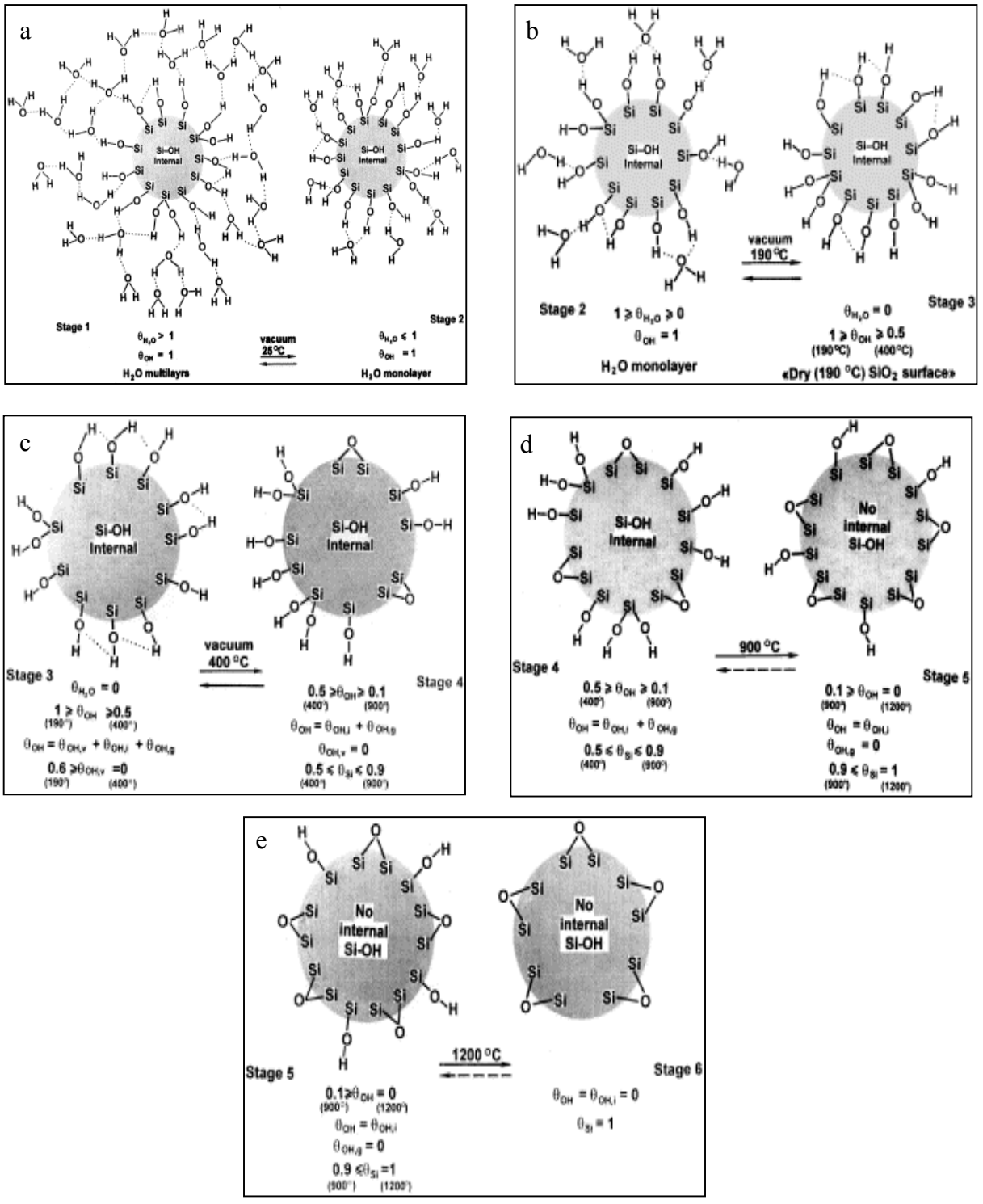

*Figure 8 The model of the surface transition of silica at different temperatures. (Description of the different stages in the text) (*ZHURAVLEV 2000)

In **stage 3 (**190-400 C°, in vacuo) the overall degree of surface hydroxylation decreases significantly ($4.60 \geq \alpha_{OH} \geq 2.35$). All the different types of silanol groups (isolated singles, geminals, vicinals) are present on the surface. The concentration of isolated single OH

groups increases and reaches the maximum at 400 C°. The concentration of vicinal bridged OH groups decreases and disappears at ~400 C°.

In the **transition from stage 3 to stage 4** (T_3= 400 C°, in vacuo) (Figure 8c) the vicinal OH groups are completely removed and only single and free geminal OH groups remain on the surface. The process is completely reversible, if excess water is introduced. Complete rehydroxylation can take place due to splitting of weakened strained SiOSi bridges.

In **stage 4 (**400-900 C°, in vacuo), the overall degree of surface hydroxylation decreases ($2.35 \geq \alpha_{OH} \geq 0.40$), there are only isolated free single and free geminal OH groups on the surface. At temperatures ~800-900 C° the geminal and internal OH groups disappear completely from silica skeleton. Concentration of siloxane bridges increases considerably and the whole silica surface becomes covered with SiOSi groups.

In **transition from stage 4 to stage 5** ($T_4 \approx$ 900 C°) (Figure 8d) the surface geminal silanol and internal OH groups are completely removed, but isolated single silanols still remain on the surface. The process is hardly reversible at room temperature if excess water is introduced (very slow process). If the silica is boiled at 100 C° in water the rehydroxylation is quite rapid.

In **stage 5** (900-1200 C°) the concentration of isolated single (free) OH groups decreases till complete disappearance. Concentration of siloxane bridges continues to increase, till the entire surface is covered with SiOSi groups and Si atoms.

In the **transition from stage 5 to stage 6** ($T_5 \approx$ 1200 C°) the OH groups are completely removed and the surface is entirely covered with SiOSi groups.

At **stage 6** (≥ 1200 C°) siloxane bridges cover the entire silica surface.

2.2.2 Interaction of silica with silanes and in particular with TMCS and HMDS

In order to study colloidal interactions, wetting phenomena and flotation mechanisms, it is desirable to work with hydrophobic surfaces. This can be achieved by adsorption of amines on the silica surface, although the interpretation of the contact angle results is complicated due to the very large hysteresis (GAUDIN ET AL., 1964). This effect is

explained by the transfer of surfactant from the air-water interface to the solid surface when the meniscus recedes across it (DIGRE AND SANDVIK, 1968).

To avoid adsorption of surfactants on the air-water interface, the one of the most widely used method for hydrophobizing silica surfaces is silanization. This is obtained by modification of silica particles with substituents of different hydrophobicities, such as dimethyldodecylchlorosilane $C_{12}H_{25}Si(CH_3)_2Cl$, (DMDS), octadecyltricholosilane, $C_{18}H_{37}SiCl_3$, (OTS), trimethylchlorosilane $(CH_3)_3SiCl$, (TMCS) (LASKOWSKI AND KITCHENER 1969; LAMB AND FURLONG 1982; TRIPP AND HAIR 1991; PONCET-LEGRAND ET AL. 2001) and hexamethyldisilazane $(CH_3)_3Si\text{-}NH\text{-}Si(CH_3)_3$, (HMDS) (YAKUBOV ET AL. 2000A,B).

Infrared spectroscopy, a powerful tool to determine the structure of adsorbed species on silica surfaces has been widely used (ARMISTEAD AND HOCKEY 1967; ZETTLEMOYER AND HSING 1977, etc.).

2.2.2.1 Reaction of chlorosilanes with dry silica surfaces

In systems where the surfaces are free of physisorbed water, (samples evacuated at temperatures below 500 C°) the chlorosilanes react with freely vibrating hydroxyl groups only, and not with the H-bond hydroxyls (DAVYDOV ET AL. 1964). The hydrophobizing reaction of silica with TMCS is described as follows:

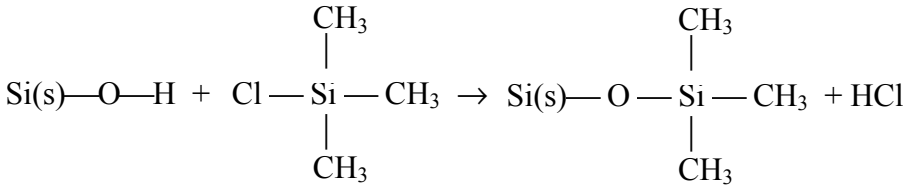

(21)

HAIR AND HERTL 1969 describes a secondary reaction, which is likely to take place on silica surfaces. In this reaction the surface hydroxyl group is simply replaced by chlorine atom.

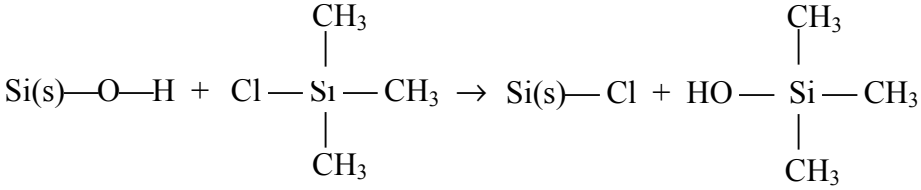

(22)

TRIP AND HAIR (1991) suggest that geminal silanols can react monofunctionally with the TMCS to result in a silanized surface as follows:

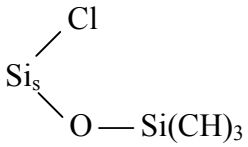

(23)

According to STÖBER (1956) the silanol groups on silica do not react quantitatively, because the large size trimethylsilyl groups, block the access to the neighbouring silanol groups. On Aerosil-silica for example he showed that only about 40 % of the silanol groups formed trimethylsiloxane groups. This explains the results obtained by LASKOWSKI AND KITCHENER (1969), who showed that the electrokinetic potential is similar on clean and hydrophobic silanated quartz.

2.2.2.2 Reaction of aminofunctional silanes with dry silica surfaces

VASANT ET AL. (1995) described the reaction of silica with aminofunctional silanes namely HMDS, as shown below:

$$\underset{\text{HMDS}}{(CH_3)_3 — Si—NH—Si—(CH_3)_3} + \underset{\text{Surface hydroxyl group}}{2{\equiv}Si—OH} \rightarrow \underset{\text{Trimethylsilyl surface group}}{2{\equiv}Si—O—Si—(CH_3)_3} + NH_3 \quad (24)$$

HERTL AND HAIR (1971) found that HMDS, in the same way as TMCS, reacts with the freely vibrating hydroxyl groups, which can be geminal [Si – $(OH)_2$] or single [Si – (OH)] , and only slightly reacts with H-bonded OH groups. As the reactivity of geminal and single hydroxyl groups is monoenergetic (reactivity of all the OH groups is the same), these groups react randomly.

GUN'KO AND CO-WORKERS (2000) suggest that a two-step reaction takes place. A fast reaction involving the non-hydrogen-bonded single silanols and disilanols, and a slow reaction resulting from the hindered reaction of HMDS with geminal silanols that already have one hydroxyl group silylated.

2.2.2.3 Interaction of chloro- and aminofunctional silanes with silica containing adsorbed water

Based on BOEHM (1966) if adsorbed water is present on the silica surface, TMCS forms hexamethyldisiloxane as described below:

$$2(CH_3)SiCl + H_2O \rightarrow (CH_3)_3Si - O - Si(CH_3)_3 + 2\ HCl \qquad (25)$$

For polyfunctional coupling agents such as HMDS, the spectroscopic results presented by HERTL AND HAIR (1971) show, that slightly larger amount of organic material is present on the surface containing adsorbed water, than on the dry samples. This is attributed to the polymerisation reaction.

Several authors consider the silylation a process that produces roughly 90° contact angle on silica with water. LAMB AND FURLONG (1982) showed that the contact angle of water on silica after silylation with TMCS is highly dependent on the number of surface silanol groups available for reaction with silylating reagent. Therefore by heating the silica to higher temperatures, the wettability of silica can be controlled (Figure 9).

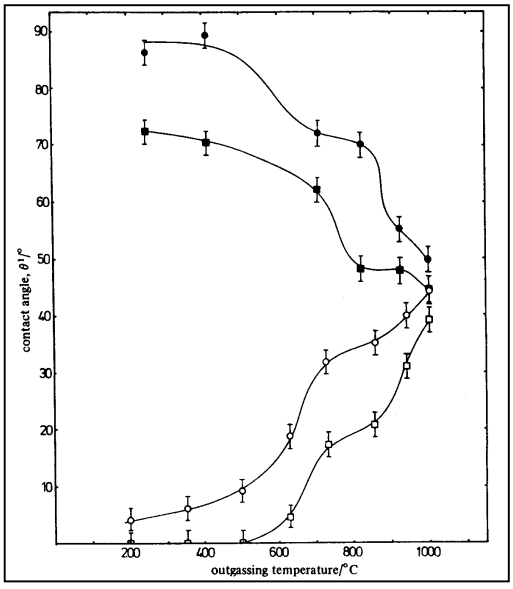

Figure 9 Summary of controlled wettability of quartz: ○□ heat treated quartz; ■● heat treated /methylated quartz. Round symbols advancing contact angle; square symbols, receding contact angle (LAMB AND FURLONG, 1982)

2.2.2.4 Interaction of water with organosilane and silazane treated surfaces

ZETTLEMOYER AND HSING (1977) were the first authors to study the interaction of water with silane-treated silica. They reacted HMDS from vapour phase with two types of silica (HiSil and Cab-o-Sil). The substrates were covered with different amounts of HMDS and adsorption isotherms of water were measured on these surfaces. The results showed that the isotherms were of Type II even at high HMDS coverage. The organic ligand did not inhibit the first-layer adsorption of water.

On the silane treated surface the breakdown of the silane coverage appears inevitable, although it has been shown (TAKACH ET AL. 1988) that stability of the silane coating on the surfaces can be improved by vapour-phase silanization. Even so, the coating still breaks down, but after longer time. MENAWAT ET AL. (1984) examined the air-water and xylene-water contact angles on silane-treated surfaces. They found a time dependent behaviour of xylene-water contact angles, which were explained with two mechanisms: rehydrolyzation and desorption of weakly adsorbed molecules. The rehydrolyzation reaction of silane-treated surfaces with water is possible due to the penetration of water molecules through the small methyl groups, as shown by the reaction below:

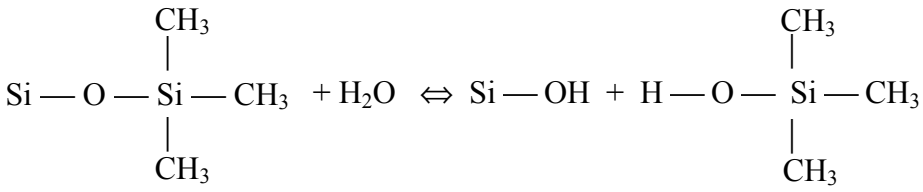

(26)

WEI AND COWORKERS (1993) studied the effect of water, air and oil on wettability of the silane treated glass surfaces. They have shown that the advancing and receding contact angles measured on the slides treated with TMCS and stored in water significantly decrease with time. The contact angle started to decrease immediately after placing the slide into water. In experiments done with quartz and silica slides the deterioration was comparable with the data obtained on glass surfaces. They precluded the possibility of desorption of weakly adsorbed silane molecules because the contact angle values were not deteriorated when the substrates were kept in air or oil.

Dependence of elipsometric film thickness on silane-treated silica

The silica surfaces are hydrophobized with silanes based on two different procedures:

- Silylation *in solution*: where the silica is immersed in a solution of silylation reagent in organic solvent, e.g. hexane or CCl_4, then rinsed with organic solvent and finally dried (LASKOWSKI AND KITCHENER 1969);
- Silylation *in vapour*: where the silica is placed into vapour of silylating reagent at room temperature or higher temperatures (YAKUBOV ET AL. 2000A,B).

TRAU ET AL. (1992) concluded that the vapour treatment produced thinner ellipsometric film thickness and smaller contact angle on silica plates, than silylation in solution.

2.3 ATOMIC FORCE MICROSCOPY IN COLLOIDAL FORCE MEASUREMENTS

The Atomic Force Microscope (AFM) invented by BINNING ET AL. (1986) has been proved to be a very valuable tool in fundamental surface science investigations, semiconductor industry, cell biology, etc. It is suitable for creating 3D images of surfaces with resolution down to nanometer or Ångström scale. In addition to the topographic imaging capabilities AFM can be used to probe nano-mechanical properties of sample surfaces e.g. taking phase-images or it can determine the local adhesive and elastic properties of samples by force measurements.

2.3.1 AFM force measurement applications

The local microscopic elastic and adhesive properties determine the behaviour of a wide variety of materials e.g. paints, glues, ceramics, paper, soil, clays, etc. The first AFM force measurements were performed in order to improve the quality of AFM images by monitoring and minimizing the attractive tip-sample forces (WEISENHORN AND HANSMA 1989). Forces were measured between standard silicon nitride cantilever and mica surface in air and water. Since the first force measurements, this technique has found its applications throughout a wide variety of disciplines, from material science to biology. Forces such as Van der Waals attraction, electrostatic repulsion, capillary forces, etc. have been measured and identified between a Ni lever and a mica surface (DUCKER ET AL. 1990), tungsten carbide tip and a gold or platinum foil (WEISENHORN ET AL. 1992), silicon nitride, Al_2O_3, glass, and diamond coated tips and mica or glass (BUTT 1991), in air and electrolytes.

The colloidal interactions have been studied over the last 60 years. Before the development of AFM, the colloidal forces could only be studied with the use of macroscopic substrates. The AFM has opened a great opportunity to directly measure the forces between colloidal particles and planar surfaces, particles or even deformable surfaces such as liquid droplets and bubbles. In 1991 Ducker and his co-workers were the first to attach colloidal particles to AFM cantilevers and measure forces between a silica sphere and silica substrate in electrolyte (DUCKER ET AL. 1991). Since then, the colloidal probe technique has been widely used. Colloidal spheres and particles of different sizes and materials such as glass (BUTT 1994), silica (DUCKER ET AL. 1991), gold (BIGGS AND MULVANEY 1994), titanium dioxide (LARSON ET AL. 1993, 1995), zirconia (BIGGS AND HEALY 1994), polystyrene (SCHAEFER ET AL. 1994; HODGES ET AL. 2002), etc. have been attached to AFM cantilevers and the force measurements have been performed in air or liquid.

2.3.2 Modified commercial AFMs and custom made instruments for force measurements

Most of the above-mentioned studies used commercially available AFMs. Although the AFMs have been successfully used in some of the experiments, their structure creates some serious limitations in some specific applications. Therefore some research groups modified their commercial setups, or built completely new custom made devices based on the AFM force measurement principle. These were optimised for the specific application of interest.

PIERCE ET AL. (1994) modified the commercial Nanoscope II AFM (Digital Instruments Inc.) in order to comply with the requirements of the force measurements on biological samples. The original AFM head was coupled with large position sensing photo detector. Custom build function generator provided the voltage signal for the piezocrystal that moved the sample in z-direction. This arrangement allowed detection of a larger range of cantilever deflections and a precise control of timing, speed and shape of the voltage function applied on the piezocrystal. This was of major importance in the study of macromolecules such as proteins.

BUTT (1994) built a completely custom made apparatus to measure particle-bubble interactions. The main advantages of the apparatus were that large cantilever deflections

could be detected, which occur in the case of particle-bubble interactions, and the measuring cell could be easily accessed and monitored from the side through a microscope.

CRAIG ET AL. (1996) built the **L**ight-**L**ever **I**nstrument for **F**orce **E**valuation (LLIFE). The strength of this instrument lies in its custom built software that gives almost complete control of surface separation and monitors surface forces under both very slow and very fast interaction conditions. Using this software control the authors provided means to investigate in more details the errors associated with this technique and develop methods to minimize or avoid them.

ECKE ET AL. (2001) developed the **P**article **I**nteraction **A**pparatus (PIA) in order to measure normal and friction forces between particles and surfaces. The apparatus was equipped with two piezo translators, one for horizontal movement for friction forces measurements, and another vertical for normal force investigations. A two-dimensional position sensitive detector used to measure the position of the laser beam reflected from the back of the cantilever. The measurement cell was easily accessible. The piezos were controlled from a PC.

TOIKKA ET AL. (2001) built a new instrument called “force ring” in order to study adhesion between fine particles and a heated sample in controlled environment. The instrument is based on AFM technique. With their arrangement a single contact could be made between a micron-sized particle and a sample surface over a controlled period of time and the pull-off force could be measured. With commercial instruments it is very difficult, if not impossible, to perform such experiments.

2.3.3 Force versus distance curves

The AFM force measurement technique is a very useful tool in quantitative studies of surface forces, such as van der Waals, capillary, electrostatic, double-layer, magnetic and adhesive forces. In this specific AFM application, one-dimensional piezo is used, and the cantilever deflection is measured as a function of piezo position.

This chapter describes the basic concept of the force versus distance curves, in case of solid surfaces and problems encountered when deformable surfaces are involved. The available methods for the determination of separation between the particle and the deformable surface are also described.

2.3.3.1 Force curves between particles and solid surfaces

In the force measurements between the AFM tip or a colloidal probe and a solid surface the evaluation and interpretation of the force vs. distance curve is quite straightforward. The actual raw data curve measured by the instrument is the detector signal [V] versus the piezo position [nm] plot, which in case of solid surfaces can be easily transformed into force [nN] versus distance [nm] curve (Figure 10).

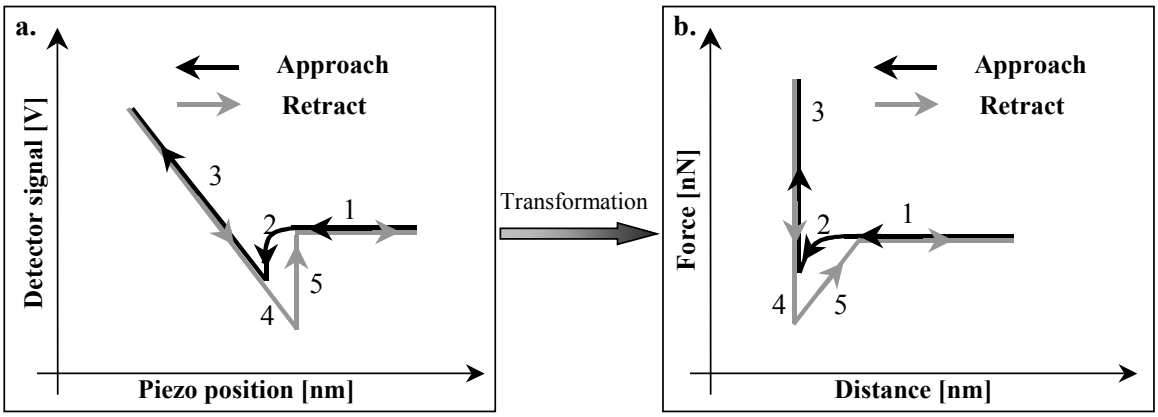

Figure 10 Schematic figure of force curve transformations. a.) Detector signal vs. piezo position curve; b.) Detector signal vs. piezo position curve transformed to Force vs. distance curve in case of non-deformable surfaces. 1. Constant force region; 2. Jump into contact (in this case due to attractive force); 3. Constant compliance region; 4. Adhesion; 5. Snap-off. The transformation is described in the text.

The transformation is obtained by multiplying the deflection with the piezo calibration coefficient and the cantilever spring constant, and adding the cantilever deflection to the piezo position as described by the following formulas:

Detector signal → Deflection: $d_c = S_d \cdot f_d$

Deflection → Force: $F = d_c \cdot K_c$

Piezo position → Distance: $D = z_p + d_c$

Where: d_c cantilever deflection
S_d detector signal
f_d detector calibration coefficient
F force
K_c cantilever spring constant
D distance
z_p piezo position

In order to obtain comparable results from several measurements, the force data is normalised by dividing it by the radius of the particle.

The resulting force vs. separation curves can then be interpreted by fitting theoretical models to the data and evaluating these fits.

2.3.3.2 Force curves between particles and deformable surfaces

The first measurements between a colloidal particle and an air bubble, and between a particle and a water droplet have been carried out by Butt (1994). Although these measurements were performed almost 10 years ago, the problem of the interpretation of the force curves in case of deformable surfaces has not yet been solved. In the case of deformable surfaces, in many cases the spring constant of the bubble/drop is lower than the spring constant of the cantilever. This means, that if there is an attractive force acting between the particle and the bubble, the bubble/drop will deform towards the particle, decreasing the separation, while in the case of a repulsive force, the separation will increase.

There have been only a few attempts to establish a method for determining the separation for such a specific application. A general procedure for the determination of the zero separation in case of deformable surfaces consists in shifting the data to coincide with the known rigid body interaction at large separations where the force is weak and the deformation is negligible (GILLIES ET AL. 2001). The disadvantage of this method is that it can only be applied to double-layer interactions where the surface potential has been independently measured.

Recently Nguyen and his co-workers described a method for analysis of the force data involving bubbles when repulsive forces dominate the interaction (NGUYEN ET AL. 2002). The equation allowing the calculation of the actual separation distance is shown below:

$$D = D_{cont} + \left(d_c - d_{cont}\right)\left\{1 + \frac{K_c}{K_b}\right\} - \left(z_p - z_c\right) \qquad (27)$$

Where:

D	actual separation distance
D_{cont}	contact value of separation distance
d_c	cantilever deflection
d_{cont}	contact value of cantilever deflection
K_c	cantilever spring constant
K_b	bubble spring constant
z_p	piezo position
z_c	contact value of piezo position

The meaning of the symbols used in their equations is detailed in Figure 11.

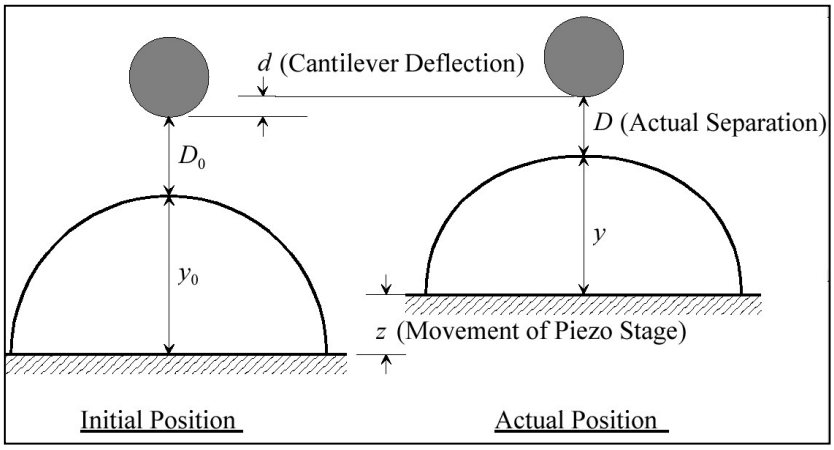

Figure 11 Schematic of the relative positions of a particle and a bubble with a surface deformation (NGUYEN ET AL 2002)

Therefore the force vs. piezo position data cannot be converted into force vs. separation data using the method described in chapter 2.3.3.1. Moreover, this also means that the jump-in curves cannot be interpreted by conventional means, which involve fitting theoretical models to the data. They can only be evaluated relative to each other. This type of force curve evaluation gives qualitative data only and it can be considered as the main limitation of the colloidal probe technique applied for measurements involving deformable surfaces.

2.3.3.3 Calculation of the bubble stiffness

Ducker et al. (1994) calculated the bubble stiffness from the slope of the constant compliance region of a force curve measured between a particle and an air bubble. In this calculation the cantilever and the bubble were modelled as two Hookean springs in a series, as given in the following equations:

$$\frac{1}{K_m} = \frac{1}{K_c} + \frac{1}{K_b} \tag{28}$$

$$K_b = \frac{K_c}{\left(\frac{K_c}{K_m} - 1\right)} = \frac{K_c}{\left(\frac{C_h}{C_b} - 1\right)} \tag{29}$$

Where: K_m - measured stiffness
K_b - stiffness of the bubble
K_c - stiffness of the cantilever
C_h - cantilever deflection per unit sample translation when pushed against hard surface

C_b - cantilever deflection per unit sample translation when pushed against the bubble

Since its publication this method has been used by several authors for the interpretation of their data involving deformable surfaces (BASU AND SHARMA 1996; PREUSS AND BUTT 1998; HARTLEY ET AL. 1999). ATTARD AND MIKLAVCIC (2001, 2002) investigated in detail the behaviour of bubbles and drops. From mathematical analysis and experimental evidence it was proved that bubbles and drops behave as Hookean springs over experimental regimes and that the effective spring constant is in scale with the surface tension.

2.3.4 Cantilever calibration

The calibration of AFM cantilevers is of major importance for the interpretation of force measurements. The force is measured between the tip and the sample, or the colloidal probe attached to the AFM cantilever and the sample. The force is calculated by multiplying the deflection of the cantilever with its spring constant.

The colloidal probe technique cannot be used without the precise knowledge of the cantilever spring constant and its determination is not an easy task. Several methods have been examined to find the most suitable and simple one. The two main approaches to the cantilevers spring constant determination are:

- the calculation from material properties and geometric dimensions;
- experimental determination .

Spring constant determination from material properties and geometric dimensions

In principle, it is possible to calculate the spring constant of AFM cantilevers by knowing the geometric dimensions and the elastic properties of the material the cantilever is made of using analytical forms (NEUMEISTER AND DUCKER 1994; TORTONESE 1997). SADER AND WHITE (1993) used a detailed finite element analysis to calculate the spring constants of an AFM cantilever. Nevertheless, the determination of exact geometrical dimensions and the elasticity modulus is not always straightforward, because of the variations due to structural defects and differences in lever geometry. In addition, cantilevers are often coated with different metallic coatings such as gold, aluminium, chromium, cobalt-chromium, etc., in order to enhance reflectivity or to render the

cantilever conductive. These coatings make the determination of elasticity modulus even more difficult, if not impossible. Therefore these methods of calibration are not very widely used.

Experimental spring constant determinations

Another approach is the experimental determination of cantilever spring constants. HUTTER AND BECHHOEFER (1993) introduced a method based on the determination of power spectral density of cantilever fluctuation due to thermal noise. CLEVELAND ET AL. (1993) attached tungsten spheres with known mass to the end of the AFM cantilevers and determined the spring constant from the change in the resonant frequency. BUTT ET AL. (1993) pushed the tip of the cantilever against the weight of a pendulum, measured the deflection of the cantilever and that of the pendulum and calculated the cantilever spring constant from the obtained values. SENDEN AND DUCKER (1994) determined the spring constant by measuring the static deflection of the cantilever under the force of a known mass applied to the end of the lever. Another calibration method is based on the measurement of deflection when the cantilever is pressed against a reference glass filament (RABINOVICH AND YOON 1994) or cantilever with a known spring constant (GIBSON ET AL. 1996; TORII ET AL. 1996; TORTONESE AND KIRK 1997). The spring constant is calculated from the slopes of the constant compliance region of the force curves with the following formula:

$$k_{test} = k_{ref} \frac{\delta_{tot} - \delta_{test}}{\delta_{test} \cdot \cos \vartheta} \tag{30}$$

The meaning of abbreviations is shown on Figure 12.

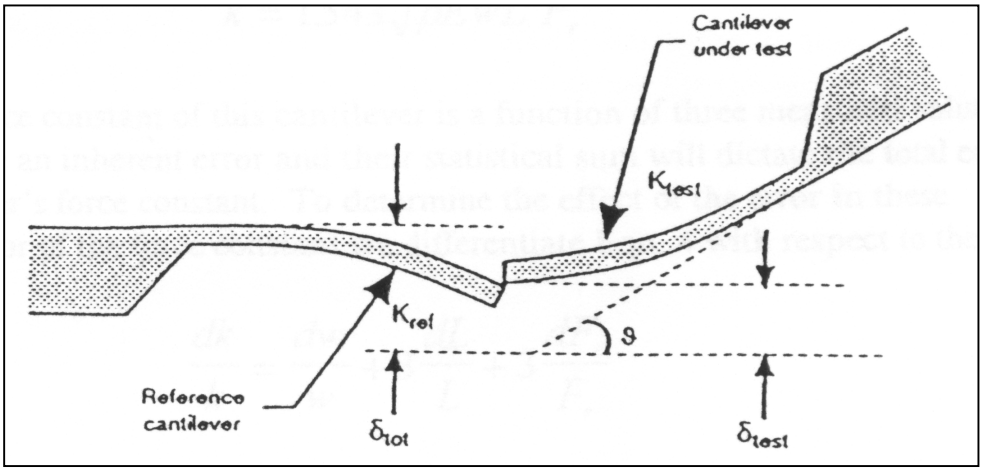

Figure 12 Schematic showing the geometry of force vs. distance measurement of test cantilever relative to a reference cantilever (TORTONESE AND KIRK, 1997)

In 1999, SADER ET AL. described a method in which the spring constant of rectangular AFM cantilevers is determined based on the measurement of the resonant frequency and quality factor of the cantilever and its plain dimensions. Recently, MAEDA AND SENDEN (2000) employed hydrodynamics for the determination of the spring constant.

In spite of the large number of papers published on cantilever calibration methods, there are no references to the instability of micro-fabricated AFM cantilevers, which was observed in the experimental part of this thesis, as shown in chapter 3.3.2.1 and Chapter 6 .

2.3.5 Pros and cons of the AFM force measurement technique

In comparison with other surface force measurement techniques such as Surface Force Apparatus (SFA) (ISRAELACHVILI AND TABOR 1972), Measurement and Analysis of Surface Interaction Forces (MASIF) (CLAESSON ET AL. 1996), the AFM has several advantages, but also some drawbacks.

The main advantage is the sample geometry, (in most of the cases a spherical particle), that can easily be determined, and therefore the Derjaguin approximation can be applied to normalize the measured force. The sensitivity of the colloidal force measurement technique is about two orders of magnitude better than the above mentioned two other techniques (SFA and MASIF). The variety of surfaces that can be employed is also much wider in AFM applications than in SFA technique. AFM is of non-interferometric type therefore the transparency of the surfaces is not a requirement.

The main disadvantages include problems in determination of the absolute distance, layer thickness, local radius and surface deformation. This makes the calculation of the surface forces versus the separation distance difficult if deformable surfaces are involved.

References chapter 2

Anderson, J.H., Wickersheim, K.A., 1964. Near Infrared Characterization of Water and Hydroxyl Groups on Silica Surfaces, *Surface Science,* **2**, 252-260.

Armistead, C.G., Hockey, J.A., 1967. Reactions of Chloromethyl Silanes with Hydrated Aerosil Silicas, *Trans. Faraday Soc*. **63**, 2549-2556.

Attard, P., Miklavcic, S.J., 2001. Effective Spring Constant of Bubbles and Droplets, *Langmuir,* **17**, (26), 8217-8223.

Attard, P., Miklavcic, S.J., 2002.Effective Spring Description of a Bubble or a Droplet Interacting with a Particle, *J. Coll. Interf. Sci.,* **247**, (1), 255-257.

Attard, P., 1989. Long-Range Attraction between Hydrophobic Surfaces, *J. Phys. Chem*., **93**, 6441-6444.

Basu, S., Sharma, M.M., 1996. Measurement of Critical Disjoining Pressure for Dewetting of Solid Surfaces*, J. Coll. Interf. Sci,* **191**, (2), 443-455.

Biggs, S., Healy, T.W., 1994. Electrostatic stabilisation of Colloidal Zirconia with Low-molecular Weight Polyacrylic Acid, *J. Chem. Soc. Faraday Trans.,* **90**, (22), 3415-3421.

Biggs, S., Mulvaney, P., 1994. Measurement of the forces between gold surfaces in water by atomic force microscopy, *J. Chem. Phys.,* **100**, (11), 8501-8505.

Binning, G., Quate, C.F., Gerber, C., 1986. Atomic Force Microscope, *Phys. Rev. Lett.,* **56**, (9), 930-933.

Boehm, H.P. 1966. Chemical Identification of Surface Groups. Sourface Groups on Silica, *In Advances in Catalysis,* **16**, 225-247.

Butt, H.-J., 1991. Electrostatic interaction in atomic force microscopy, *Biophys. J*., **60**, (4), 1438-1444.

Butt, H.-J., 1994. A Technique for Measuring the Force between a Colloidal Particle in Water and a Bubble, *J. Colloid Interface Sci*., **166**, 109-117.

Carambassis, A., Jonker, L.C., Attard, P., Rutland, M.W., 1998. Forces Measured between Hydrophobic Surfaces due to a Submicroscopic Bridging Bubble, *Phys. Rev. Lett.*, **80**, (24), 5357-5360.

Chang, Y.-I., Chang P.-K., 2002. The role of hydration force on the stability of the suspension of Saccharomyces cerevisiae–application of the extended DLVO theory, *Coll. Surf. A: Physicochem. Eng. Asp.,* **211**, (1), 67-77.

Christenson, H.K., Claesson, P.M., Berg, J., Herder, P.C., 1989. Forces between Fluorocarbon Surfactant Monolayers: Salt Effects on the Hydrophobic Interaction, *J. Phys. Chem*., **93**, (4), 1472-1478.

Christenson, H.K., Fang, J., Ninham, B.W., Parker, J.L., 1990. Effect of Divalent Electrolyte on the Hydrophobic Attraction, *J. Phys. Chem*., **94**, 8004-8006.

Claesson P.M., Christenson, H.K., 1988. Very Long Range Attractive Force between Uncharged Hydrocarbon and Fluorocarbon Surfaces in Water, *J.Phys. Chem.* **92**, (6), 1650-1655.

Claesson, P.M., Blom, C.E., Herder, P.C., Ninham, B.W., 1986. Interactions between Water-Stable Hydrophobic Langmuir-Blodgett Monolayers on Mica, *J. Coll. Interf. Sci*., **114**, (1), 234-242.

Claesson, P. M., Ederth, T., Bergeron, V., Rutland, M. W., 1996. Techniques for measuring surface forces, *Advances in Colloid and Interface Science*, **67**, 119-183.

Cleveland, S. J., Manne, P., Bocek, D., Hansma, P.K., 1993. A nondestructive method for determining the spring constant of cantilevers for scanning force microscopy, *Rev. Sci. Instr.,* **64**, (2), 403-405.

Craig, V.S.J., Hyde, A.M., Pashley, R.M., 1996. Application of the Light-Lever Technique to the Study of Colloidal Forces, *Langmuir,* **12**, (15), 3557-3562.

Davydov, V.Ya., Kiselev, A.V., Zhuravlev, L.T., 1964. Study of the Surface and Bulk Hydroxyl Groups of Silica by Infra-red Spectra and D2O-exchange, *Trans. Faraday Soc.,* **60** (II), 2254-2264.

Derjaguin, B.V., Dukhin, S.S., 1961. Kinetic Theory of Flotation of Small and Medium-size Particles, *Trans. Ist. Min. Metall.,* **70,** 221-246.

Derjaguin, B.V., Landau, L., 1941. Theory of the Stability of Strongly Charged Lyophobic Sols and of the Adhesion of Strongly Charged Particles in Solutions of Electrolytes, *Acta physicochimica U.S.S.R.,* **14**, (6), 633-662.

Digre, M., Sandvik, K.L., 1968. Adsorption of amine on quartz through bubble interaction, *Trans. Inst. Mining Met.C*, **77,** (739), 61-64.

Ducker, W. A., Cook, R. F., Clarke, D. R., 1990. Force measurement using an ac atomic force microscope, *J. Appl. Phys.,* **67**, (9), 4045-4052.

Ducker, W.A., Senden, T.J., Pashley, R.M., 1991. Direct measurement of colloidal forces using an atomic force microscope, *Nature,* **353,** 239-241.

Ducker, W.A., Xu, Z., Israelachvili, J.N., 1994. Measurement of Hydrophobic and DLVO Forces in Bubble-Surface Interactions in Aqueous Solutions, *Langmuir*, **10**, (9), 3279-3289.

Dzyaloshinskii, I.E., Lifshitz, E.M., Pitaevskii, L.P., 1961. The General Theory of Van der Waals Forces, *Adv. Phys.,* **10**, (38), 165-209.

Ecke, S., Raiteri, R., Bonaccurso, E., Reiner, C., Deiseroth, H.-J., Butt, H.-J., 2001. Measuring normal and friction forces acting on individual fine particles, *Rev. Sci. Instrum.,* **72**, (11), 4164-4170.

Ederth, T.E., Claesson, P., Liedberg, B., 1998. Self-Assembled Monolayers of Alkanethiolates on Thin Gold Films as Substrates for Surface Force Measurements. Long-Range Hydrophobic Interactions and Electrostatic Double-Layer Interactions, *Langmuir*, **14**, (17), 4782-4789.

Eriksson, J.C., Ljunggren, S., Claesson, P.M., 1989. A Phenomenological Theory of Long-range Hydrophobic Attraction Forces based on a Square-gradient Variational Approach. *J. Chem. Soc. Faraday Trans. II*, **85**, (3) 163-176.

Fripiat, J.J., Uytterhoeven, J., 1962. Hydroxyl Content in Silica Gel ”Aerosil”, *J. Phys. Chem*. **66**, 800-805.

Fröberg J. C., Rojas, O. J., Claesson, P. M., 1999. Surface forces and measuring techniques, *Int. J. Min. Process.,* **56**, (1-4), 1-30.

Gaudin, A.M., Bangs, L.B., Witt, A.F., 1964. Hysteresis of Contact Angles inFogadjunk. the System Benzene-Water-Quartz, *Proc. 7th Intern. Min. Process. Congress*, New York, 321-328.

Gibson, T.C., Watson, G.S., Myhra, S., 1996. Determination of the spring constants of probes for force microscopy/spectroscopy, *Nanotechnology,* **7**, 259-262.

Gillies, G., Prestidge, C.A., Attard, P., 2001. Determination of the Separation in Colloid Probe Atomic Force Microscopy of Deformable Bodies, *Langmuir*, **17**, (25), 7955-7956.

Graciaa, A., Morel, G., Saulner, P., Lachaise, J., Schechter, R. S., 1995. The ζ-Potential of Gas Bubbles, *J. Coll. Interf. Sci.,* **172**, (1), 131-136.

Griot, O., Kitchener, J.A., 1965. Role of Surface Silanol Groups in the Flocculation of Silica Suspensions by Polyacrylamide. Part 2. – Surface Changes of Silica Suspensions on Ageing, *Trans. Faraday Soc*., **61**, 1032-1038.

Gun’ko, V.M., Vedamuthu, M.S., Henderson, G.L., Blitz, J.P., 2000. Mechanism and Kinetics of Hexamethyldisilazane Reaction with Fumed Silica Surface, *J. Coll. Interf. Sci.,* **228**, 157-170.

Hair, M.L., Hertl, W., 1969. Reactions of Chlorosilanes with Silica Surfaces, *J. Phys. Chem.,* **73**, (7), 2372-2378.

Hamaker, 1937. The London-Van der Waals Attraction between Spherical Particles, *Physica* **IV**, 10, 1058-1072.

Hartley, P.G., Grieser, F., Mulvaney, P. Stevens, G.W., 1999. Surface Forces and Deformation at the Oil-Water Interface Probed Using AFM Force Measurement, *Langmuir,* **15**, (21), 7282 - 7289;

Hertl, W., Hair, M.L., 1971. Reaction of Hexamethyldisilazane with Silica, *J. Phys. Chem,* **75**, (14), 2181-2185.

Hodges, C. S., Cleaver, J. A. S., Ghadiri, M., Jones, R., Pollock, H. M., 2002. Forces between Polystyrene Particles in Water Using the AFM: Pull-Off Force vs Particle Size, *Langmuir,* **18**, (15), 5741-5748.

Hogg, H., Healy, T.W., Fuerstenau, D.W., 1966. Mutual coagulation of Colloidal Suspensions, *Trans. Faraday Soc.*, **62**, (522), 1638-1651.

Hutter, J. L., Bechhoefer, J., 1993. Calibration of atomic-force microscope tips, *Rev. Sci. Instrum.,* **64**, (7), 1868-1873.

Iler, R. K., 1955. The colloid chemistry of silica and silicates, *Cornell University Press, New York*.

Iler, R.K., 1979. The chemistry of Silica. Solubility, Polymerization, Colloid and Surface Properties, and Biochemistry, *Wiley-Interscience Publication, John Wiley & Sons, New York*.

Israelachvili, J.N., 1972. The calculation of van der Waals dispersion forces between macroscopic bodies, *Proc. Royal. Soc. London A*, **331**, (1584), 39-55.

Israelachvili, J.N., 1991. Intermolecular and Surface Forces, *Academic Press, London*.

Israelachvili, J.N., Adams, G.E., 1976. Direct measurement of long range forces between two mica surfaces in aqueous KNO_3 solutions, *Nature,* **262**, (5571), 774-776.

Israelachvili, J.N., Pashley, R.M., 1982. The hydrophobic interaction is long range, decaying exponentially with distance, *Nature*, **300**, (5890), 341-342.

Israelachvili, J.N., Pashley, R.M., 1984. Measurement of the Hydrophobic Interaction between Two Hydrophobic Surfaces in Aqueous Electrolyte Solutions, *J. Coll. Interf. Sci.,* **98**, (2), 500-514

Israelachvili, J.N., Tabor, D., 1972. The measurement of van der Waals dispersion forces in the range 1.5 to 130 nm, *Proc. R. Soc. Lond.* **A331**, 19-38.

Karaman, M.E., Meagher, l., Pashley, R.M., 1993. Surface chemistry of emulsion polymerisation, *Langmuir*, **9**, (5), 1220-1227.

Lamb, R.N., Furlong, D.N., 1982. Controlled wettability of Quartz Surfaces, *J. Chem. Soc. Faraday Trans.* 1, **78**, 61-73.

Lange, K.R., 1965. The Characterization of Molecular Water on Silica Surfaces, *J. Colloid Sci.,* **20**, 231-240.

Larson, I., Drummond, C.J., Chan, D.Y.C., Grieser, F., 1993. Direct force measurements between TiO_2 surfaces, *J. Am. Chem. Soc.,* **115**, (25), 11885-11890.

Larson, I., Drummond, C.J., Chan, D.Y.C., Grieser, F. 1995. Direct Force Measurements between Dissimilar Metal Oxides, *J. Phys. Chem.*, **99**, (7), 2114-2118.

Laskowski, J. S, Kitchener, J.A., 1969. The Hydrophilic-Hydrophobic Transition of Silica, *J. Coll. Interf. Sci.,* **29**, 4, 670-679.

Laskowski, J.S., 1986. The Relationship between Floatability and Hydrophobicity, *Advances in Mineral Processing, Soc. Mining. Eng. Inc., Littleton, Colorado*, 189-208.

Laskowski, J.S., Yordan, J.L., Yoon, R.H., 1989. Electrokinetic potential of microbubbles generated in aqueous solutions of weak electrolyte type surfactants, *Langmuir*, **5**, (2), 373-376.

Li, C., Somasundaran, P., 1991. Reversal of Bubble Charge in Multivalent Ionic Salt Solutions – Effect of Magnesium, *J. Coll. Interf. Sci,* **146**, (1), 215-218.

Lifshitz, E.M., 1956. The Theory of Molecular Attractive Forces between Solids, *Soviet Phys. JETP*, **2**, (1), 73-83.

Maeda, N., Senden, T., 2000. A Method for the Calibration of Force Microscopy Cantilevers via Hydrodynamic Drag, *Langmuir,* **16**, (24), 9282-9286.

McShea, J.A., Callaghan, I.C., 1983. Electrokinetic potentials at the gas-aqueous interface by spinning cylinder electrophoresis, *Colloid & Polymer Sci*., **261**, (9), 757-766.

Meagher, L., Craig, V.S.J., 1994. Effect of Dissolved Gas and Salt on the Hydrophobic Force between Polypropylene Surfaces, *Langmuir,* **10**, (8), 2736-2742.

Menawat, A., Henry, J., Siriwardane, R., 1984. Control of Surface Energy of Glass by Surface Reactions: Contact Angle and Stability, *J. Coll. Interf. Sci*, **101**, (1), 110-119.

Meyer, D.E., Hackerman, N., 1966. Adsorption Thermodynamics of the Interaction of Water and Various Silica Powders, *J. Phys. Chem.,* **70**, (7), 2077-2086.

Molina-Bolívar, J. A., Galisteo-González, F., Hidalgo-Alvarez, R., 1999. The role played by hydration forces in the stability of protein-coated particles: non-classical DLVO behaviour, *Colloid. Surf. B: Biointerf.*, **14**, (1-4), 3-17.

Neumeister, J.M., Ducker, W.A., 1994. Lateral, normal, and longitudinal spring constants of atomic force microscopy cantilevers, *Rev. Sci. Instrum.,* **65**, (8), 2527-2531.

Nguyen, A.V., Nalaskowski, J., Miller, J.D., 2002. Measurements of bubble-particle interaction forces by atomic force microscopy, *Proc. of 9th APCChE 2002 and Chemeca 2002*, 29 September – 3 October, Christchurch, New Zealand.

Nguyen, A.V., Schulze, H.J., 2003. Colloidal Science of Flotation, *Marcel Dekker, Inc.,* New York (in press).

Parker, J.L., Claesson, P.M., Attard, P., 1994. Bubbles, Cavities, and Long-Ranged Attraction between Hydrophobic Surfaces*, J. Phys. Chem.*, **98**, 8468-8480.

Pashley, R.M., 1981. DLVO and Hydration Forces between Mica Surfaces in Li^+, Na^+, K^+, and Cs^+ Electrolyte Solutions: A Correlation of Double-Layer and Hydration Forces with Surface Cation Exchange Properties, *J. Coll. Interf. Sci*., **83**, (2), 531-546.

Paulson, O., Pugh, R.J., 1996. Flotation of Inherently Hydrophobic Particles in Aqueous Solutions of Inorganic Electrolytes, *Langmuir*, **12**, (20), 4808-4813.

Pierce, M., Stuart, J., Pungor, A., Dryden, P., Hlady, V., 1994. Adhesion Force Measurements Using an Atomic Force Microscope Upgraded with a Linear Position Sensitive Detector, *Langmuir*, **10**, (9), 3217 – 3221

Poncet-Legrand, C., Bordes B., Lafuma, F., 2001. Surface modification of colloidal silica particles*, Colloid Polym. Sci.,* **279**, 114-121.

Preuss, M., Butt, H.-J., 1998. Direct Measurement of Particle-Bubble Interactions in Aqueous Electrolyte: Dependence on Surfactant, *Langmuir*, **14**, (12), 3164 – 3174.

Rabinovich, Ya. I., Yoon, R.-H., 1994. Use of Atomic Force Microscope for the Measurements of Hydrophobic Forces between Silanated Silica Plate and Glass Sphere, *Langmuir,* **10**, (6), 1903-1909.

Rabinovich, Ya., Derjaguin, B.V., 1988. Interaction of Hydrophobized Filaments in Aqueous Solutions, *Colloids and Surfaces*, **30**, (3/4), 243-251.

Ruckenstein, E., Churaev, N.V., 1991. A Possible Hydrodynamic Origin of the Forces of Hydrophobic Attraction, *J. Coll. Interf. Sci.,* **147**, (2), 535-538.

Sader, J.E., Chon, J.W.M., Mulvaney, P., 1999. Calibration of rectangular atomic force microscope cantilever, *Rev. Sci. Instrum.,* **70**, (10), 3967-3969.

Sader, J.E., White L., 1993. Theoretical analysis of the static deflection of plates for atomic force microscope applications*, J. Appl. Phys.,* **74**, (1), 1-9.

Senden, T.J., Ducker, W.A., 1994. Experimental Determination of Spring Constants in Atomic Force Microscopy, *Langmuir,* **10**, (4), 1003-1004.

Takach, N.E., Benett, L.B., Douglas, C.B., Andersen, M.A., Thomas, D.C., 1988. Wettability Alteration of Model Sandstone Surfaces by Vapor-Phase Treatment with Organosilanes, *J. Am. Chem. Soc.*, **33**, (3), 525-529.

Toikka, G., Spinks, G.M., Brown, H.R., 2001. Fine Particle Adhesion Measured at Elevated Temperatures Using a Dedicated Force Rig, *Langmuir*, **17**, (20), 6207-6212.

Torii, A., Sasaki, M., Hane, K., Okumat, S., 1996. A method for determining the spring constant of cantilevers for atomic force microscopy, *Meas. Sci. Technol.,* **7**, (2), 179-184

Tortonese, M., 1997. Cantilevers and Tips for Atomic Force Microscopy, *IEEE Engineering in Medicine and Biology,* **16**, (2), 28-33.

Tortonese, M., Kirk, M., 1997. Characterization of application specific probes for SPMs, *SPIE* **3009**, 53-60.

Trau, M., Murray, B.S., Grant, K., Grieser, F., 1992. An Ellipsometric Study of Thin Films on Silica Plates Formed by Alkylchlorosililation Reagents, *J. Coll. Interf. Sci.,* **148**, (1), 182-189.

Tripp, C.P., Hair, M.L., 1991. Reaction of Chloromethylsilanes with silica: A Low-Frequency Infrared Study, *Langmuir,* **7**, 923-927.

Vasant, E.F., Van Der Voort, P., Vrancken, K.C., 1995. Characterization and Chemical Modification of the Silica Surface, *Elsevier, Amsterdam*.

Verwey, E.J.W., Overbeek, J.T.G., 1948. Theory of the Stability of Lyophobic Colloids, *Elsevier, Amsterdam.*

Wei, M., Bowman, R.S., Wilson, J.L., Morrow, N.R., 1993. Wetting Properties and sziaStability of Silane-Treated Glass Exposed to Water, Air, and Oil, *J. Coll. Interf. Sci.,* **157**, (1), 154-159.

Weisenhorn, A. L., Maivald, P., Butt, H.–J., Hansma, P. K., 1992. Measuring adhesion, attraction, and repulsion between surfaces in liquids with an atomic-force microscope, *Phys. Rev. B, Condens. Matter,* **45**, (19), 1126-1132.

Weisenhorn, A.L., Hansma, P., 1989, Forces in atomic force microscopy in air and water, *Appl. Phys. Lett.,* **54**, (26), 2651-2653.

Yakubov, G.E., Vinogradova, O.I., Butt, H.J., 2000a. Contact angle of hydrophobic microparticles at water-air and water-hexadecane interfaces, *J. Adhesion Sci. Tech*., **14**, (14), 1783-1799.

Yakubov, G.E., Butt H.-J., Vinogradova O.I., 2000b. Interaction forces between hydrophobic surfaces. Attractive jump as an indication of formation of "stable" submicrocavities, *J. Phys. Chem. B*, **104**, 3407-3410.

Yoon, R.-H., 2000. The role of hydrodynamic and surface forces in bubble-particle interaction, *Int. J. Miner. Process.,* **58**, (1-4), 129-143.

Yoon, R.-H., Flinn., D.H., Rabinovich, Y.I., 1997., Hydrophobic interactions between Dissimilar Surfaces, *J. Coll. Interf. Sci.,* **185**, (2), 363-370.

Young, G.J., 1958. Interaction of Water Vapour with Silica Surfaces, *J. Colloid Sci.,* **13**, (1), 67-85.

Zettlemoyer, A.C., Hsing, H.H., 1977. Water on Organosilane-Treated Silica Surfaces, *J. Coll. Interf. Sci.,* **58**, (2), 263-274.

Zhuravlev, L. T., 2000. The surface chemistry of amorphous silica. Zhuravlev model, *Colloids and Surfaces A: Physicochemical and Engineering Aspects,* **173**, (1-3), 1-38.

Zhuravlev, L. T., 1993. Surface characterization of amorphous silica – a review of work from former USSR, *Colloids and Surfaces A: Physicochemical and Engineering Aspects,* **74**, (1), 71-90.

CHAPTER 3 INSTRUMENT DESIGN AND DEVELOPMENT

Men often become what they believe themselves to be. If I believe I cannot do something, it makes me incapable of doing it. But when I believe I can, then I acquire the ability to do it even if I didn't have it in the beginning.

Mohandas Gandhi

In this chapter a new instrument called **C**olloidal **I**nteraction **F**orce **M**easurement **A**pparatus (CIFMA) is described. It was specially designed and built for this thesis. The instrument was customized to meet the requirements of force measurement between particles and deformable surfaces.

The basic working principle is identical to the principle of AFM force measurements. A colloidal particle is glued to an AFM cantilever and moved towards a surface, bubble or droplet with the help of a high precision piezo-translator. When force acts on the particle, the cantilever is deflected, that is measured by light lever technique. The main differences relative to commercial AFM-s are that this instrument has:

(1) no scanning capability in xy-directions;
(2) extended, piezo-translator range;
(3) extended position-sensing detector size;
(4) large sample holder quvette holding over 50 ml of liquid;
(5) video imaging system with side view;
(6) advanced data archiving-retrieval software.

These improvements make the instrument suitable for measurements between colloidal particles and deformable surfaces such as air bubbles or oil droplets.

3.1 FUNCTIONAL SPECIFICATIONS

The functional specifications of the CIFMA were created after a preliminary study performed with commercial AFM and the instrument built by Butt (1994).

In case of measurements with deformable surfaces, the deformation of the bubble or drop at the moment of detachment can easily be as large as 30-50 μm (Figure 13) therefore a large piezo range is needed to facilitate the detachment.

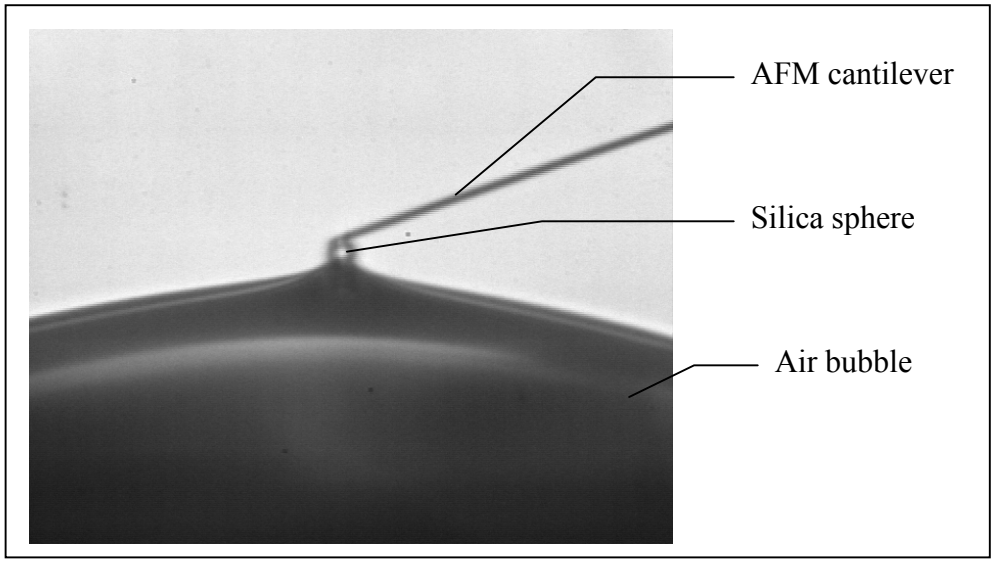

Figure 13 Video snapshot taken during the detachment process of the particle from an air bubble

In commercial AFM-s, the piezo-translator is usually located under the sample holder liquid cell that introduces a high risk of damaging the piezo-translator if the sample cell is leaking.

When measuring forces between particles and deformable surfaces, the deflection of the AFM cantilever is usually much larger than in normal AFM applications. The size of the conventional split photodiode is far to small to detect such large deflections. Therefore the position-sensing device should have a large size and large detection range in order to comply with the requirements of these measurements.

An open design for good side-view and easy accessibility for sample manipulation and cell cleaning, and possibility to accommodate additional sensors was very important. The facility to record the events with CCD camera were also of key importance. The bubble-size must be measured very precisely.

Previous experience with scientific instruments has shown that one of the most time consuming and complicated part of the work is the retrieval and manipulation of archive data. Taking into consideration that one experiment consists of several (usually 5-40), measurement series, and each measurement series contains 5-30 force curves, the number of curves to manipulate and interpret is rather large. One low-resolution curve contains more than 2000 points. All the relevant experimental conditions and the resulting force

curve data have to be stored for later analysis. Therefore an easy use of the data handling facility is essential.

Moreover, for higher flexibility it is desired to control from software all essential actuators and measurement devices.

3.2 DESIGN OF THE CIFMA

The CIFMA was designed by considering the guidelines described in chapter 3.1. The following chapter gives a detailed description of the hardware and software component implementation.

3.2.1 Hardware design

The structure of the CIFMA is presented in Figure 14. The layout follows the so-called stand-alone design, where the sample is in rest, while the cantilever is scanned with the help of a piezo-translator. The main components of the setup are the *head*, the *sample holder quvette* and the *optical- and video recording system*.

The *head* consists of three main parts: the piezo-translator, the laser and the position-sensing detector. The main design issue when planning the mechanical structure of the instrument was to create a stable, vibration free structure. Therefore, the measuring *head* was built on a commercially available dual stable rod system, which dampens the vibrations. The rod system also provides the rough translation in z-direction of the head, by a lead-screw driven platform. The lead-screw adjustment has 0.01 mm vertical resolution.

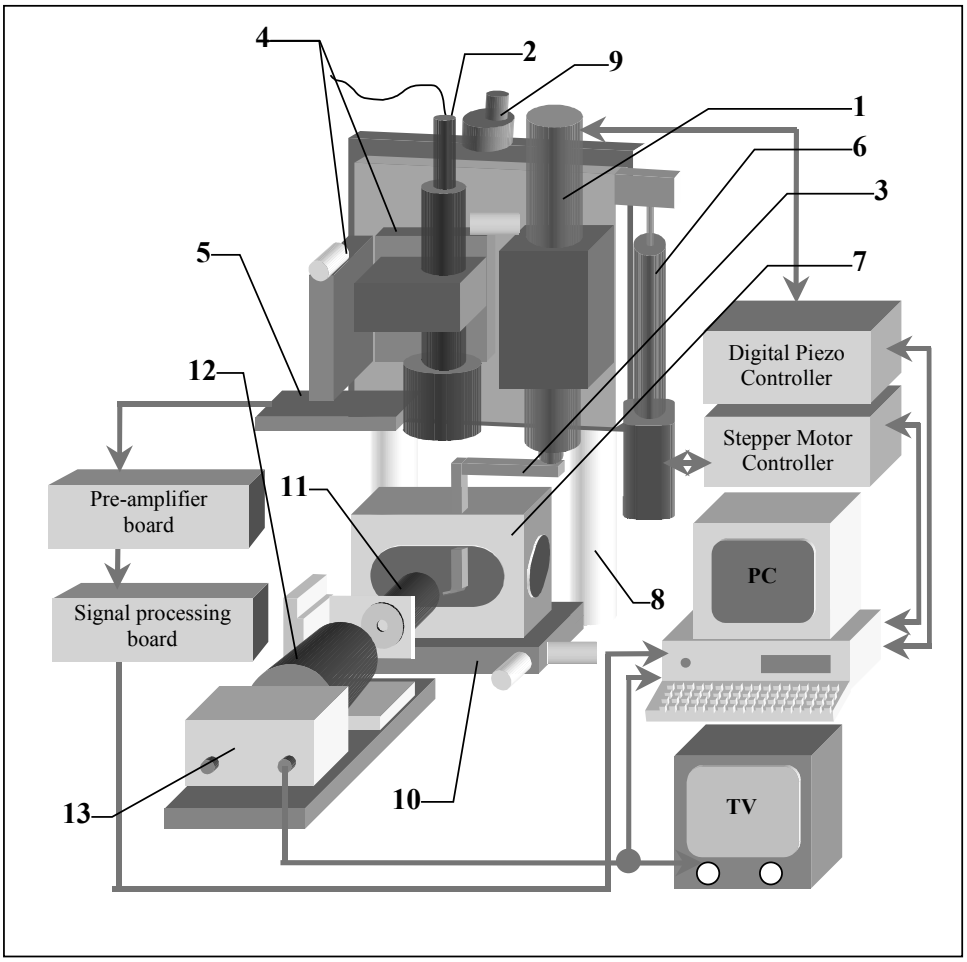

Figure 14 Schematic structure of the experimental setup for particle-bubble interaction measurements 1. Piezo-translator, 2. Laser diode with focusing optics, 3. Cantilever holder with AFM cantilever, 4. Translation stages for laser alignment, 5. Position Sensing Detector, 6. Stepper Motor, 7. Sample holder quvette, 8. Stable rod system, 9. Lead screw of the stable-rod system, 10. XY translation stage for sample positioning, 11. Long working distance microscope objective, 12. Photo lens, 13. CCD camera

The base plate of the head is mounted vertically on a *cross roller bearing one directional translation stage* equipped with a high-torque *actuator* (Nanomover, Melles Griot BV.). The actuator is needed for the second level of head positioning. It has a travel range of 25 mm (10 nm resolution and ±100 nm bi-directional repeatability) and electric position output. The actuator is used for positioning the particle couple of microns above the sample (bubble, drop, particle or flat surface) as well, as for measuring the size of the bubble/drop. The latter is determined by touching the end of the cantilever first to the bottom of the quvette, where the bubble is located, and reading the position of the actuator, then moving to the top of the bubble and reading the position again. The difference of the two readings gives the height of the bubble.

The *piezo-translator* (SDL Queensgate, DPT-C-L-A) providing the z-direction movement with a range of 75 μm is mounted on the base plate with a mounting bracket. It is placed upside-down, with the cantilever-holder attached to it. The cantilever is moved towards the solid surface, bubble or droplet placed onto the sample holder quvette. This construction eliminates the risk of damaging the piezo-translator by a leaking quvette. The position of the piezo-translator is measured by an internal capacity-sensor with picometer accuracy. The piezo-translator is controlled in closed-loop, which eliminates the hysteresis and creep of the piezo.

The digital controller (SDL Queensgate, NPS-3331-LN) is connected to a PC via parallel interface (National Instruments, PC-DIO-24), which provides a high-speed link, up to 4000 commands per second. The error-specifications of the piezo translator and control electronics are given in chapter 3.3.1.

The *cantilever-holder* is an L shaped block of PEAK plastic attached to the piezo-translator. The holder design enables easy detaching from the piezo-translator, necessary to change cantilevers. The cantilever is mounted on the end of the cantilever-holder with a flexible stainless steel clip.

The *diode laser* (Power Technology Inc., 670 nm, adjustable power, factory equipped with focusing optics, focal length: 45 mm) is mounted on xy-translation stage (installed using two one-dimensional translation stages placed perpendicular to each other). The laser beam is focused and pointed to the back of the cantilever. The laser beam is reflected into the position-sensing detector. If the measurements are operated in liquid, an optical window is attached to the cantilever-holder in order to minimize the refraction effects of the laser beam when passing through the air-liquid/liquid-air interfaces.

The *position-sensing detector (PSD)* (SiTek Electro Optics AB.) has an active area of 30 x 4 mm. It is mounted directly into the path of the reflected laser beam, without mirror, thus maximizing the intensity of the laser spot in the detector. The PSD indicates the position of the centroid of the laser spot reflected from the back of the cantilever as a current signal proportional to the position. The signal of the PSD is pre-amplified with a one-channel preamplifier board then forwarded to the computer through a *signal processing and data acquisition* board. The advantage of using a PSD instead of split

photodiod in addition to the large dynamic range is the sensitivity, which does not depend on the size and shape of the reflected spot.

The *sample holder quvette* is 80x40x55 mm large, made of Teflon and equipped in four sides with Plexiglas windows as can be seen in Figure 15.

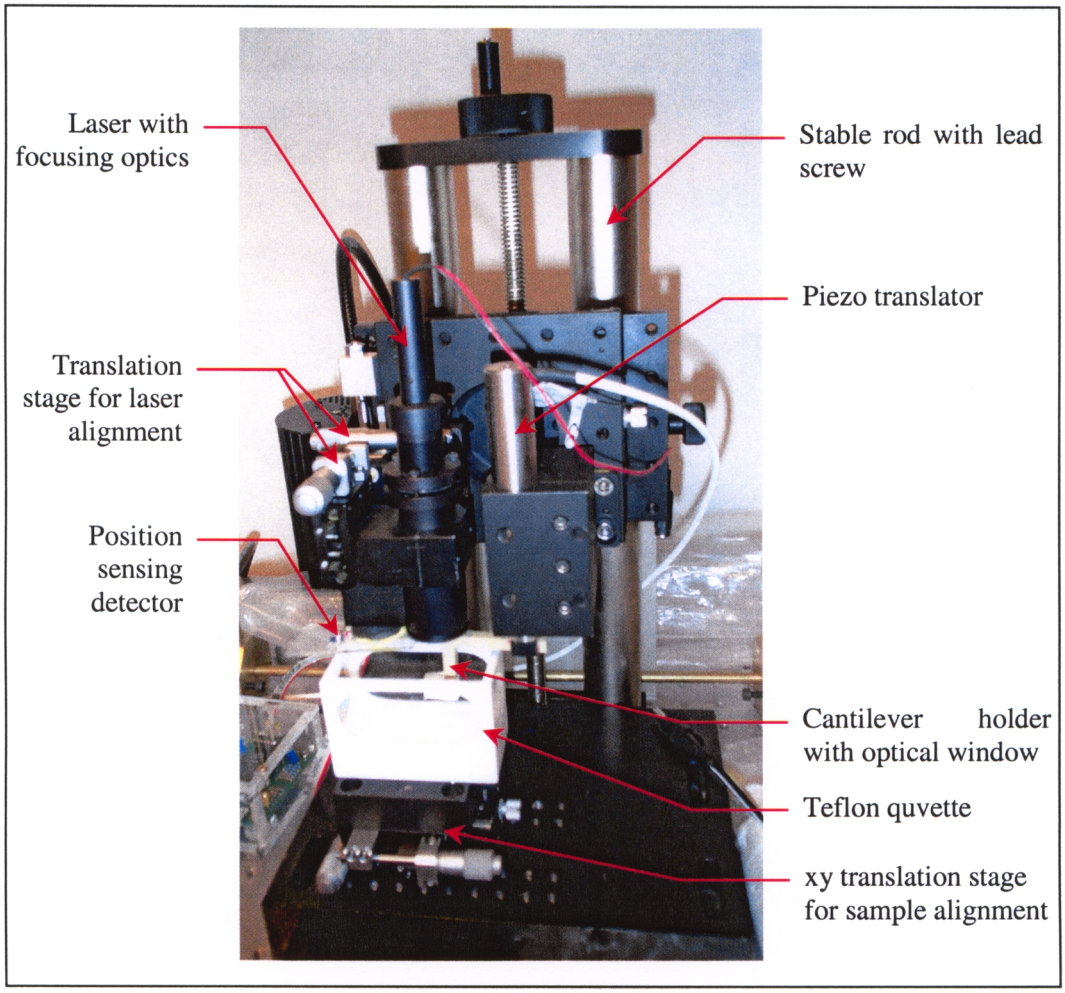

Figure 15 Photograph of the measuring head of the CIFMA and the sample holder quvette

Teflon was chosen as construction material because it is inert to most of the chemicals and can be cleaned in hot acid to prevent contamination. Teflon has very hydrophobic nature facilitating the placement and keeping of the bubble on the bottom of the quvette. The quvette is mounted to an xy-translation stage using a magnetic holder. The translation stage allows for precise positioning of the sample (air bubble, droplet, particle or solid surface) relative to the cantilever (having attached the particle) with a precision of 3 µm in a total range of 13 mm. The volume of the liquid used in the measurements is usually 40 ml, which is much higher than any AFM liquid cell could support. The large size of the

quvette offers the possibility to insert different sensors into the cell, such as pH- and E_h-electrodes, thermometers, etc. in order to record the exact experimental conditions.

An *optical system* (Figure 16) is used to position the particle over the bubble. The optical system is composed of: microscope objective with long working distance (20 mm), photo lens and CCD camera. The microscope objective is placed on a xyz-positioning stage in order to facilitate the focusing of the optics on the cantilever. The photo lens (Tokina 75-300 mm, f/4.5-5.6) is set to ∞ distance since the focusing is done by the microscope objective.

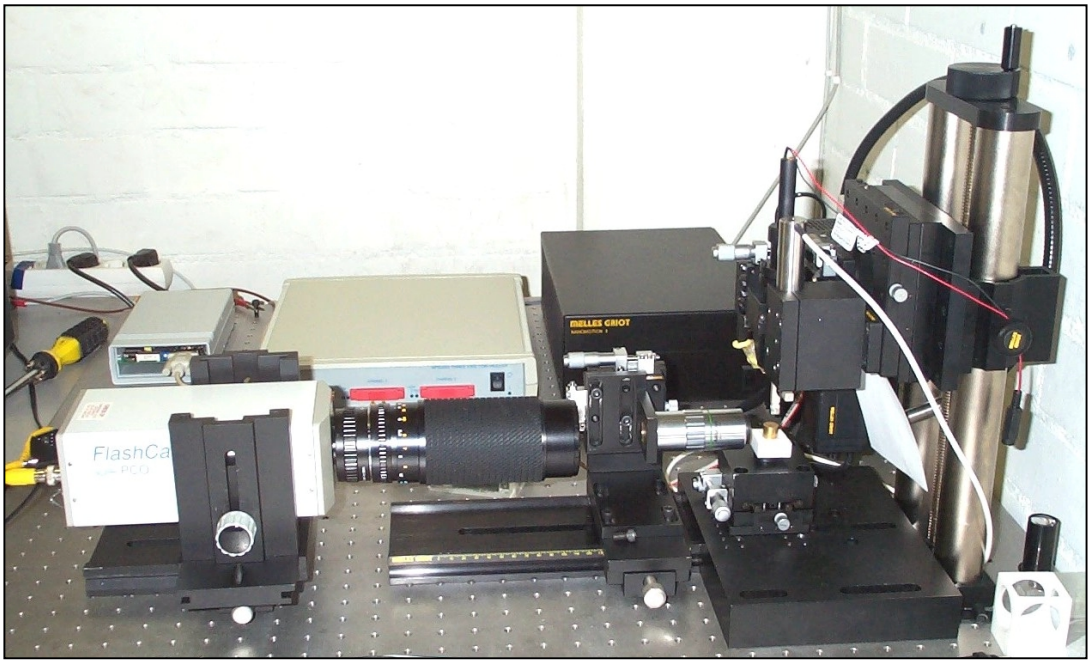

Figure 16 Side view of the CIFMA including the optical system

The zoom function of the photo lens allows the user to get a large and clear image of the cantilever with the glued particle. The illumination comes from the back by a collimated light source, through a white Plexiglas sheet, in order to get an even lighting. The photo lens is mounted on a CCD camera, which is connected to TV, video and computer in order to monitor and record the measurements to videotape and/or image files for further analysis.

The setup is placed on a high quality *vibration isolation table* in order to achieve a disturbance-free environment for the measurements.

Some experiments require a well-defined gas atmosphere. Therefore, the whole setup is placed into a *polyethylene glove bag*, which can be sealed and filled with gas (Figure 17). An internal frame holds the polyethylene glove bag. The cabling (to the controllers, computer, etc) is inserted through holes made in the glove bag and sealed with Teflon tape. The air is sucked out from the bag with a vacuum cleaner and filled with the required gas. With this arrangement, overpressure can be kept around the sample cell, and therefore the effect of dissolved gases in liquid solutions can be studied.

Figure 17 The experimental setup placed inside the polyethylene glove bag

3.2.2 Data acquisition and control software

The experimental system is managed from a PC, running on Pentium III 500 MHz processor, 256 MB RAM and Windows NT operating system. The pre-amplified and processed analogue signal from the PSD is connected to the data acquisition card (National Instruments PCI-6024E), which works with 12-bit resolution and maximum sampling rate of 200 kS/s. The communication between the digital piezo-controller and the PC is done through a digital IO card (National Instruments PC-DIO-24).

3.2.2.1 Relational database

One key issue in the software development work was to develop a comprehensive and independent database in order to promote the easy access to the measurement data. Data related to experimental conditions are stored together with every force curve data. Because

of the variable length and large amount of data within a force curve, these are stored in separate files. The location and name of these files obviously are set in the database. A relational database management system (Microsoft Access) was used, that is accessed through ODBC (Open Database Connectivity) mechanism with the help of LabView SQL Toolkit. The ODBC connection allows us to move the database in future to any other computer platform and database system, if needed.

The main idea was to structure systematically the information about the measurement parameters and conditions. The highest unit of the structure is the *'Experiment'*. The unique parameter that defines this unit is the particle glued to AFM cantilever and stored in a well-defined place. If the cantilever with the glued particle is changed, a new *'Experiment'* is started. The second unit is the *'Measurement'*. If an experimental parameter e.g. reagent concentration, bubble, etc. is changed, a new *'Measurement'* is started. Each *'Experiment'* consists of several (usually 5-40) 'Measurements'. In every *'Measurement'* usually 5-30 force curves are recorded. The data structuring system is illustrated in Figure 18.

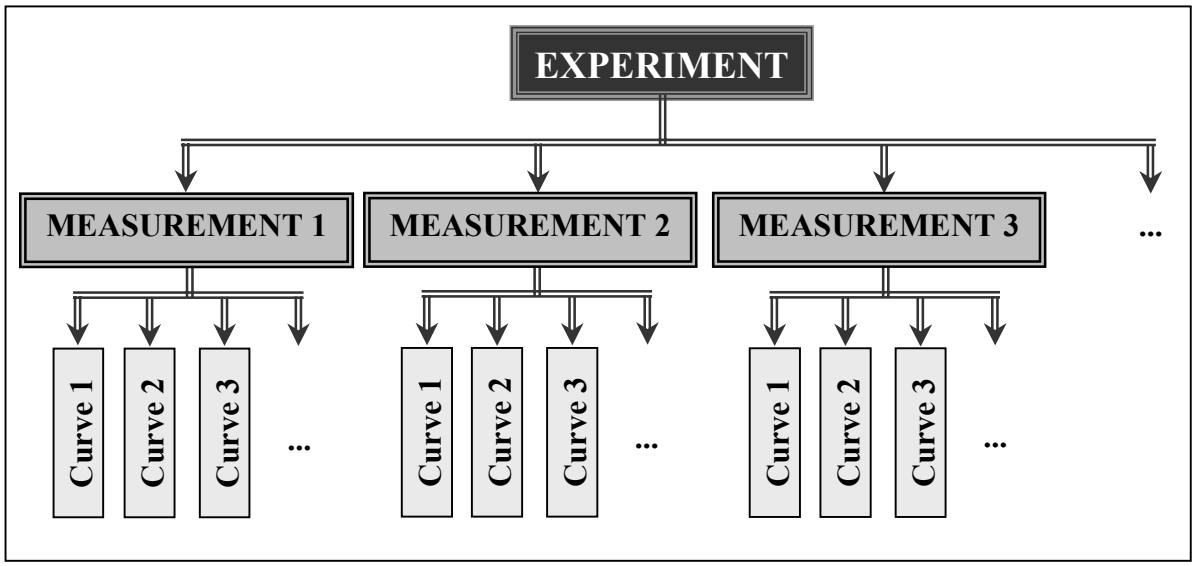

Figure 18 Data structuring system

The database consists of 11 tables and each table contains 2-12 fields. The relational model is presented on Figure 19.

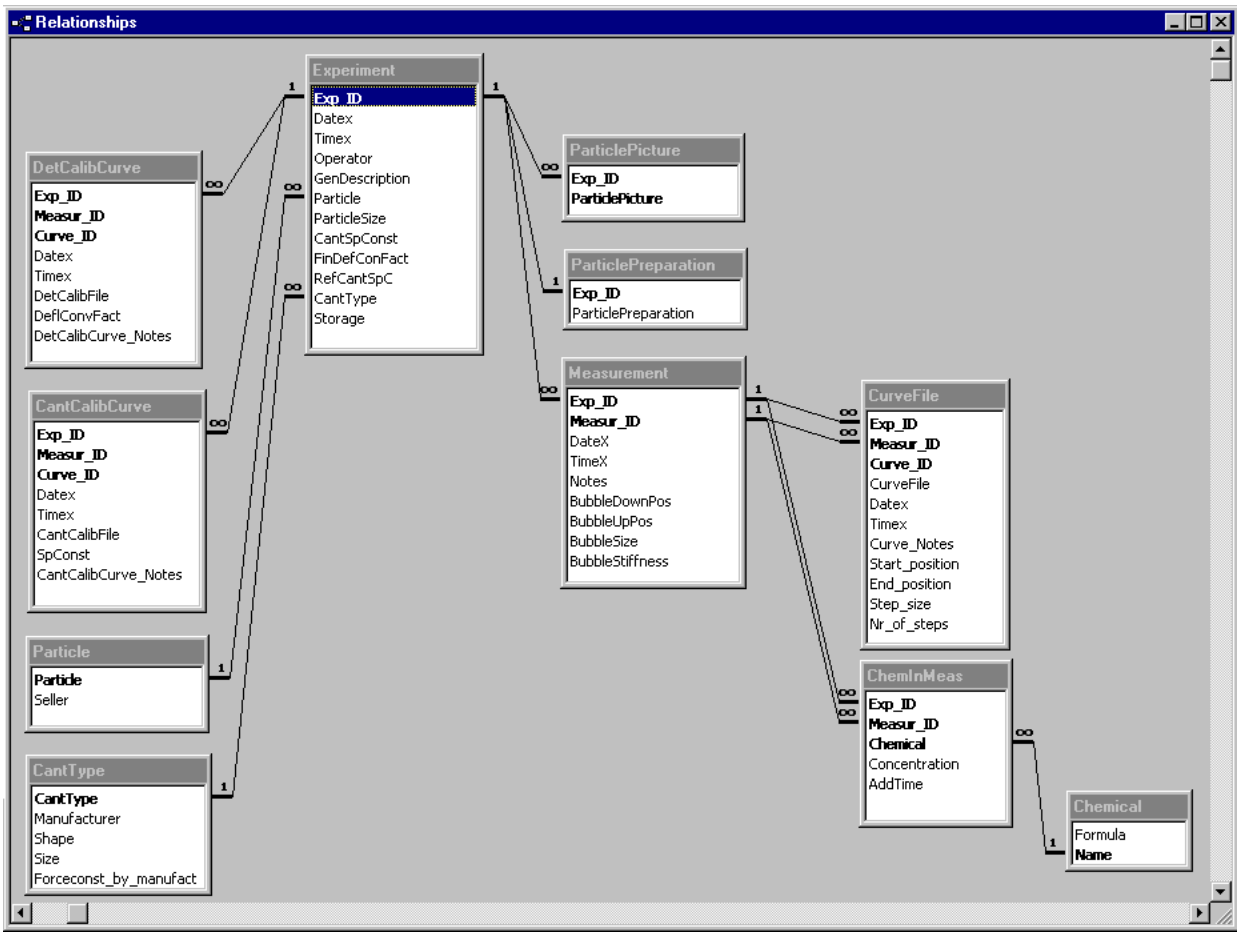

Figure 19 Relational model of the database

3.2.2.2 Application software

The application software was written with LabView (National Instruments), a 4th generation graphical programming tool. LabView was chosen because it is relatively easy to learn and building the graphical user interface is easy having at reach a large library of ready-made components. The architecture of the software is shown in Figure 20.

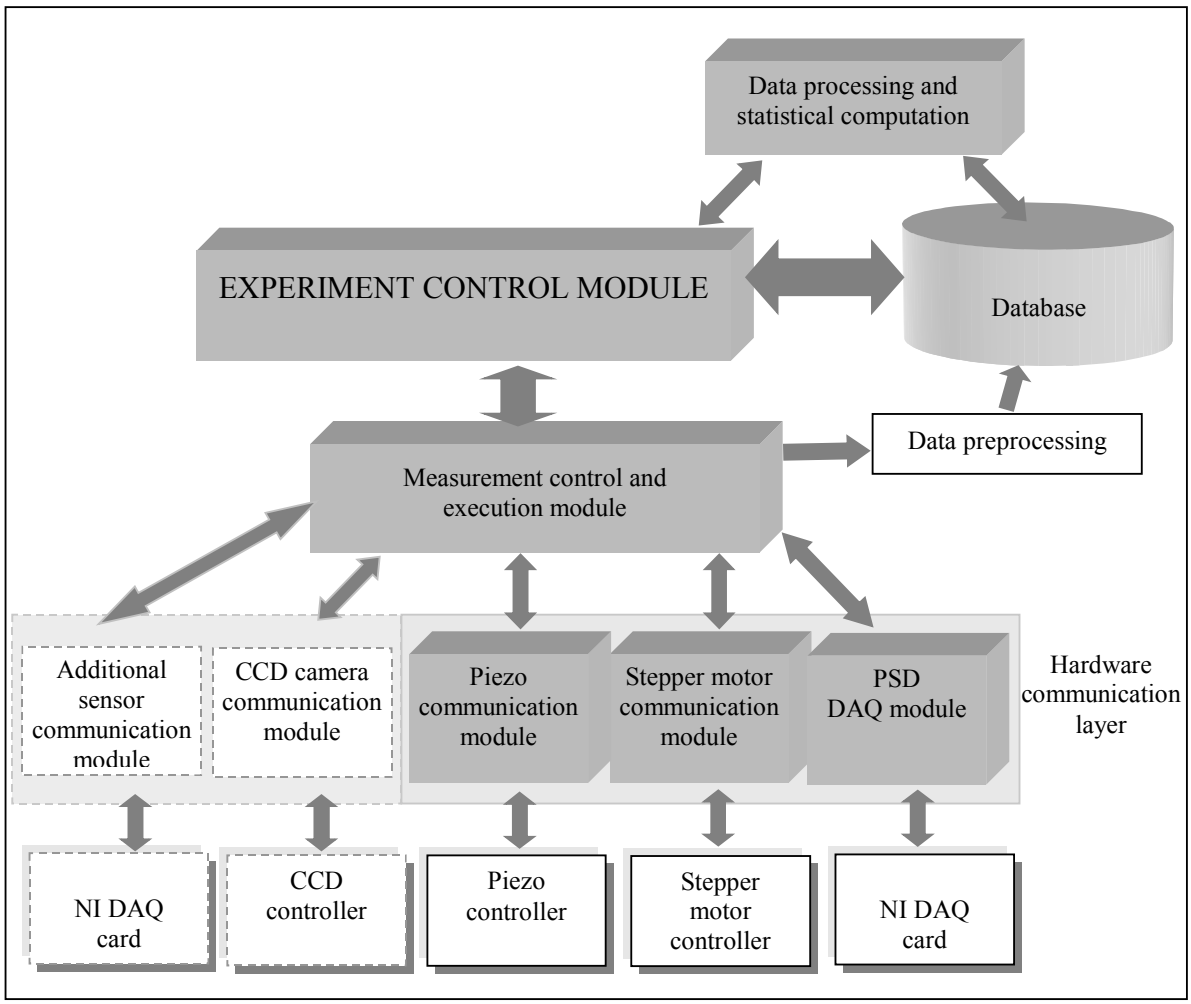

Figure 20 Schematic figure of the software architecture

The software system consists of two main parts: on-line command and data acquisition and off-line data processing and analysis.

The *on-line command and data acquisition* modules control and supervise the instrument during the measurements. The experimental conditions, such as date and time, general description, particle information, cantilever information, SEM pictures of particles, used chemicals, etc. are stored together with every force curve data in the database.

The force curves are processed by the *off-line data processing and analysis* modules. PSD voltage vs. piezo-translator position raw data is converted into the force vs. piezo-translator position curves as described in chapter 2.3.3.1. The normalizing process of the force curves will be described in chapter 5.3.3.

3.2.2.3 Graphical User Interface (GUI)

The relation between user interface panels is presented in Figure 21. The '*Main control panel'* of the software, the '*Data acquisition panel'* and the control window of the z-direction high-torque actuator ('*Nanomover control'*) is shown in Figure 22. The following user interface panels can be launched from the '*Main control panel'*:

(1) New Experiment Info panel;
(2) New measurement info panel;
(3) Data acquisition panel;
(4) Nanomover control panel;
(5) Database access panel.

Information concerning the experimental procedure and conditions is entered into the '*New Experiment Info'* and '*New measurement info'* panels and finally is saved to the database. The most important experimental information records are automatically passed to the data acquisition application and displayed in the '*Data acquisition panel'*. The piezo translator and data acquisition is controlled through this panel. Basic parameters for the measurement (piezo translator start- and end position, step size, scan rate and number and type of curves to acquire) can be set from here. If the experiment requires retention of the particle in contact with the sample (bubble or droplet), at a given load, the required parameters (time in contact, piezo position at contact) can also be set. The force curves appear on-line on the data graph as well as the PSD signal vs. time curve. The file name for each force curve is created automatically as a combination of the experiment, measurement and curve ID, and it is stored in the database.

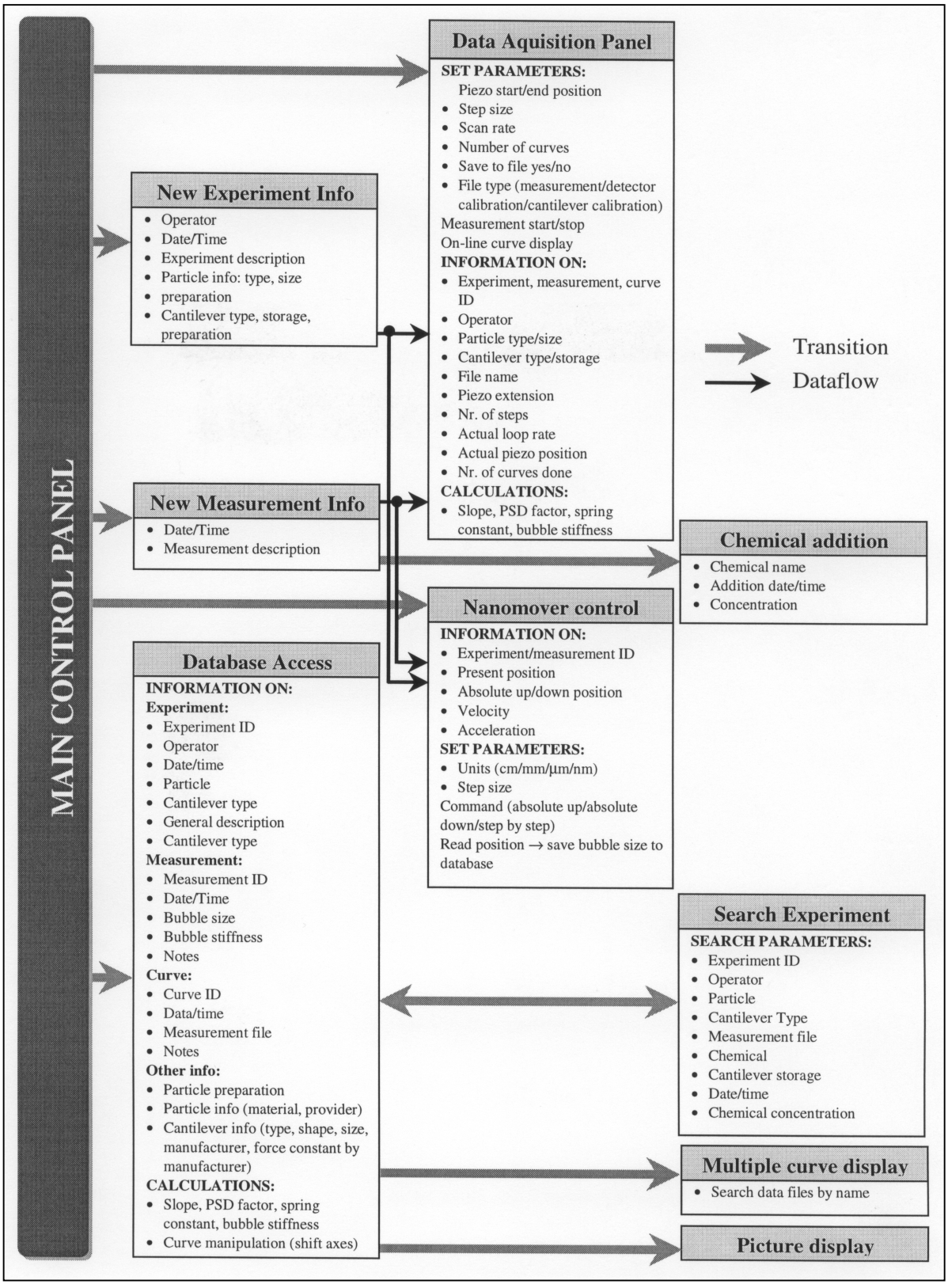

Figure 21 Relation of panels in the graphical user interface

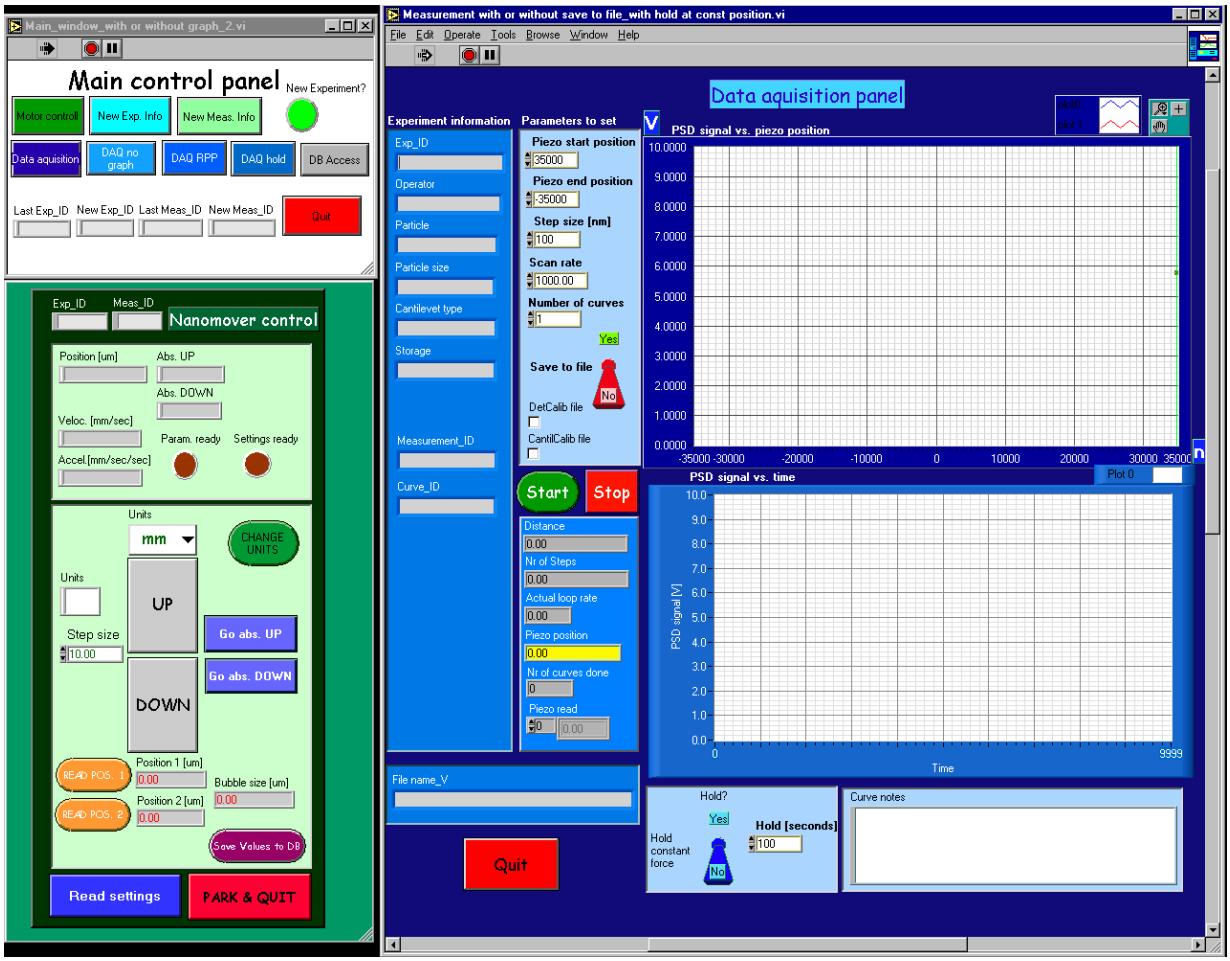

Figure 22 The 'Main control panel' of the software, the 'Data acquisition' panel and the 'Nanomover control' panel

The high torque actuator is controlled from the '*Nanomover control panel'*. The window allows velocity and acceleration setting for the actuator. The step size can be specified in cm, mm, μm or nm and the exact position of the stepper-motor can be read. This feature facilitates the measurement of the bubble size and its value can be stored in the database for every measurement.

The '*Database access'* panel shown on Figure 23 is the front panel of the *off-line data processing and analysis module.* The retrieval of archive data about any measurement stored in the database and the off line processing and statistical analysis of the measurement data can be initiated from this panel.

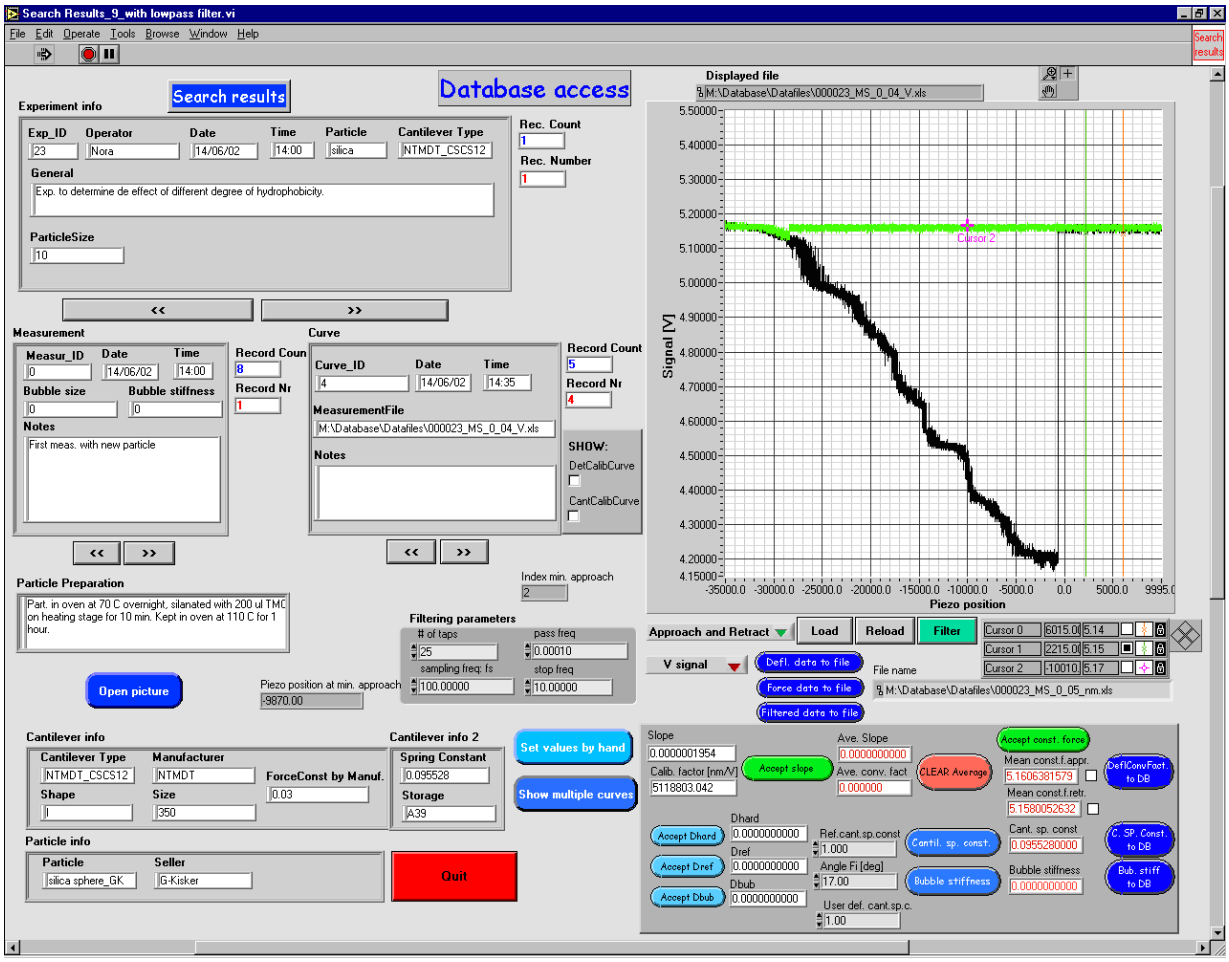

Figure 23 'Database Access' panel

The database query is built automatically from the parameters chosen in the *'Search experiment'* panel (Figure 24). The query results are displayed in the '*Database access'* panel. The number of records found is displayed and the arrow buttons facilitate the viewing of the records. The off-line processing of the data is carried out from this panel. Basic measurements and calculations such as PSD factor and cantilever spring constant and bubble stiffness determination can be performed from the '*Data acquisition panel'*.

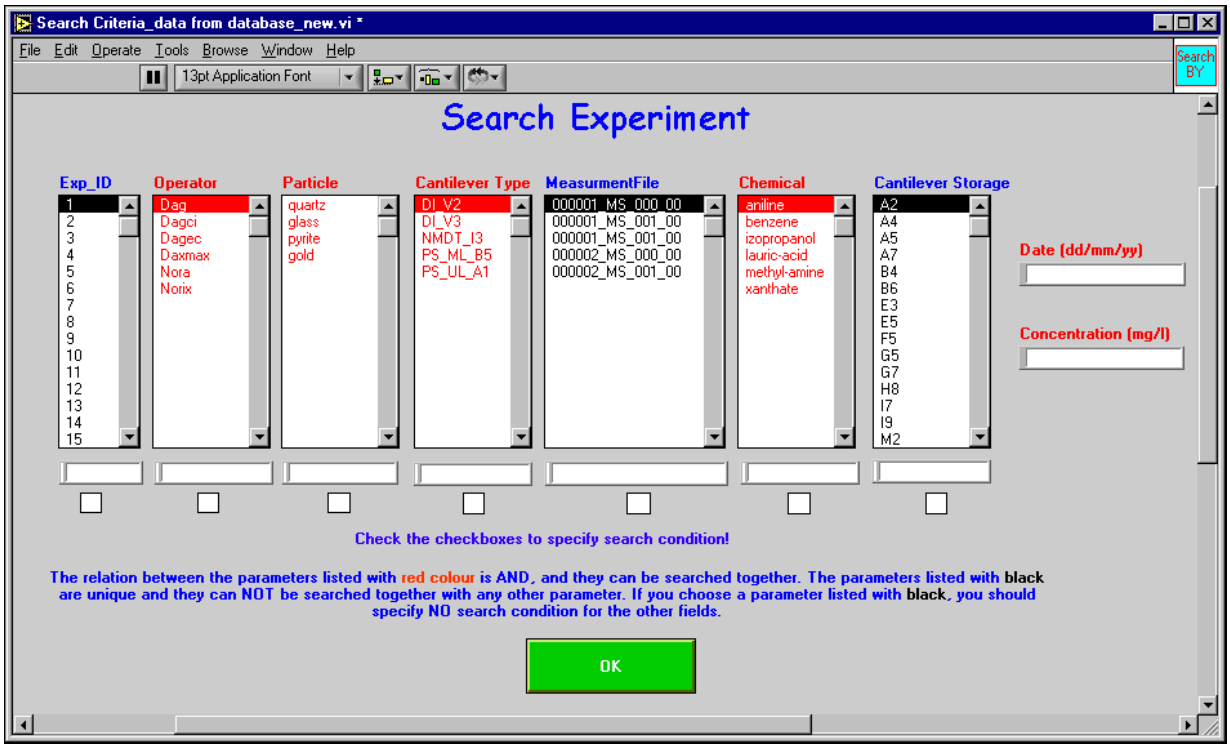

Figure 24 The 'Search Experiment' panel of the software

For easier comparison of experimental results, multiple curves can be displayed in *'Multiple curve display'* panel.

If SEM pictures of the particles glued to cantilevers are available, these pictures can be viewed by opening them directly form the *'Database Access'* panel.

3.3 ERROR DETERMINATION

In the measurements conducted using CIFMA two main types of errors are possible: systematic errors and random errors. This chapter examines the reasons and scale of these errors in order to minimize them during the measurements. When designing the CIFMA one of the most important issues were to minimize the possible of errors. The reproducibility and the artefacts encountered in the measurements are also reviewed.

3.3.1 Systematic errors

Systematic errors during the measurements occur due to the error of the CIFMA's hardware components. These errors are specified and quantified by the manufacturer of each component.

Piezo translator and control electronics

The main error source of the piezo translators is due to the hysteresis, creep and non-linearity of the piezo crystal. However in the CIFMA this effect is eliminated with the use of a piezo translator equipped with internal capacitance position sensor and a closed loop digital controller. The controlled piezo-translator system has the following performances (measured by the manufacturer for every system):

- 0.01 %, linearity error over the full motion range
- 0.03 % peak-to-peak hysteresis

The controller has a 21-bit resolution to provide positioning noise better than 1 part in $2x10^6$ (equivalent to 0.05 nm in 100 μm), PID feedback and linearity error better than 0.02 %. (SDL QUEENSGATE, 2000). A plot of the piezo command position vs. the real piezo position measured by the internal capacitance position sensor of the piezo translator is shown on Figure 25.

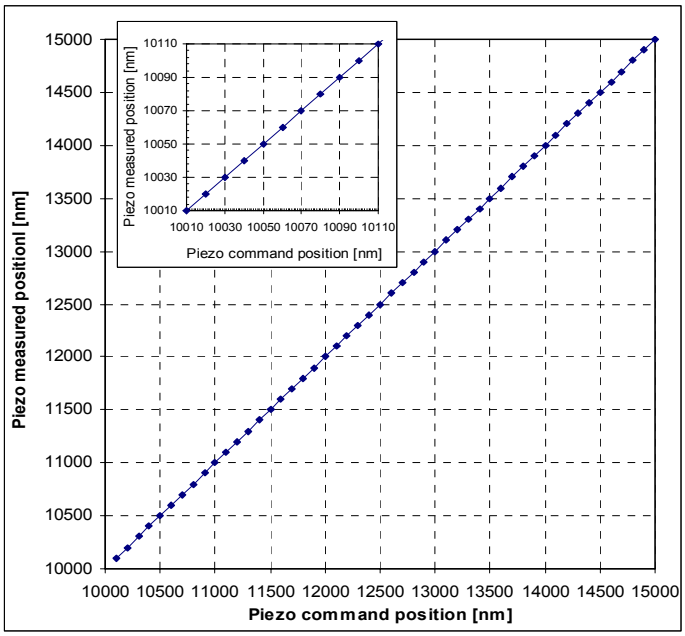

Figure 25 Plot of piezo command position vs. measured piezo position when the piezo moves in 100 nm steps. The inset shows the same plot, but then the piezo moves with 10 nm steps

Although the piezo response is linear, the internal capacitance sensor has a noise level in the 5 kHz bandwidth, which is many times higher than the actual, 0.27 nm motion noise of the translator. Therefore to further increase the accuracy of the measurements, the piezo command position values are used to plot the force vs. piezo position curves. This method

is appropriate only in the case when the piezo step size is around 100 nm or lower, and the response time of the piezo translator is negligible.

PSD and connected electronic boards

The PSD has a specified resolution better than one part in one million and a position non-linearity of ±0.1 %. The connected electronic signal processing board has a full-scale inaccuracy of ±0.5 % (SITEK, 1996).

3.3.2 Random errors and error minimization procedures

The random errors during the measurements with CIFMA occur due to external effects. These effects can be categorised in four large groups:

(1) Cantilever induced errors
(2) Environment induced errors
(3) Instrument induced errors
(4) Human factor

3.3.2.1 Cantilever induced errors

RADMACHER ET AL. (1995) have shown, that cantilevers tend to bend due to ambient temperature changes and due to laser heating. The displacement of the silicon nitride cantilevers due to temperature change can be in the order of several hundred nanometers. However most of the experiments with CIFMA are performed in liquid environment in a relatively large sample holder cell, with a minimum liquid volume of 40 ml. Therefore it is likely that the bending effect is not as significant as for measurements performed in air, due to the high specific heat of the liquid.

The largest source of error (up to 45 %) in the force measurements is likely due to the change of the cantilever spring constant over time. There are only a few publications referring to these issues, and in most of the cases this effect is overlooked. For determining the error caused by this cantilever instability, a detailed study on the spring constant of the measurement cantilevers was done and will be discussed in the experimental Chapter 6. A method to minimize the errors occurring due to this effect will also be presented.

3.3.2.2 Environment induced errors

The sources of environment-induced errors in the force measurements are mechanical and acoustic vibrations and electric noise.

In order to enhance the resolution of the instrument, the random noise level of the different components has to be minimized. The environmental vibrations that could affect the experiment vary between 10 to 200 Hz, depending on their origin. They can be due to acoustic effects (>20 Hz), street traffic (5-100 Hz), construction and machinery (10-200 Hz). These vibrations are avoided by placing the CIFMA on a high performance vibration isolation table which provides a virtually vibration free environment.

Electric noise is also a source of error in measurements. As the components of the CIFMA are supplied with DC current, this effect is not very significant. In order to reduce any residual noise due to electrical interference the different components were connected to each other with shielded cables.

3.3.2.3 Instrument component induced errors

Thermal drift might also be a source of random error in the measurements. As an example, the piezo controller alone could produce a thermal drift of 140 $nm°C^{-1}$, while the piezo translator 35 nm C^{-1}. As an example, a 3 °C change in the temperature would cause 525 nm drift on a 70 μm translation distance, which means a 0.75 % error. By performing the measurement at a constant temperature this effect can be eliminated.

During the measurements care has to be taken to avoid errors resulting from the warm up drift of the different components. By rigorously keeping the warm up time specified by the component manufacturer (after switching on the instrument), the error is negligible.

3.3.2.4 Human factor

The operator performing the data analysis may introduce error into measurements in the force curve processing stage, when the piezo position at contact point or the point where the repulsive term begins to contribute to the interaction force has to be determined. This mainly happens because the determination of the contact point between the particle and the surface is difficult especially in the repulsive case, as there is no discrete point or sudden

change in the force curve, only a change in the curvature of the graph. The magnitude of the error introduced at this stage depends on the resolution of the force curve. At a high-resolution (small step size) of force curve, the error is within couple of nm-s limit, while if the curve is recorded with a low resolution (high step size), the error can be in the range of 20-50 nm.

3.3.3 Reproducibility, repeatability

The estimation of the reproducibility of the results is quite difficult as there are no other instruments available with which the results could be duplicated.

It was observed, that the repeatability of the measurements was highly influenced by the sample preparation procedure and the measurement procedure itself. The sample preparation procedure adapted in the experiments is quite complex and therefore great care was taken when this procedure was followed.

The measurement itself is also influenced by several factors that have to be taken into consideration in order to obtain comparable and repeatable results. Comparable results can only be obtained if the measurement parameters e.g. approach velocity, load, contact time, etc. are nearly identical.

3.4 ARTEFACTS IN FORCE-DISTANCE MEASUREMENTS

Although the first force curves obtained using AFM were recorded more than 10 years ago, a number of features of these curves are not yet understood.

The most common artefacts in the AFM measurements arise from the piezo hysteresis and creep, which are characteristic for every piezo crystal. As the piezo actuator built into the CIFMA contains a capacitance sensor, and the actuator is connected to a closed loop piezo controller, these two most common artefacts are avoided. Other observed artefacts are discussed below.

Loading/unloading hysteresis

One very common feature is the hysteresis between loading and unloading (approach and retraction) parts of the force curves at high scan rates (Figure 26)

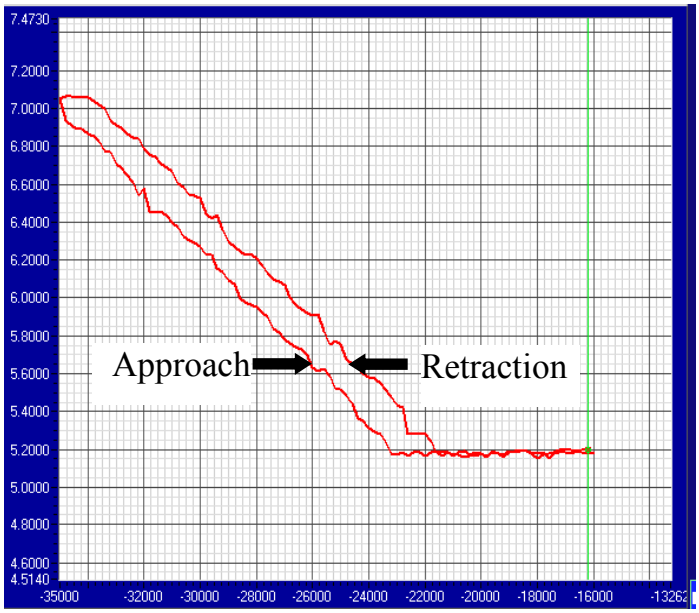

Figure 26 Force curve recorded at high scanning speed

HOH AND ENGEL (1993) have also described this artefact. They proposed that this phenomenon is caused by the friction between the tip and the sample, which makes the cantilever bow forward after the tip makes contact with the surfaces resulting in an offset in the contact line.

This theory was thoroughly studied using CIFMA. The basic idea of the study was, that if the laser is focused on the very end of the cantilever, the hysteresis due to the cantilever bow should be larger, than in the case when the laser spot is more towards the chip body (Figure 27).

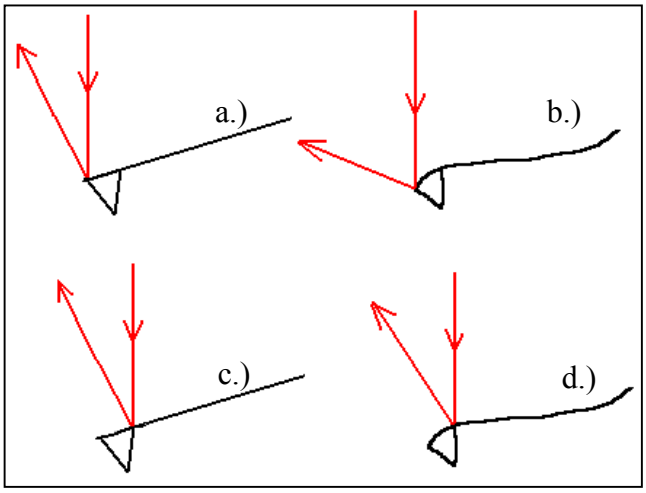

Figure 27 Basic idea of testing the reasons for loading/unloading hysteresis

With the help of the optical system, the laser spot was focused on two different parts of the cantilever. The interaction between the tip and the sample was also followed with the optical microscope and the measurements were recorded in .avi files. The results revealed that the hysteresis was not dependent on the location of the spot on the back of the cantilever therefore the cause of the hysteresis is most probably not the bow of the cantilever.

Steps in the zero-line

Steps in the zero-line can be often observed as shown on Figure 28.

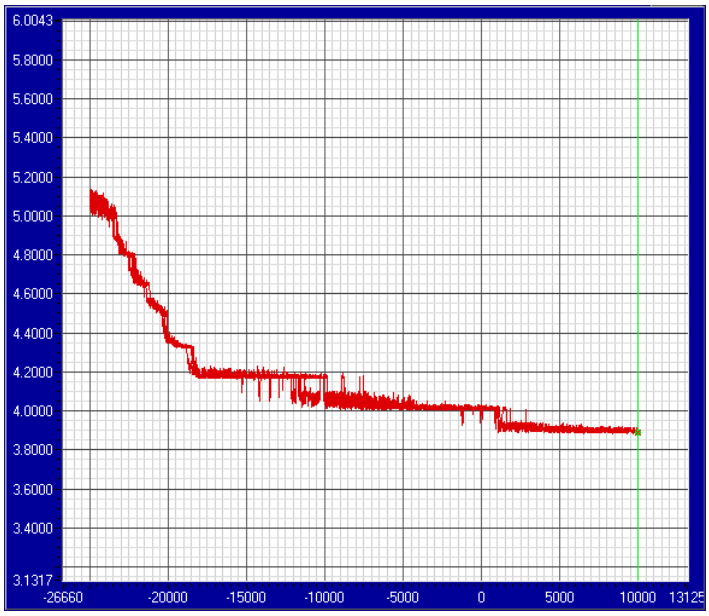

Figure 28 Graph showing steps in zero line

This artefact is most probably caused by improper focusing of the laser beam on the back of the cantilever, which is then reflected into the PSD. The improper focusing causes a change in the intensity of the laser spot reflected into the PSD.

The artefact can be eliminated, by proper focusing of the laser beam on the back of the cantilever.

Zero-force line hysteresis

Figure 29 shows a graph of the zero-force line hysteresis.

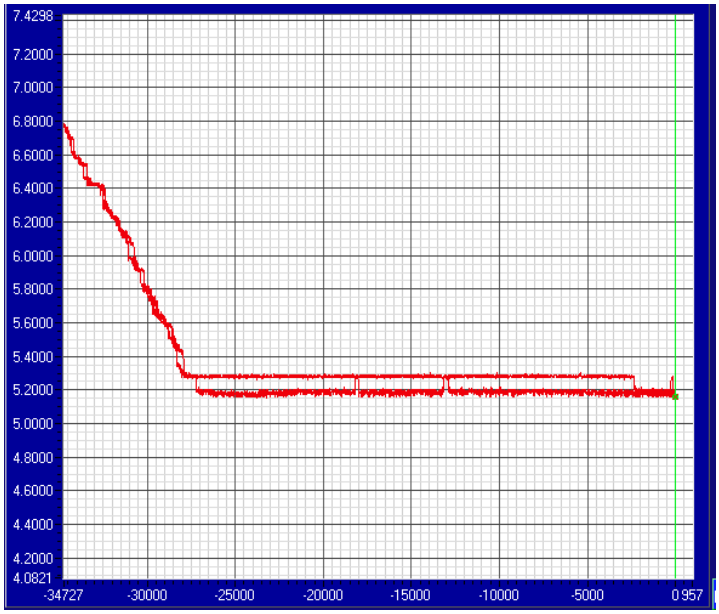

Figure 29 Graph showing the hysteresis of the zero force line

This artefact is often present when particle-bubble interaction forces are measured. The origin of the artefact is not yet clear, but proper alignment of the laser beam to the back of the cantilever eliminates it in most cases.

3.5 EVALUATION OF CIFMA

CIFMA has proved to be a flexible and powerful tool in the particle-bubble interaction studies.

The resolution of the instrument is in the pN range, depending on the spring constant of the cantilever that is rather high relative to the nominal force values in 5-500 mN range. The high resolution is combined with a large measurement range provided by the 75 µm

movement range of the piezo translator and the large surface area of the PSD. This way, weak long-range forces, and strong forces (e.g. adhesion) can be detected without saturation of the PSD signal (e.g. no interpolation is needed to obtain the adhesion force data, as it is usual with commercial instruments).

Another very important feature of CIFMA is its high flexibility to make modifications of the hardware and/or software components depending on the specific experimental needs. This issue has proved to be very important during the experimental work.

The open design gave a good access to the large sample holder quvette. The optical and video imaging system facilitated the observation of so far undetected phenomena in the particle-bubble interaction measurements. These observations will be discussed in the experimental chapter.

CIFMA opened the possibility to study adhesion forces between particles and air bubbles, which was not possible before due to the lack of a suitable experimental technique.

The database implemented as part of the instrument control and data acquisition software promoted easy archive data retrieval that turned out to be useful in analysis and synthesis involving large amount of data from several measurements.

The limitations encountered during the experimental work were not due to the experimental setup itself, they were rather due to the principle of force measurement technique. The main limitation results from the deformation of the bubble or drop surface that cannot be detected. There is a need for an independent mean to measure surface deformation. This kind of addition to CIFMA or commercial instruments would help clarify remaining questions of the surface chemistry.

As a summary it can be concluded, that CIFMA lived up to the expectations.

References chapter 3

Butt, H.-J., 1994. A Technique for Measuring the Force between a Colloidal Particle in Water and a Bubble, *J. Colloid Interface Sci*., **166,** (1), 109-117.

Radmacher, M., Cleveland, J.P., Hansma, P.K., 1995. Improvement of Thermally Induced Bending of Cantilevers Used for Atomic Force Microscopy, *Scanning*, **17**, 117-121.

SDL Queensgate Ltd., 2000. Test results for NPS3331-LN-PAR-B serial number 702015, DPT-C-L-A serial number 2645, system specification booklet of the piezo translator system.

SiTek Electro Optics AB, 1996. PM-Kit User's Manual.

Tortonese, M., 1997. Cantilevers and Tips for Atomic Force Microscopy, *IEEE Engineering in Medicine and Biology,* **16**, (2), 28-33.

CHAPTER 4 HYPOTHESIS AND AIM OF EXPERIMENTS

A fact is a simple statement that everyone believes. It is innocent, unless found guilty. A hypothesis is a novel suggestion that no one wants to believe. It is guilty, until found effective.

Edward Teller

4.1 CANTILEVER STABILITY STUDY

The hypothesis was assumed that the cantilever spring constant is not constant over an extended period of time. The hypothesis was based on personal experience and discussions with PREUSS AND ECKE (1999).

Therefore it was decided to determine the possible variation of the cantilever spring constant over time and to determine an experimental procedure that could be utilized to minimize the errors resulting from such variations.

4.2 CONTACT ANGLE MEASUREMENTS AND AFM IMAGING

The aim of the contact angle measurements was to determine the wettability after hydrophobizing the silica plates and particles used later in the particle-bubble interaction studies. For a better understanding of the particle-bubble interactions the surfaces used in the experiments were also imaged with AFM to determine their roughness.

4.3 PARTICLE-BUBBLE INTERACTION STUDY

The hypothesis put forward in the particle-bubble interaction experiments was that long-range non-DLVO surface force acts between particles and bubbles, with the hydrophobic force being likely the most important one. The origin of the force is still unknown, as discussed in chapter 2.1.1.2.1.

The aim of the experiments was to provide additional data to shed new light on particle-bubble interactions. The research was focused on ultrapure, electrolyte containing and gas

saturated aqueous systems. In addition, the effects of approach velocity, applied load and contact time on the particle-bubble adhesion were aimed to be studied.

References chapter 4

Preuss, M., Ecke, S., 1999. Personal communication.

CHAPTER 5 MATERIALS AND METHODS

All things are difficult before they are easy.

Thomas Fuller

5.1 CANTILEVER STABILITY STUDIES

The cantilever calibration procedure was based on the method suggested by TORTONESE AND KIRK (1997) described in chapter 2.3.4.

The reference cantilevers were purchased from Veeco Instruments Inc. Four reference cantilevers were mounted on a specially designed stage shown on Figure 30.

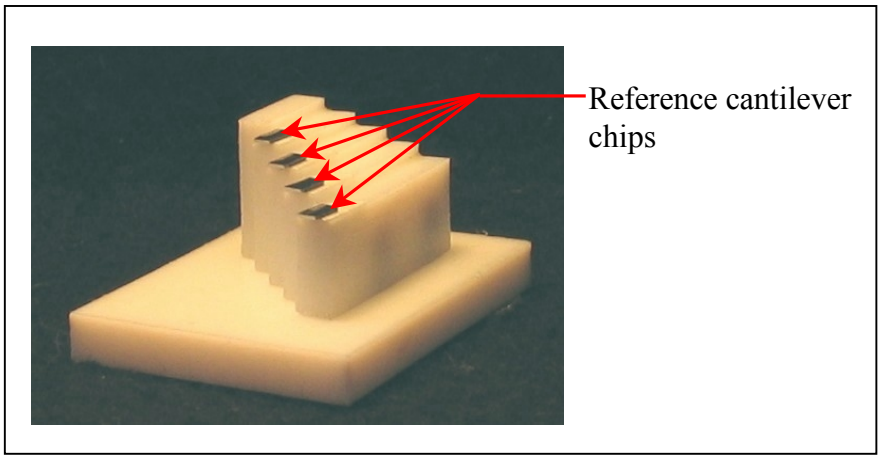

Figure 30 Reference cantilever and bubble holder

The cantilevers tested in the cantilever stability study were calibrated against each of the references 4 to 5 times.

5.2 CONTACT ANGLE MEASUREMENTS AND AFM STUDIES

The contact angles on heat-treated and silylated silica particles were determined using the microsphere tensiometric method, as described by PREUSS AND BUTT (1998). The contact angles were also measured on fused silica plates used as control substrates with captive drop method. Advancing and receding contact angles were measured using Cam 200 Optical Surface Tension/Contact Angle meter (KSV Instruments ltd.).

The contact mode AFM imaging was carried out using Autoprope CP (Park Scientific Instruments) atomic force microscope. Topography images were taken on the silica plates and the particles used in the force measurements to determine their surface roughness.

5.3 PARTICLE-BUBBLE INTERACTION STUDIES

5.3.1 Samples, reagents and sample preparation procedures

Fused silica spheres (10, 15 and 20 μm in size) from G.Kisker GbR. and fused silica plates supplied by Finnish Specialglass Oy were used as substrates. The silica spheres were utilized to prepare colloid probes for the force measurements, while the silica plates were used to determine the contact angle under different sample preparation techniques.

All the reagents used in sample preparation and measurements were of analytical grade and were used without further purification. The water used in the measurement was ultra high purity water, cleaned in five-steps: mechanical removal of the solid particles, ion exchange, active carbon treatment, reverse osmosis and reversed bed ion exchange. The resistance of the water was higher than 18 MΩcm, and the pH was 5.4±0.2. In some experiments the water was saturated with CO_2 or Ar. The pH of the CO_2 saturated water was pH 4.1. Ar did not change the pH of the water (5.4±0.2). The preparation of the gas-saturated solutions will be described in chapter 5.3.1.2.4

The bubbles were created with the use of a micropipette on the bottom of a Teflon quvette. Laboratory air, Ar or CO_2 were utilized in different experiments. The bubbles were stable for several days. The bubble height, measured from the substrate surface, varied between 650-950 μm.

In the experiments only surfactant free systems were used. Because of the uncertainty with regard to the behaviour of surfactant molecules adsorbed on bubble surface when a solid particle approaches the bubble surface, it was decided to utilize surfactant-free systems only. Such uncertain behaviour could lead to interpretational difficulties. The other uncertainty would arise from the patch-like adsorption of surfactant molecules at silica surfaces, which would also make the interpretation of the results difficult. Therefore the surface hydrophobicity of the particles was only modified by silylation, as described in chapter 5.3.1.2.

The measurement cantilevers used for preparation of the colloidal probes were purchased from MikroMasch.

5.3.1.1 Preparation of the colloidal probe

A tipless AFM cantilever with the desired spring constant was selected from the chip. Usually there are two or three cantilevers on each side of the chip, but only one can be used in the force measurements. The other cantilevers were removed from the chip by breaking them with an ultra-thin copper wire. The ultra-thin copper wire was prepared by partially dissolving normal copper wire in a mixture of sulphuric and nitric acid. The silica particles were heat treated at different temperatures (see chapter 5.3.1.2.2). After heating, the particles were spread on a microscope cover glass. Very small droplets of epoxy glue (5 Minute Super Epoxy, OCI Professional) were placed on the microscope cover glass by using the ultra-thin copper wire. The cover glass was attached to a Park Scientific Instruments Autoprobe CP AFM sample stage. A tipless AFM cantilever was placed into the standard cantilever holder of the instrument. With the help of the CP optical microscope a suitable particle was chosen from the microscope cover glass. Using the AFM's XY translation stage as a micromanipulator, the cantilever was positioned over the small glue droplet and dipped into the glue. Then, the cantilever was pressed against the microscope cover glass to reduce the size of the glue droplet roughly to the diameter of the particle to be attached. The chosen particle was then picked up with the glued end of the cantilever and allowed to dry until firmly set (Figure 31). With this method 2-20 μm particles can easily be glued to cantilevers.

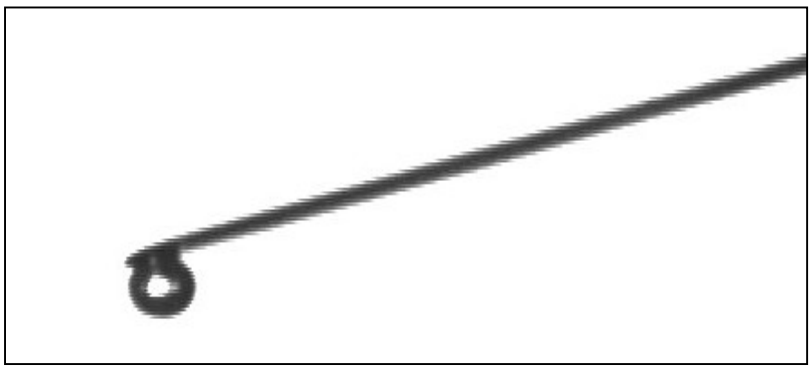

Figure 31 Photograph of the AFM cantilever with an attached 15 μm diameter silica particle as seen with the CIFMA's optical microscope

The manufacturer specified the epoxy glue to be inert to water and electrolytes. It was therefore assumed, that no contamination is introduced into the experiment by the glue.

5.3.1.2 Sample preparation: cleaning, heat treatment and methylation

The same cleaning procedure was strictly followed prior all experiments. The silica particles were originally suspended in water. As specified by the manufacturer, no further cleaning of the particles was necessary. The cleanness and therefore the hydrophilicity of the particles was checked using the method suggested by CHAMEROIS ET AL. (2000), that is based on the observation of the behaviour of particles sprinkled to the surface of liquid, (in this case water).

The silica plates were cleaned in hot, 37 % HCl for 1 hour, then rinsed 10 times with ultrapure water, followed by a 2 minute cleaning in 12 M NaOH and rinsing 10 times in ultrapure water. The cleaned silica plates were stored under ultrapure water prior the heat treatment and methylation. The cleanness of the plates was checked by placing an air bubble on the plate immersed in water. If the bubble did not cling (as observed under microscope), the plate was assumed to be clean and hydrophilic.

5.3.1.2.1 Sample preparation for experiments carried out in ultrapure system

The colloidal probes were prepared from hydrated 15 μm silica particles as described in chapter 5.3.1.1. The colloidal probes were then hydrophobized with 1,1,1,3,3,3-hexamethyl-disilazane (HMDS) vapour at 70 C° for 150 minutes. The hydrophobized colloidal probes were kept in a dessicator over silica gel until used for measurements.

The experiments were performed in ultrapure water at pH 5.4 without salt and/or surfactant addition. The bubble was formed from laboratory air and the experiments were carried out in normal air atmosphere.

5.3.1.2.2 Sample preparation for experiments carried out with particles varying in hydrophobicity

In order to achieve different degree of hydrophobicity, the silica samples (plates and particles) were prepared following the method suggested by LAMB AND FURLONG (1982). For heat treatment a droplet of the suspension containing 10 μm silica particles was put on a cleaned silica plate and together with another cleaned silica plate it was placed inside the preheated oven and kept at constant temperature overnight. This procedure depending on the oven temperature (70, 110, 200, 400 or 1050 °C), removed a controlled amount of OH

groups from the surface, which serve as adsorption sites for the silane, as described in chapter 2.2.

The heat-treated silica particles were glued to AFM cantilevers as described previously. The colloid probe prepared this way and the silica plate used as control substrate, were placed into a small closed jar. Excess amount of TMCS (trimethyl-chlorosilane) was added and the jar was placed into the heating chamber at 70 °C for 10 minutes. After silylation the colloid probe and the control plate were placed in the oven at 110 °C in order to remove the excess amount of hydrophobizing agent. Between silylation and measurement the substrates were kept in a dessicator over silica gel, in order to avoid adsorption of water molecules.

All the measurements were conducted in 10^{-3} M KCl aqueous solutions. The cantilevers were attached to the cantilever holder of the instrument and immersed into the liquid. The date and time of the immersion was recorded. Some experiments were performed over an extended time period (up to 12 days) in order to study the time dependency of the interactions. The electrolyte and the bubble were changed from time to time. In some experiments the particles attached to cantilevers were placed into the oven either at 110, or 190 C° in order to restore the hydrophobicity lost most probably due to hydration of the silica surfaces.

5.3.1.2.3 Sample preparation for the study on the effect of applied load, contact time and approach velocity on adhesion

20 μm silica particles were heat treated at 400 °C and colloidal probes were prepared from these particles. The colloidal probes were then hydrophobized with TMCS vapour as described in chapter 5.3.1.2.2. The measurements were performed in 10^{-3} M KCl aqueous solutions.

5.3.1.2.4 Sample preparation for experiments carried out to study the effect of type of gas and electrolyte concentration

Colloid probes were prepared from 15 μm silica spheres based on the procedure described above. The probes were washed in ethanol and n-Heptane then kept for 150 minutes in 1,1,1,3,3,3-hexamethyl-disilazane (HMDS) vapour at 70 C°, washed again in ethanol and n-heptane to remove the un-reacted HMDS. The cantilevers with already glued

particles were stored in a dessicator over silica gel to avoid adsorption of water molecules on the particle surfaces.

The experiments were carried out in air-equilibrated, Ar or CO_2 saturated ultrapure water and KCl electrolyte, in air, Ar or CO_2 atmosphere. For gas saturated solutions the ultrapure water and electrolyte were first frozen, then melt and degassed (MAHNKE ET AL. 1999) finally saturated with Ar and CO_2 by bubbling the gases through the liquid for 60 minutes. The electrolyte concentrations were 10^{-4} M and 10^{-2} M KCl. The gas atmosphere around the sample holder quvette was provided with the help of the glove-bag in which the instrument was placed, as described in chapter 3.2.1.

5.3.2 Standard procedure prior to measurements

First, before any measurement, the laser beam had to be aligned on the back of the cantilever and the reflected spot had to point into the middle of the PSD. The noise/signal ratio had to be minimized over the full range of the PSD. This was done by manual fine tuning of the laser-translation stages and following the signal from the PSD, while the piezo-translator was scanning in z-direction with large tip sample separations (tip not touching the surface). The linearity error over the entire piezo-translator range should be under 0.2% (0.02V on 0-10V scale). This was important to avoid the artefacts described in chapter 3.4.

Second, prior the force measurements between particles and bubbles, the *PSD factor* and spring constant of the cantilever have to be determined. The PSD factor is the constant showing the deflection of the cantilever per change of output voltage of the PSD. It is calculated from the slope of the constant compliance region (reasonably accurate for stiff samples) of the force curve taken by pressing the cantilever against a hard surface. As the PSD factor is a key element in transforming the voltage into force data, it is very important to keep its value as stable as possible during one experiment. In case of any small change in the hardware settings during one experiment, the PSD factor was measured and compared with previous values in order to minimize the error.

The measurement cantilevers were calibrated by pressing them against a *reference cantilever* with known spring constant following the method described in chapter 2.3.4. The slope of the curves can be calculated directly from the data graph. The angle between

cantilevers pressed against a hard surface and against each other is required in order to calculate the spring constant of the measurement cantilever. Images were recorded in order to measure this angle. The value of PSD factor and the cantilever spring constant was recorded for each experiment.

The bubble was placed on the reference cantilever holder stage shown on Figure 30. This arrangement facilitates the calibration of the cantilever at any time during the measurement against several references within a short time period, without the need to remove the cantilever from the liquid phase.

5.3.3 Force curve processing and analysis

In the measurements, approach and retraction curves were recorded. The curves were later processed off-line. The voltage vs. piezo-position curves were converted to force vs. piezo-position curves by multiplying first the voltage values by the PSD factor (specific for the PSD), and then by the spring constant of the measurement cantilever. The curves were shifted vertically so that the constant force region corresponds to the zero force value, and horizontally so that the jump-in point corresponds with zero distance value. The force vs. piezo-position curves were not converted to force vs. separation, as the constant compliance region in case of bubbles and particles can not be defined in the same way as for solid surfaces. The constant compliance region in this case is a measure of both, cantilever deflection and bubble deformation. An additional problem in converting from force vs. piezo-position to force vs. separation curves is that sometimes it is difficult to distinguish whether stable water film or TPC line is formed between the particle and air bubble. Therefore it was decided to ignore any corrections for the bubble deformation and not to convert from force vs. piezo-position to force vs. separation. Optionally the voltage, deflection and force data can be filtered for noise reduction.

The force curves obtained in the measurements were analysed from attractions (jump-in) and adhesion (jump-off) point of view. The jump-in point was taken as a measure of attraction, while the jump-off as a measure of adhesion Figure 32. As convention, the more negative values mean larger jump-in force. For easier understanding, in the case of figures comparing adhesion forces (e.g. Fig. 45-49), the negative adhesion forces were plotted vs. different variables. Therefore in these figures more positive adhesion values mean larger force.

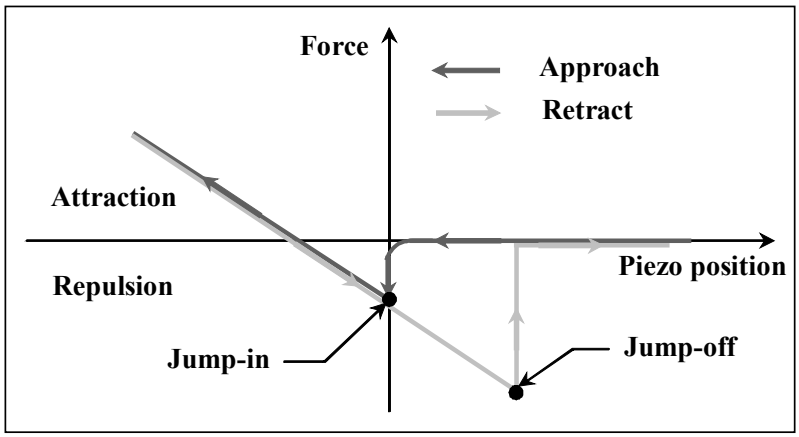

Figure 32 Force vs. piezo position curve showing the jump-in and jump-off points used as measures of attraction, respectively adhesion

The measurements were carried out preferably in the same range of applied load. The load was determined from the force curves as shown in the figure above. The measurement data was normalized in every case by the radius of the used particle.

The fitting of the measurement data with theoretical models was not attempted because of the reasons described in theoretical chapter 2.3.3.2.

References chapter 5

Chamerois, M., Francois, M., Villiéras, F., Yvon, J., 2000. Modification of calcium carbonate surface properties: macroscopic and microscopic investigations, in *Apparent and Microscopic Contact Angles*, ed. Drelich, J., Laskowski, J.S., Mittal, K.L., VSP, Köln, 405-417.

Lamb, R.N., Furlong, D.N., 1982. Controlled wettability of Quartz Surfaces. *J. Chem. Soc. Faraday Trans.,* **1**, (78), 61-73.

Mahnke, J., Stearnes, J., Hayes, R.A., Fornasiero, D., Ralston, J., 1999. The influence of dissolved gas on the interactions between surfaces of different hydrophobicity in aqueous media Part I. Measurement of interaction forces, *Phys. Chem. Chem. Phys.,* **1,** (11), 2793 – 2798.

Preuss, M., Butt, H.-J., 1998. Direct Measurement of Particle-Bubble Interactions in Aqueous Electrolyte: Dependence on Surfactant, *Langmuir*, **14**, (12), 3164 – 3174.

Tortonese, M., Kirk, M., 1997. Characterization of application specific probes for SPMs, *SPIE* **3009**, 53-60.

CHAPTER 6 CANTILEVER STABILITY STUDY

In all science, error precedes the truth, and it is better it should go first than last.

Hugh Walpole

The spring constant of several cantilevers was measured to verify the hypothesis. As an example, Figure 33 and Figure 34 illustrate the cantilever spring constant values measured with the reference cantilever method (TORTONESE AND KIRK 1997) as described in theoretical chapter 2.3.4.

The spring constants of the cantilevers were measured against four different reference cantilevers, five times within roughly one hour time intervals. Each spring constant value was calculated from an average of five consecutive measurements.

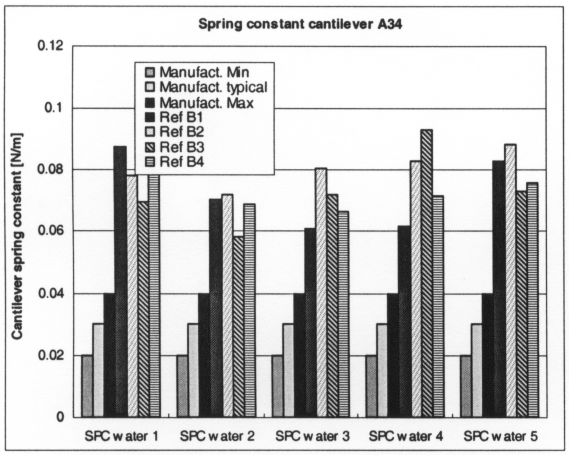

Figure 33 Spring constant values of cantilever A34 measured against four reference cantilevers

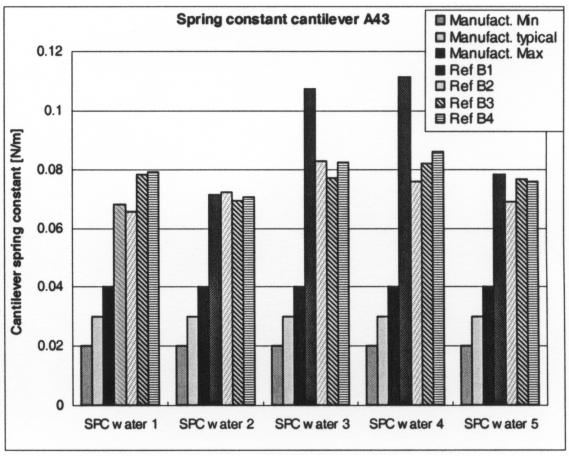

Figure 34 Spring constant values of cantilever A43 measured against four reference cantilevers

According to the manufacturer's specifications, the spring constant of the above mentioned example cantilevers should have been between 0.02 and 0.04 N/m. The measured mean value of the cantilever spring constants of the two cantilevers were 0.075 and 0.079 N/m respectively, which means a high coefficient of variation of 45.8 % and 43.3 % respectively within a time interval of 6 hours. As the measured force is calculated by multiplying the cantilever deflection with the spring constant, this variation would mean 45.8 and 43.3 % respectively variation in the measured force. As it can be seen from

Figure 33 and 34 the spring constant values also change when measured against different reference cantilevers. This fact suggests that the reference spring constant changes too.

The exact reason for the change of the cantilever spring constant is not yet clear. The reasons might include: chemical change in the cantilever coating material caused by the electrolyte, structural change in the cantilever material due to the heat emitted by the laser, etc.

As the reasons of these changes are not known, these errors cannot be avoided. Based on this study it was decided, that if an experiment lasts for several hours, the cantilever will be calibrated several times during the course of the experiment and the actual spring constant value will be used for calculating the force. This is the only possibility to reduce the error induced by this factor. It is also essential to choose a stable reference cantilever, which does not change its spring constant.

References chapter 6

Tortonese, M., Kirk, M., 1997. Characterization of application specific probes for SPMs, *SPIE* **3009**, 53-60.

CHAPTER 7 CONTACT ANGLE MEASUREMENTS AND AFM IMAGING

Just because something doesn't do what you planned it to do doesn't mean it's useless.

Thomas A. Edison

Figure 35 shows the resulting contact angle values measured on silica spheres and fused silica plates after heat and TMCS treatment and only heat treatment (at 1050 °C). As it can be seen from the figure the resulting contact angles on silica plates were generally higher than on particles. For some unknown reason the heat treatment at 1050 °C combined with TMCS gave an unexpectedly high contact angle value on particles. After heat-treatment at 400 °C the receding contact angle measured on sphere was 0°. The trend of change in hydrophobicity of silica plates follows well that described by LAMB AND FURLONG (1982). In the case of particles, this trend was far from being clear.

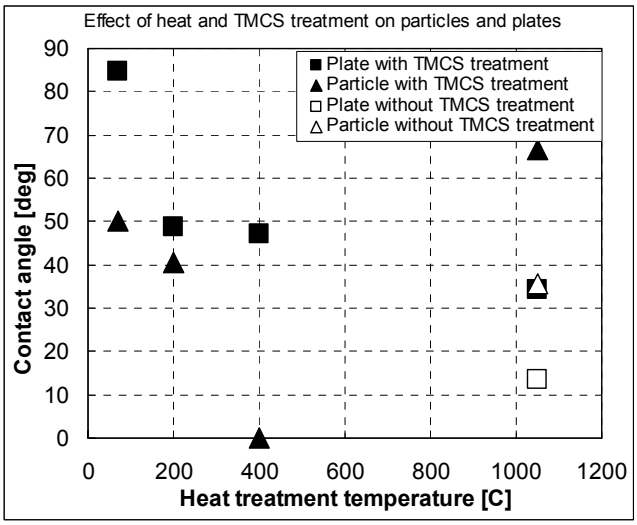

Figure 35 Receding contact angles measured on silica particles and silica plates as a function of heat treatment temperature

To determine the reason for this difference and the discrepancy in the contact angle values, AFM images were taken from the particles and plates and the average roughness of the surfaces were determined. The 3D AFM images of one of the 10 µm silica sphere is shown in Figure 36, while the image of the 20 µm silica sphere is shown in Figure 37.

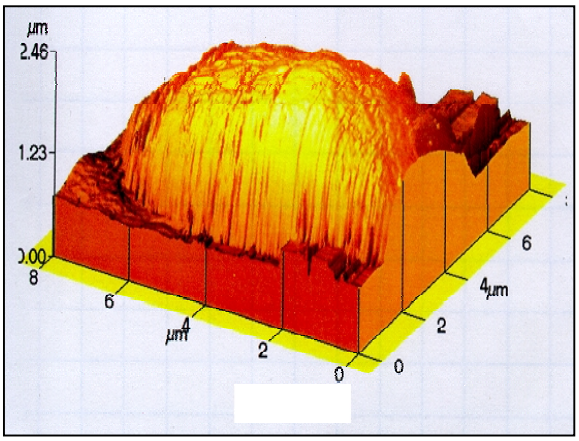

Figure 36 3D AFM image of a 10 µm fused silica sphere used in the force measurements

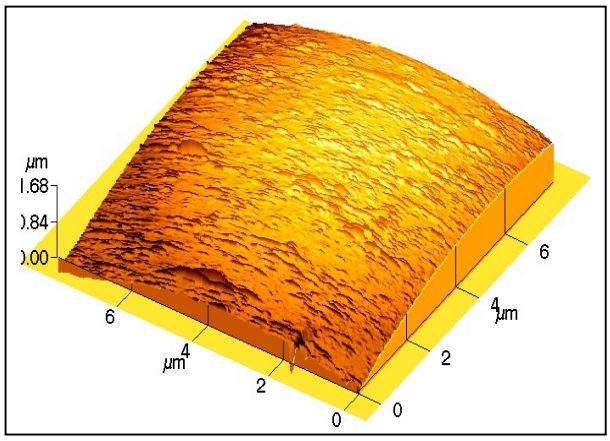

Figure 37 3D AFM image of 20 µm fused silica sphere used in the force measurements

The average roughness values measured on different substrates are given in Table 1. The roughness of the particles is shown after subtracting the curvature.

Table 1

Substrate	**Average roughness [Å]**	**Measured area [µm^2]**
Plate	5.8	1
10 µm sphere	98.2	1
20 µm sphere	110.2	1

The difference in the contact angle values can probably be explained by the very different surface roughness of the substrates. Therefore, presumably the particle surface is heterogeneous, and the apparent contact angle measured on the silica particle surface is a combination of different microscopic contact angles. The effect of heterogeneity increases with roughness.

The particles treated with HMDS (treatment described in chapters 5.3.1.2.1 and 5.3.1.2.4), had contact angles between 70° and 80°.

References chapter 7

Lamb, R.N., Furlong, D.N., 1982. Controlled wettability of Quartz Surfaces, *J. Chem. Soc. Faraday Trans.* 1, 78, 61-73.

CHAPTER 8 PARTICLE-BUBBLE JUMP-IN STUDIES

Science... never solves a problem without creating ten more.

George Bernard Shaw

This chapter presents the result of the jump-in studies. First part describes the effect of ultrapure water and electrolyte containing solution, while in the second part the effect of gas saturation with different type of gas is shown.

8.1 EFFECT OF ELECTROLYTE CONCENTRATION

8.1.1 Experiments carried out in ultrapure system

The first experiments involved interactions between 15 μm diameter HMDS treated silica spheres and air bubbles in ultrapure water without any surfactant or ion addition. The colloidal probe was prepared as described in chapters 5.3.1.1 and 5.3.1.2.1. The contact angle of the hydrophobized particles was 59°.

The most important observation of these tests was a phenomenon not described before in the literature. A very violent and extremely long-range jump of the air bubble towards the hydrophobized particle was observed with the CIFMA's optical system. The distance from where the bubble jumped into contact with the particle was estimated from the image files, being in the range of micrometers.

The other important observation was that, the deformation of the bubble did not result in a change in the local curvature of the bubble surface, but rather the bubble surface jumped as a whole towards the particle.

8.1.2 Experiments carried out in electrolyte

Colloidal probes prepared from 10 μm silica spheres were heat treated at 70, 200 and 1050 °C and hydrophobized with TMCS as described in chapter 5.3.1.2.2. Experiments were also performed with silica particles heat-treated at 1050 °C, but without TMCS

coating. The force measurements were conducted over extended time periods (up to several days). All the experiments were performed in 10^{-3} M KCl electrolyte. The contact angles of the particles treated at different temperatures were presented in Chapter 7.

Unlike in the ultrapure system, in these experiments performed in an electrolyte solution the violent jump of the bubble towards the particle (contact angles between 40° to 67°) was not observed. Although, a smaller deformation of the bubble very likely occurred, this deformation could not be objectively detected.

Figure 38 shows the approach force curves recorded between air bubbles and a silica particle heat-treated at 200 C° and hydrophobized with TMCS. Figure 39 shows the approach curves recorded with air bubbles and a silica particle heat treated at 1050 C°, and hydrophobized with TMCS. The curves were recorded over an extended period of time (up to 1.5 days).

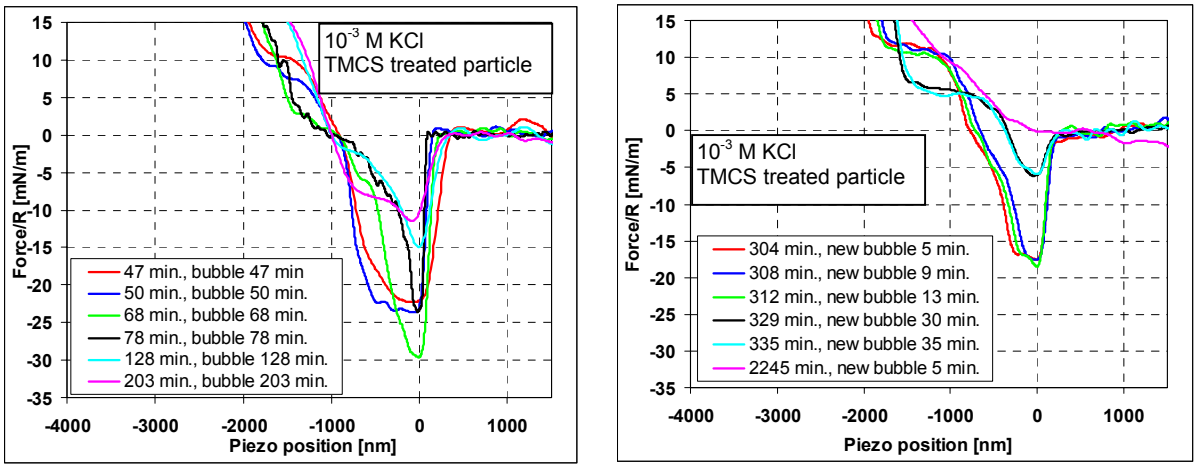

a.) *b.)*

Figure 38 Approach curves taken with particles heat treated at 200 C° and hydrophobized with TMCS. The first column of the legend denotes the time elapsed since the particle has been immersed into solution, while the second the time since the bubble has been placed into the bottom of the quvette. a) First bubble, b) New bubble

As described in chapter 5.3.3, the force vs. piezo-position curves were not converted into force vs. separation distance curves.

The very important observation was, that the jump-in force was highly dependent on the time elapsed since the particle was immersed into the electrolyte, and on the age of the bubble. The results presented in Figure 38 and Figure 39 show that the jump-in force

decreases with time and it can completely disappear within about 5 hours after placing the particle into the electrolyte.

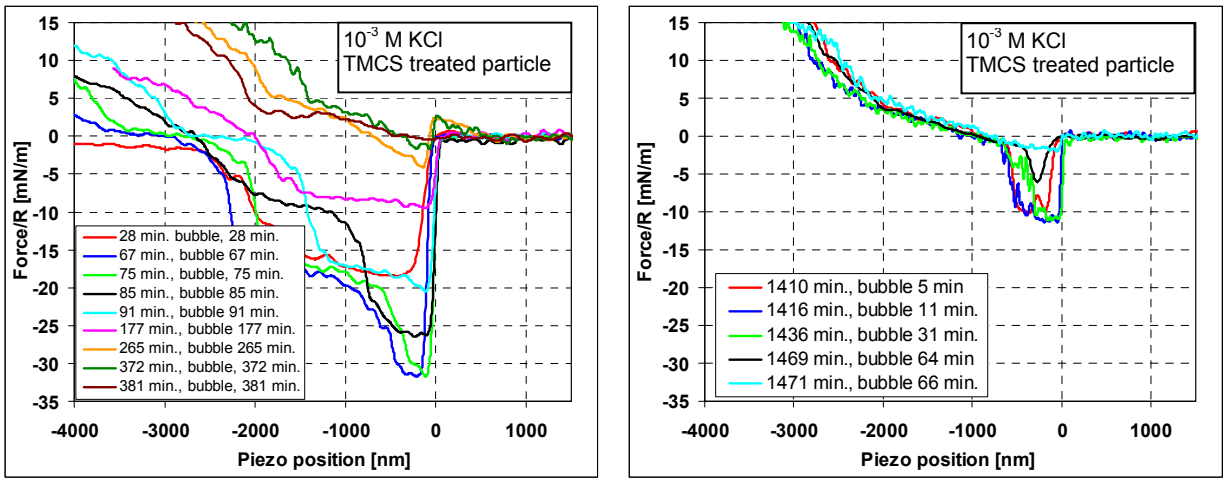

a.) *b.)*

Figure 39 Approach taken with particles heat treated at 1050 C°, hydrophobized with TMCS. The first column of the legend denotes the time elapsed since the particle has been immersed into solution, while the second the time since the bubble has been placed into the bottom of the quvette. a) First bubble, b) New bubble

Another very important observation in this experimental series was the effect of bubble age on the jump-in force. If a new bubble is placed into the quvette after the jump-in disappeared, the jump-in re-appears, but with a lower strength (Figure 38b and Figure 39b). This phenomenon can be repeated within a time limit of maximum 24 hours, but the jump-in cannot be restored after the particle has been in the solution for more than one day. It has also been noted, that before the disappearance of the jump-in force repulsion starts to act between the particle and bubble (Figure 39a).

In order to verify the idea of changing jump-in force, and therefore hydrophobicity (contact angle decrease) due to hydration, after the disappearance of the jump-in force, the particles were placed into the oven and re-heated at temperature of 110 C° overnight. The assumption was that this heat-treatment should remove the adsorbed hydroxyle layer and restore the hydrophobicity. No change in the surface hydrophobicity could be detected. A higher temperature (190 C°) was also tested, as suggested by TRIPP AND HAIR (1991). At 190 C° the surface hydrophobicity was restored as shown on Figure 40, which serves as a proof to the idea that jump-in disapears with time due to hydration of the silica surfaces. The relatively high noise level of the curves is attributed to the reduced reflectivity of the AFM cantilever caused by the long residence time in electrolyte and heat-treatment.

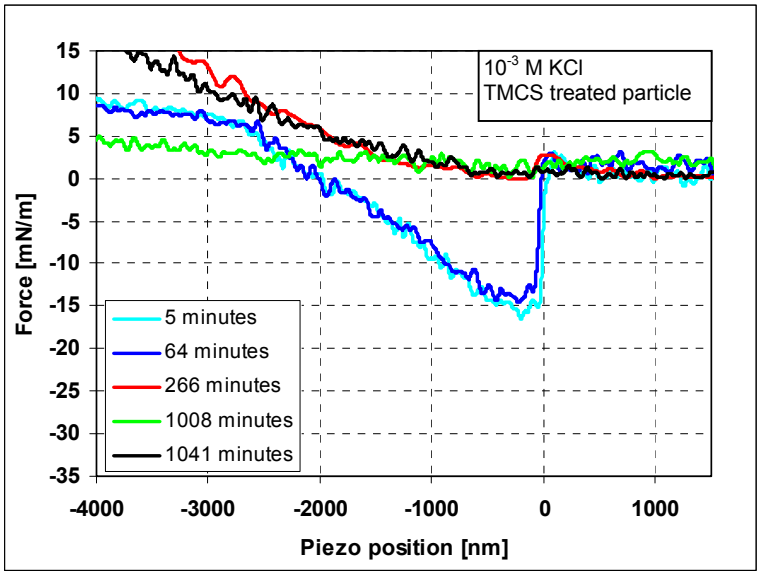

Figure 40 Approach curve taken after the particle was stored at 190 C° overnight. Same particle as on Figure 39. The bubble and the particle were placed into the liquid in the same time

Figure 41 summarizes the results of the jump-in tests carried out with particles treated at 200 and 1050 °C.

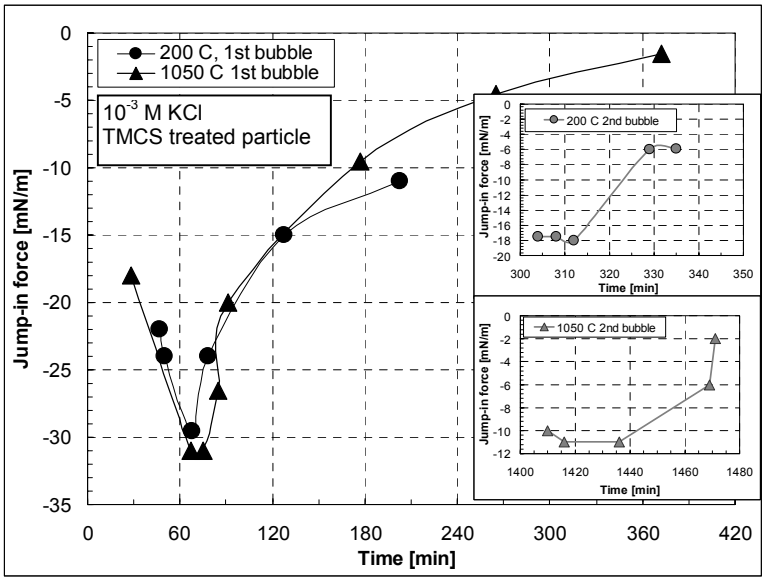

Figure 41 Jump-in forces as function of time with particles treated at different temperatures and hydrophobized with TMCS. The insets show the jump-in forces measured after a new bubble was placed into the solution (more negative jump-in values mean larger jump-in force)

The jump-in force first increased with time then it started decreasing rapidly until it disappeared. A similar trend was observed when the same particle was tested in the same

solution, but a new bubble was produced, although with the second bubble the magnitude of the force was smaller and the decrease in the force magnitude was much faster.

The varying form and slope of the constant compliance line in the different measurements is a phenomenon that has no explanation yet. It might be caused by the change in bubble and cantilever stiffness, although we cannot preclude the possibility of an artefact caused by some reflected light from the deforming bubble or undulating movement of the bubble due to hydrodynamic forces.

8.2 EFFECT OF A TYPE OF GAS AND ELECTROLYTE CONCENTRATION

The aim of these experiments was to determine whether dissolved gases and the specific gas atmosphere affect the particle-bubble interactions. For these measurements the colloidal probes and the specific gas saturated ultrapure water and electrolytes were prepared as described in chapter 5.3.1.2.4. The bubble of the specific gas was placed on the bottom of the Teflon quvette with a micropipette. First air equilibrated ultrapure water in air, Ar saturated ultrapure water in Ar atmosphere, and CO_2 saturated ultrapure water in CO_2 atmosphere were tested. In the second set of measurement the effect of Ar and CO_2 was tested at different KCl electrolyte concentrations. The pH of the air and Ar saturated solutions was 5.16±0.2, while for CO_2 saturated water it dropped to 4.1.

The effect of air, Ar and CO_2 gases on the jump-in force between a hydrophobized silica sphere and an air bubble in pure water are shown in Figure 42.

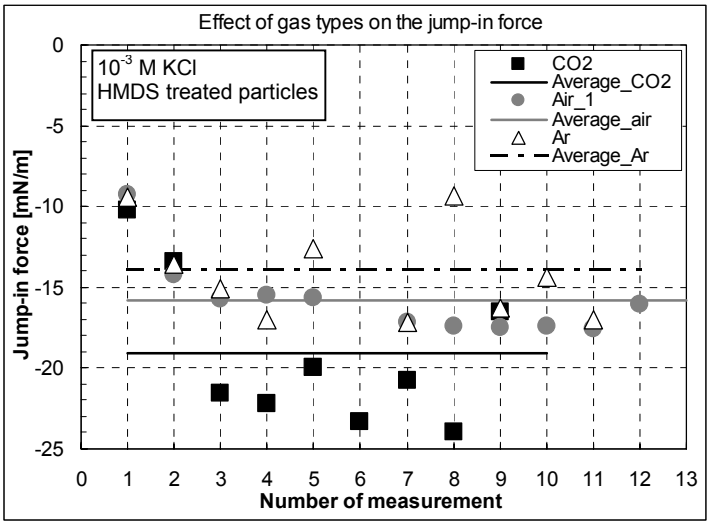

Figure 42 Effect of a gas type on the jump-in force measured (HMDS treated silica).

Although the average jump-in force measured with the force measurement technique was larger in case of CO_2 saturated water than in the case of air and Ar saturated water, the video files recorded during the measurements showed a jump of the bubble towards the particle only in the case of air-equilibrated ultrapure water. It also has to be noted, that in the behaviour of the jump-in force at the first approach of the particle towards the bubble, the kind of gas did not seem to have any effect. In case of Ar and CO_2 the jump-in values were highly variable, while in the case of air, the results were more consistent.

In the second set of tests the effect of Ar and CO_2 at different electrolyte concentrations was tested. The results are shown in Figure 43.

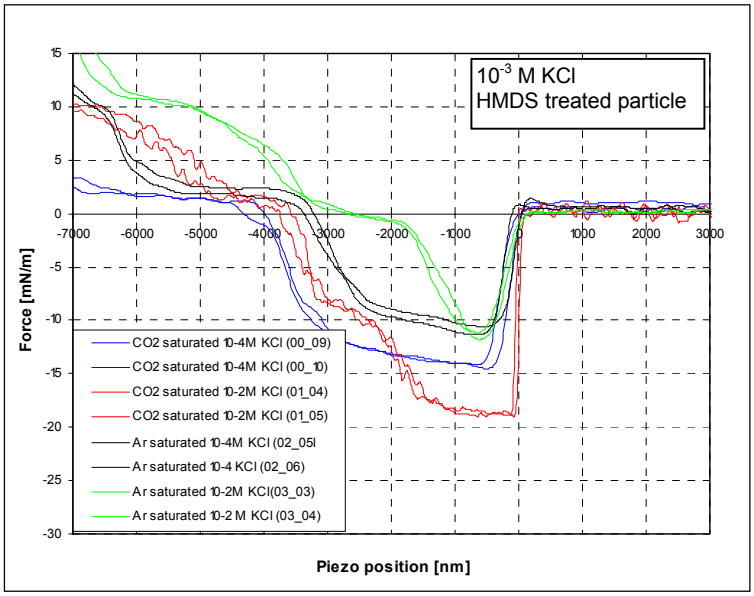

Figure 43 Effect of gas types and electrolyte concentration on the attachment of HMDS treated silica sphere to air bubble

When the KCl concentration was increased from 10^{-4} to 10^{-2} M the jump-in force increased significantly in CO_2 saturated solution, while in Ar saturated solution no significant change was detected. In electrolyte solutions no violent jump of the bubble was observed.

References chapter 8

Tripp, C.P., Hair, M.L., 1991. Reaction of Chloromethylsilanes with Silica: A low frequency infrared study, *Langmuir*, **7**, (5), 923-927.

CHAPTER 9 PARTICLE-BUBBLE ADHESION STUDIES

Aerodynamically, the bumblebee shouldn't be able to fly, but the bumblebee doesn't know it so it goes on flying anyway.

Mary Kay Ash

The detachment-force was studied by analysing the maximum force needed to detach the particle from the bubble (Figure 32), independently of bubble deformation. A video sequence of the pull-out of a 15 μm silica particle from an air bubble is shown in Figure 44.

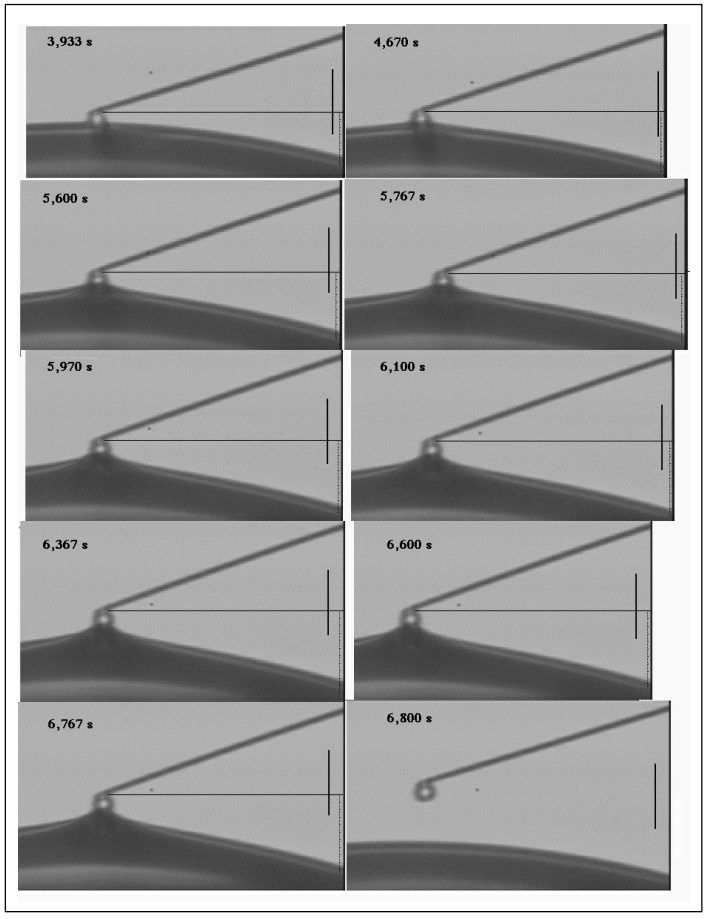

Figure 44 Video sequence showing the air bubble deformation when detaching from a 15 μm particle.

The adhesion study, first describes the effect of applied load, contact time and approach velocity. In the second part the results obtained in electrolyte containing and gas saturated systems are presented.

9.1 EFFECT OF APPLIED LOAD, CONTACT TIME AND APPROACH VELOCITY ON ADHESION

There are only a few publications, which briefly mention the adhesion between particles and air bubbles, (most likely because commercial AFMs are not suited for this type of experiments due to their small measurement range). Even so, some authors have noticed that the adhesion force is dependent on the applied load (FIELDEN ET AL. 1996; PREUSS AND BUTT 1998). The effects of contact time, applied load and approach velocity have not been extensively studied.

The experiments were performed in 10^{-3} M KCl solution at pH 5.16 with 20 μm silica spheres prepared as described in chapter 5.3.1.2.3. The particles were moved towards the air bubble and pressed to it. No jump-in force was detected, and the interaction at approach was monotonically repulsive, therefore it can be assumed, that the apparent receding contact angle was 0° and no TPC formation occurred. This was confirmed also by the visual observation of the particle-bubble interaction with the help of CIFMA's video imaging system. The adhesion force was measured at three different applied load intervals and three different approach velocities (the applied load was determined as described in chapter 5.3.3).

In the first measurements the particle was pressed against the air bubble, and retracted immediately after the desired loading force value was reached. In the next tests the particle was kept in contact with the bubble at a given loading force for 1, 3, 6 and 10 seconds respectively. Experiments were carried out in three load ranges: 5, 10 and 20 mN/m. The measurements were conducted within a short period of time (30 minutes) therefore it was assumed that the time dependent effects could be neglected. Figure 45 shows the results of the tests on the effect of loading and contact time.

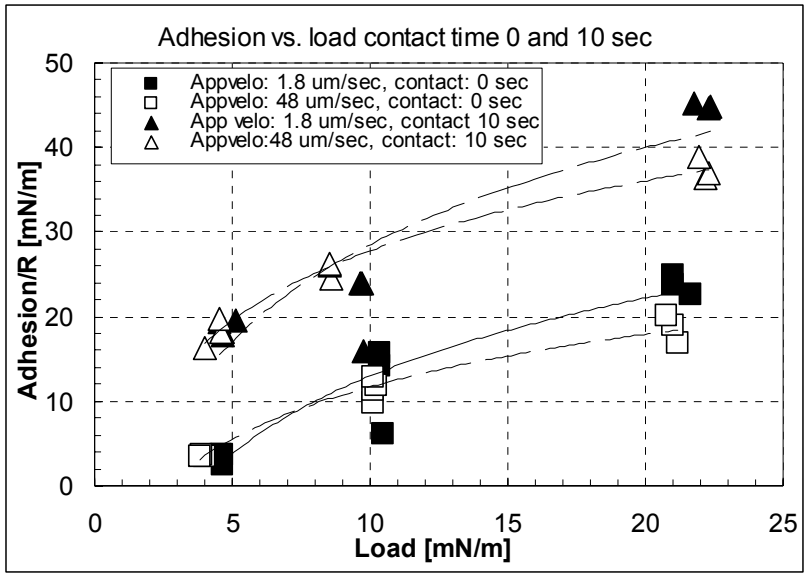

Figure 45 Effect of applied load and contact time on the adhesion force between silica particle and air bubble (approach velocity 1.8 and 48 μm/sec)

Although the apparent receding contact angle was 0° and there was probably no film-rupture between the particle and bubble, adhesion between them still occurred. However the adhesion force was only about 10 to 20 % of the force that was measured when the particle was hydrophobic.

The adhesion force was strongly affected by the applied load: adhesion increased with increasing loading force. When the applied load was increased from ~5 mN/m to ~20 mN/m, but the particle was immediately retracted after reaching the desired load value (contact time 0 seconds), the force needed to detach the particle from the air bubble increased by a factor of 4.

The effect of contact time was also significant. Increasing the contact time from 0 to 10 seconds increased the adhesion force from ~5 mN/m to ~20 mN/m in the case of low load values and from ~20 mN/m to ~40 mN/m in case of high load values. Figure 46 and Figure 47 provide further details showing the effect of contact time on adhesion force between a particle and air bubble.

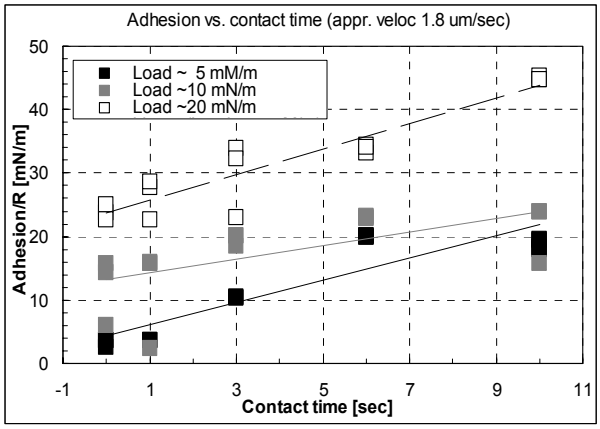

Figure 46 Effect of contact time on the adhesion force at three different applied loads (approach velocity 1.8 μm/sec)

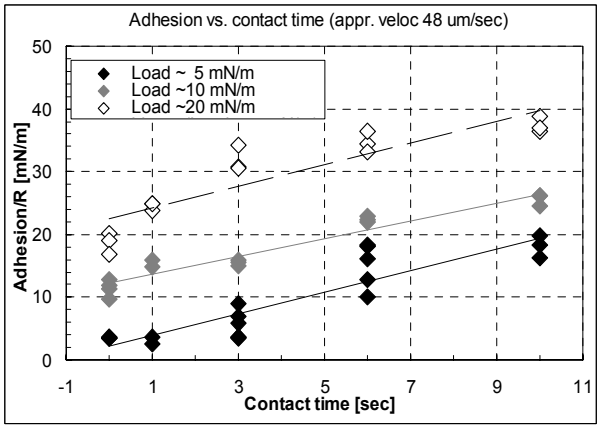

Figure 47 Effect of contact time on the adhesion force at three different applied loads (approach velocity 48 μm/sec)

In order to test whether the adhesion is affected by the drainage of the liquid from the gap between the particle and bubble, the particle was pushed to the bubble with 1.8, 21 and 48 μm/sec velocities. The results of these experiments are shown in Figure 48.

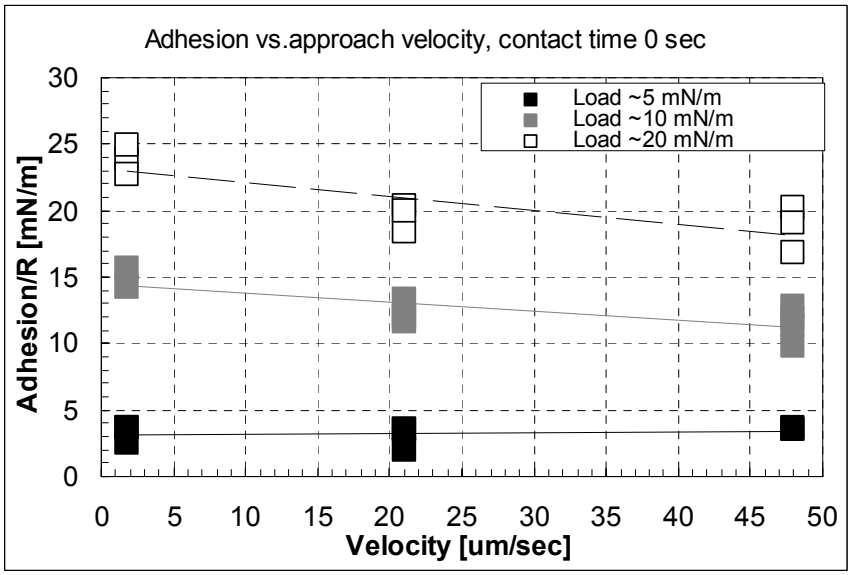

Figure 48 Effect of approach velocity on the adhesion force between a silica particle and an air bubble at different loading force ranges

Increased velocity had a slight effect on the adhesion force. For low load values the increased approach velocity did not affect the adhesion, while for medium and high loading force values the adhesion decreased slightly with increased approach velocity.

9.2 EFFECT OF TIME

The values of the adhesion force were plotted as a function of time elapsed since the particle was immersed in electrolyte for the particles treated at different temperatures, as shown in Figure 49. The actions taken (e.g. placing a new bubble, or changing electrolyte) during the course of the experiment are also marked on the figure.

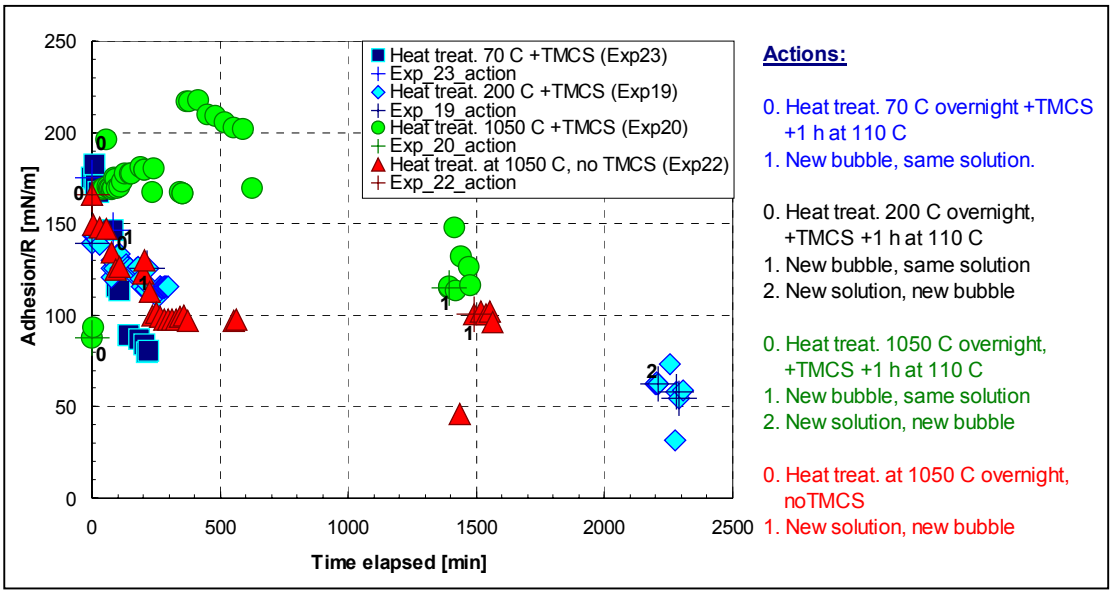

Figure 49 Maximum adhesion values (jump-off force) vs. time (particles treated in different conditions)

It was observed, that as expected, initially the adhesion force decreased with decreasing contact angle, although for some unknown reason in the case of particles treated at high temperature (1050 °C) the data was not consistent with this trend, and the adhesion force was highly variable.

The dependency of the adhesion force on the time elapsed since the particle was immersed in electrolyte solution was striking. The adhesion decreased significantly during the first 5 hours of the experiment. The adhesion force decreased by as much as 60 % in some of the experiments within 4 hours of residence time. Contrary to the jump-in force, the dependence of adhesion force on bubble age was not so clear. This result shows that the bubble-particle adhesion is most probably affected only by the processes happening on the particle surface, and not by the ones occurring at the gas-liquid interface.

9.3 EFFECT OF TYPE OF GAS AND ELECTROLYTE CONCENTRATION

The adhesion force in the measurements carried out in the presence of Ar and CO_2 was very high. The exact adhesion values could not be determined, because even the extended position sensing limits of the experimental setup did not provide large enough range for the detection of these forces. Further improvement of the experimental apparatus or the use of much stiffer cantilevers could probably solve this problem. However with the use of stiffer cantilevers the sensitivity of the measurements will be much lower.

9.4 COMPARISON OF MEASURED AND ESTIMATED ADHESION VALUES

The maximum capillary force was calculated using Eq. 20, presented in chapter 2.1.2.1. The calculated maximum capillary force and measured maximum adhesion force was plotted as a function of contact angle in Figure 50.

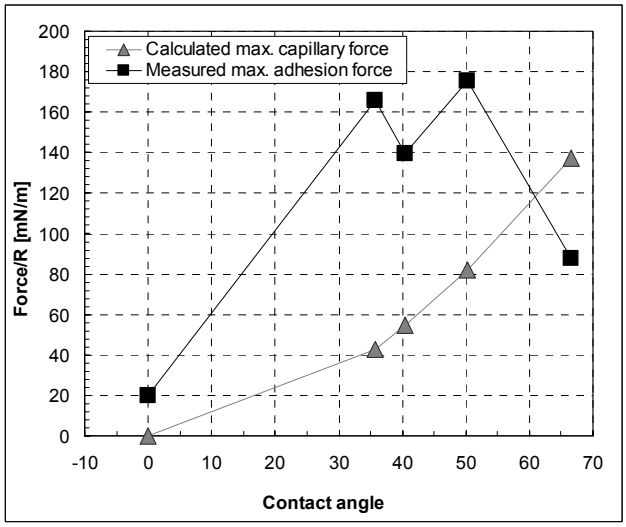

Figure 50 Calculated capillary force and measured adhesion as a function of contact angle

As it can be seen from this figure, the measured adhesion was in almost all the cases higher than the calculated maximum capillary force.

The adhesion force is very low in case of low load values (~5 mN/m) and 0 sec contact time. In this case the correlation is much better with the calculated capillary force values, than in the case of higher applied load and contact time values. Although it has to be noted, that the exact capillary force acting on the particle is difficult to be calculated, as it seems

that microscopic sites having a different contact angle from the apparent macroscopic contact angle dominate the interaction.

References chapter 9

Fielden, M.L., Hayes, R.A., Ralston, J., 1996. Surface and Capillary Force Affecting Air Bubble-Particle Interactions in Aqueous Electrolyte, *Langmuir,* **12**, (15), 3721-3727.

Preuss, M., Butt, H.-J., 1998. Direct Measurement of Particle-Bubble Interactions in Aqueous Electrolyte: Dependence on Surfactant, *Langmuir*, **14**, (12), 3164 – 3174.

CHAPTER 10 DISCUSSION

The most exciting phrase to hear in science, the one that heralds new discoveries, is not 'Eureka!' but 'That's funny...'

Isaac Asimov

The CIFMA has been proved to be a powerful tool in studying particle-bubble interactions. Because CIFMA is not a commercial instrument and because it was built as part of this research project, the daily work with it has revealed several insights, which probably wouldn't be observed with commercial equipment.

The results of the tests raise several questions:

- utility of the colloidal probe technique for particle-bubble interaction measurements;
- interaction of particles and air bubbles (important in building flotation models);
- utility of certain materials (in this case silica as a model substrate in AFM force measurements).

Fitting experimental results to the available theoretical models was considered inadequate for particle-bubble interactions, because the real separation between the particle and air bubble could not be precisely determined due to the deformation of the bubble. Therefore in this work the experimental data was not fitted in any case to the theoretical models, rather the results were analysed relative to each other.

In this discussion first the effect of measurement parameters, such as applied load, contact time and approach velocity on the adhesion force are discussed. Then the effect of electrolyte concentration and type of gas are examined on both the jump-in and the adhesion force between particles and bubbles.

10.1 EFFECT OF APPLIED LOAD, CONTACT TIME AND APPROACH VELOCITY ON THE ADHESION

Even if the apparent receding contact angle measured on the silica particles was 0°, adhesion could be detected between the particle and air bubble. This peculiar phenomenon

has already been experimentally observed and in the flotation literature it is referred to as *contactless flotation* (DERJAGUIN AND DUKHIN 1979).

The surface of silica at pH ~5 is negative similar to the bubble surface therefore a repulsive force was expected and measured. With increasing loading force this repulsion is probably surmounted and adhesion occurs even without TPC formation. Similar behaviour was observed by FIELDEN ET AL. (1996) with dehydroxylated silica particles in aqueous electrolyte, and by PREUSS AND BUTT (1998) for hydrophilic silica particles in dodecyltrymethylammonium bromide (DTAB) solution.

As shown in chapter 9.4, the adhesion of the particles to the air bubbles was in almost every case higher than estimated from the maximum capillary force values. Therefore, it is very likely that the adhesion is not only influenced by the contact angle, but also by other factors.

As already described in Chapter 7 particle surfaces were not completely smooth, and therefore microscopic sites for adhesion could form. These sites bear different, probably higher degree of hydrophobicity than the overall particle surface. The increase of adhesion with increased loading force leads to the conclusion that microscopic hydrophobic sites are most probably in the "valleys" of the surface, while the peaks are hydrophilic. This argument is also supported by the theory presented by ILER (1979) which says, that the surfaces with a small positive radius of curvature ("hills") are easily dehydroxylated, while the dehydroxylation of the surfaces with small negative curvature ("valleys") is way more difficult. Therefore when silylating the heat-treated silica particles, the valleys provide more sites for adsorption of silane than the peaks, and these sites will play a key role in the particle-bubble adhesion.

In the case of apparently hydrophilic but not completely smooth particles, the capillary force is most probably not dominating the adhesion interaction over the whole particle surface, rather acts only on the nanometer sized asperities present on the surface.

The formation of a firm link between the particle and air bubble could be enhanced with increasing the contact time. At first glance this could be attributed to the drainage rate between the particle and bubble, but it has been shown that with increasing approach velocity of the particle towards the air bubble the adhesion is not affected significantly.

However, the approach velocities were still quite low in these experiments (max. 48 μm/sec), and perhaps higher approach velocities should be further tested.

10.2 DISCUSSION ON ULTRAPURE AND ELECTROLYTE CONTAINING SYSTEMS

Very long-range interaction between HMDS treated silica particles and air bubbles was observed by optical means. The measurement of the range of interaction was unfortunately not possible. The bubble deformation could not be measured, only visually observed. This is not a limitation of the CIFMA, but a limitation of the force measurement technique itself, which only allows the measurement of the cantilevers deflection, but has no means to detect deformational changes on the surface.

The long-range interaction manifested itself through a violent and large deformation of the air bubble towards the particle. The observed range is several orders of magnitude larger than the range predicted by the van der Waals force. The observed deformation involving the whole bubble surface not only a local curvature also suggests that the energy involved in the interaction is much higher than predicted from the theories.

This phenomenon was only present in experiments carried out in ultrapure water equilibrated with air. This suggests that the phenomenon is confined to a very restricted system and might be another manifestation of the hydrophobic force.

The hydrophobic force should not be affected by the change in electrolyte concentration, therefore the presence of the violent jump of the bubble in ultrapure water and its disappearance in electrolyte suggests, that the change in electrolyte concentration is most probably not affecting the interaction, but it affects the bubble elasticity. This theory is supported by the bubble stiffness calculations. The stiffness of the air bubbles was calculated from the force curves using Eq. 29 discussed in theoretical chapter 2.3.3.3. The bubble stiffness results as a function of KCl electrolyte concentration are presented in Figure 51.

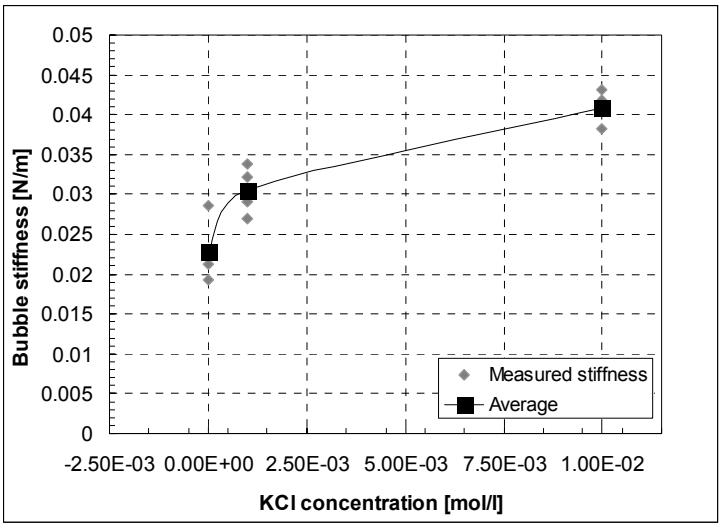

Figure 51 Bubble stiffness at different KCl concentrations

The spring constant of the cantilevers used in the measurements in most of the cases exceeds 0.04-0.12 N/m. The spring constant of the air bubble in ultrapure water is around 0.02 N/m, while in 10^{-3} M KCl electrolyte this value increases to around 0.04 N/m. Therefore it is not surprising that in the ultrapure water the bubble having a much lower spring constant than the cantilever, deforms towards the particle attached to the cantilever, while at higher electrolyte concentrations, this jump cannot be observed anymore. This of course does not necessarily mean that the very long-range interaction does not exists in electrolyte containing systems, but it rather means that it cannot be observed.

The work with silica in surfactant free electrolyte solutions revealed that the changes occurring in the silica-water-air bubble system are much more complex than thought before. The time dependent behaviour of both jump-in and adhesion force probably results from the slow changes occurring on silica surface, caused by hydration of the hydrophobic surface. This phenomenon was first described by LASKOWSKI AND KITCHENER (1969). VIGIL ET AL. (1994) in their measurements performed using SFA also reported a similar behaviour of silica surfaces. It is important to emphasise that this study showed for the first time such time dependent phenomena in the experiments carried out using AFM type of equipment.

The bubble age seems also to be an important factor influencing the particle-bubble interaction. EIGELES AND VOLVENKOVA (1963) showed dependence of the induction time on bubble age during the adhesion of quartz in NaOH and $CaCl_2$ electrolyte. Although the

time scale is slightly (with about 20 minutes) shifted, the trend in the behaviour of the induction time and the trend in the jump-in force presented in Figure 41 are very similar.

These two very important results of the jump-in study suggest that two parallel phenomena take place at the same time, one on the particle surface and other one on the bubble surface. The phenomena taking place on the particle surface most likely involves hydration of the surface as is discussed in chapter 2.2; what is going on the bubble surface is still unknown. A speculative explanation could be the hydrogen bond aided organization of the double layer, although some authors (VIGIL ET AL. 1994) suggest that change in water structure at the interface should occur in milliseconds rather than in minutes or days. EIGELES AND VOLVENKOVA (1963) suggest, that a polymolecular film forms on the surface of the bubble. For a more exact explanation further experimental evidence will be needed.

The violent jump of the bubble towards the TMCS treated silica surface (contact angle between 40 and 67°, depending on heat treatment temperature) was not observed in this study as it was observed with HMDS treated surfaces (contact angles between 70 and 80°). Therefore it is most likely that the particle-bubble jump-in interaction is dependent on the contact angle as well as on the sample preparation procedure as it has been discussed in chapter 2.1.1.2.1.

10.3 EFFECT OF TYPE OF GAS

In order to determine the origin of the long-range interaction observed in ultrapure systems, experiments were conducted in liquid phase saturated with Ar, CO_2 or air. The interaction was highly dependent on the type of gas present in the system. The range and magnitude of the measured jump-in force was increasing in Ar $\rightarrow$ air $\rightarrow$ CO_2 order. Seemingly the CO_2 affected not only the magnitude of the jump-in force, but also the properties of the bubbles. When using CO_2, the bubble deformation was not as large as in the case of air bubbles. The real difference caused by the presence of air and CO_2 couldn't be precisely assessed since with air a smaller jump-in force was measured, and a large bubble deformation towards the solid particle was observed by optical means, while with CO_2 the bubble deformation was small and the jump-in force was large. As already mentioned in chapter 5.3.1, the pH of the CO_2 saturated ultrapure water was 4.1 due to the dissolved CO_2, compared with the non-saturated water, which pH was 5.4±0.2. The change of the pH shows that the ionic strength of the solution changed, which as discussed in

previous chapter, most probably caused a change in the bubble elasticity and also a change in the bubble charge.

Although the exact number values of the forces couldn't be expressed due to above described reasons, it could be concluded, that both CO_2 and air seem to have a significant effect on the bubble-particle interaction.

These results, and the ones obtained with Ar and CO_2 saturated solutions at different electrolyte concentrations are in excellent agreement with the results of the capture efficiency study by DAI ET AL. (1998). They found that the capture efficiency of particles by bubbles was improved in CO_2 saturated electrolyte compared with Ar, and this effect was further enhanced when the electrolyte concentration was increased from 1.2×10^{-4} M to 10^{-2} M. MAHNKE ET AL. (1999) also showed that the CO_2 increased the jump-in distance between hydrophobic solid surfaces.

Argon did not seem to affect the interaction between particles and air bubbles. Therefore, it can be assumed that non-polar inert gases having very low solubility in water don't have an effect on the interaction, while polar gases such as CO_2 and non-polar oxidizing gases such as air increase the jump-in force.

In the recent years many authors (e.g. CARAMBASSIS ET AL. 1998; TYRRELL AND ATTARD 2001, etc.) support the theory that the long-range forces between hydrophobic surfaces are caused by formation of sub-microscopic bubbles on the solid surfaces. This theory cannot be ruled out in explaining the results presented in this thesis, although the range of the interaction and the observed violent jump of the bubble in air equilibrated system suggests that the energies involved in this process are much larger than what could be expected from the presence of sub-micron bubbles. The range of the force would rather suggest presence of micron-sized bubbles, which could be detected by optical means. In the experiments, such bubbles were not observed on the surfaces.

The difference in bubble behaviour in different liquid environments (air equilibrated ultra-pure water, and air equilibrated KCl electrolyte) seems to indicate that the peculiar behaviour of bubbles is rather influenced by the electrolyte concentration than the presence of micro or nano-bubbles on the solid surface.

10.4 IMPACT OF THE OBTAINED RESULTS ON MODELLING OF FLOTATION

Industrial flotation is a complex process involving the interaction of treated (hydrophobized) mineral surfaces with air bubbles in a hydrodynamically turbulent environment.

The scale of the system causes that depending on the size of the bubbles and particles different forces are dominating. For coarse particles the adhesion force and the gravitational force less buoyancy are close to each other and any random fluctuation in the drag force and/or the inertial effects of bubble vibration induced acceleration can cause the particle bubble aggregate to break. For fine particles the adhesion is much higher than any gravitational force. The rate determining is the particles ability to overcome the energy barrier in an effective way. This process is strongly dependent on particle size.

The presence of an energy barrier described by LASKOWSKI ET AL. (1991) was not observed to happen under all experimental conditions tested (e.g. Figure 39a). In most of the experiments an unstable film formed between the hydrophobic particle and the bubble, which ruptured spontaneously and jump-in occurred. In some experiments, the macroscopic contact angles detected on the particles were 0 or very close to 0 and no TPC was formed when the particle and the bubble were pressed against each other. Even in such cases a hysteresis could be detected between the approaching and retracting force curves, meaning that the particles adhered to the bubble, although with a different (lower) strength than in experiments with higher contact angle. From flotation point of view this is of importance mainly in the case of small (<20 μm) particles, which could adhere to the bubbles and be carried into the froth phase despite their very low hydrophobicity. In case of large particles the gravity force and inertial effects overcome the weak "contactless" adhesion of the particles to the bubbles and break up the particle-bubble aggregate. It has been seen in practice (HEISKANEN ET AL. 2000, 2001) that reducing the turbulence causes big particles (+105 μm) having large (bulk) contact angles (abt 80 deg) to float. At the same time small particles (-32μm), which have a much smaller contact angle (50 deg) start floating as well.

The chemically treated surface gives rise to the formation of a three phase contact line. The interaction forces (DLVO and non-DLVO) co-exist with the hydrodynamic drag forces, buoyancy and gravity.

In order to take all these effects into account a force balance must be formulated over the particle bubble aggregate.

The hydrodynamic forces can be estimated using CFD techniques. It is of great importance that the behavior and time dependency of the netforce at approach and as a function of the distance is clarified. The development of the CIFMA measurement technique allows also the measurement (in terms of force) of differences of the surface treatment.

The processes taking place on the particle surfaces occur in a time interval of a couple of hours, which is comparable with the time that mineral particles spend in suspension from the grinding phase to the end of flotation process. This finding is in accordance with the observation that under similar conditions the flotation of coarse particles has a lower recovery in the scavenger circuit compared to rougher flotation.

Therefore it is very important to treat the particle-bubble interaction as a dynamic, time dependent phenomena, and this has to be taken into account when building new, more precise flotation models.

Besides to the dynamic, time dependent behaviour, the importance of nanometer-sized asperities of the particle surface was shown. The single bubble capture experiments done by ANFRUNS AND KITCHENER (1977) are in accordance with this observation. They have found, that spherical glass beads show much lower collection efficiency than natural, irregularly shaped quartz particles. Generally in the industrial flotation process, and other applications including three-phase systems, the particles involved are not spherical, but angular, with several corners and projections. These corners and projections are most likely influencing the strength of the adhesion force in an even higher extent than the nanometer size asperities. Therefore modelling the strength of the particle-bubble aggregates with spherical particle interactions has to be reassessed.

The very large bubble deformation observed in ultrapure systems might not be of outstanding importance in the flotation, as in the industrial process electrolytes are always present. As previously discussed, at increased electrolyte concentration the elasticity of the air bubbles increases, which prevents the deformation. At the same time it has to be emphasized that the long-range, non-DLVO interaction itself might still be present in the system, which can highly influence the formation of particle-bubble aggregates.

The analysis of the obtained results in relation with the flotation rate was considered. For a detailed analysis and comparison with flotation results, flotation tests would have been needed. Flotation experiments were out of the scope of this thesis and therefore this type of analysis was omitted and will be carried out as a continuation of this project.

10.5 SILICA AS A MODEL SUBSTRATE

Over the last several years, silica has been frequently used as a model substrate in the systems studied in different fields, from paper industry to biology. The results of the present study revealed that the use of silica as a model material in AFM force measurements has to be reassessed.

The changes in the surface structure of silica over time were observed in-situ with the use of CIFMA. The changes that might be attributed either to the slow hydration of the surface (GRIOT AND KITCHENER 1965) or to structural changes of silica surface (VIGIL ET AL. 1994) can significantly affect the results of the force measurements and can lead to misleading conclusions.

Therefore, when using silica as a model material in AFM measurements conducted over a longer time period (several hours), one has to be aware of the dynamic surface processes.

References chapter 10

Anfruns, J.F., Kitchener, J.A., 1977. Rate of capture of small particles in flotation, *Trans. Inst. Min. Metall.*, C, **86**, C9-C15.

Carambassis, A., Jonker, L.C., Attard, P., Rutland, M.W., 1998. Forces Measured between Hydrophobic Surfaces due to a Submicroscopic Bridging Bubble, *Phys. Rev. Lett.*, **80**, (24), 5357-5360.

Dai, Z., Fornasiero, D., Ralston, J., 1998. Influence of dissolved gas on bubble-particle heterocoagulation, *J. Chem. Soc. Faraday Trans.*, **94**, (14), 1983-1987.

Derjaguin, B.V., Dukhin, S.S., 1979. Kinetic Theory of the Flotation of Fine Particles, *Proc. XIII. International Mineral Processing Congress 1979*, Elsevier, ed. J.S. Laskowski, Part A, 21-62.

Eigeles, M.A., Volvenkova, V.S., 1963. Inorganic Electrolytes and Colloids in Elementary Flotation, *Pergamon Press, Mineral Processing, Proc. Sixth Int. Congr., 26 May-2 June, Cannes,* 513-526.

Fielden, M.L., Hayes, R.A., Ralston, J., 1996. Surface and Capillary Force Affecting Air Bubble-Particle Interactions in Aqueous Electrolyte, *Langmuir,* **12**, (15), 3721-3727.

Griot O., Kitchener, J.A., 1965. Role of Surface Silanol Groups in the Flocculation of Silica Suspensions by Polyacrylamide, Part 2. – Surface Changes of Silica Suspensions on Ageing, *Trans. Faraday Soc.,* 61, 1032-1038.

Heiskanen K., Föhr K., Junnikkala S., Aho J., Lampinen P. and Honkivaara K., 2000. Flotation of different particle sizes as a function of bubble surface area flux, *Proc. Canadian Mineral Processors Conference, Ottawa, CIM*, paper 12, 197-211.

Heiskanen K., Junnikkala S. and Föhr K., 2001. Results from Pyhäsalmi Concentrator on Bubble Surface Area Flux and Flotation Rate Relationship as a Function of Particle Size, *Proc. Canadian Mineral Processors Conference, Ottawa, CIM.*

Iler, R.K., 1979. The chemistry of Silica. Solubility, Polymerization, Colloid and Surface Properties, and Biochemistry, *Wiley-Interscience Publication, John Wiley & Sons, New York.*

Laskowski, J.S., Kitchener, J.A., 1969. The Hydrophilic-Hydrophobic Transition of Silica, *J. Coll. Interf. Sci.,* 29, 4, 670-679.

Laskowski, J.S., Xu, Z., Yoon, R.-H., 1991. Energy Barrier in Particle-to-bubble attachment and its Effect on Flotation Kinetics, *Preprints XVIIth Int. Min. Proc. Congr.,* Dresden, 23-28 Sept., 237-249.

Mahnke, J., Stearnes, J., Hayes, R.A., Fornasiero, D., Ralston, J., 1999. The influence of dissolved gas on the interactions between surfaces of different hydrophobicity in aqueous media, *Phys. Chem. Chem. Phys.*, **1**, (11), 2793-2798.

Preuss, M., Butt, H.-J., 1998. Direct Measurement of Particle-Bubble Interactions in Aqueous Electrolyte: Dependence on Surfactant, *Langmuir*, **14**, (12), 3164 – 3174.

Tyrrell, J.W.G., Attard, P, 2001. Images of Nanobubbles on Hydrophobic Surfaces and Their Interactions, *Physical Review Letters*, **87**, (17), 176104-1 – 176104-4.

Vigil, G.; Xu, Zh.; Steinberg, S.i; Israelachvili, J., 1994. Interactions of silica surfaces, *J. Coll. Interf. Sci.*, **165**, (2), 367-385.

CHAPTER 11 CONCLUSIONS AND RECOMMANDATIONS

Sit down before fact as a little child, be prepared to give up every conceived notion, follow humbly wherever and whatever abysses nature leads, or you will learn nothing.

Thomas H. Huxley

11.1 CONCLUSIONS

The following conclusions can be drawn from this research project:

1. An experimental setup, named CIFMA, which overcomes the limitations of commercial instruments, (caused mainly by the limited measurement range) was designed and built.

2. An easy to use archive data access system was implemented that is a bottleneck of many scientific instruments.

3. Very long range and violent bubble deformation towards the hydrophobic silica particle was observed by optical means. The long-range force is not detectable with the AFM force measurement technique due to the low spring constant of the bubble.

4. The violent bubble deformation disappeared with increased electrolyte concentration, probably because the elasticity of the bubble also increased.

5. Air and CO_2 affect the particle-bubble interaction, while Ar seems to be indifferent.

6. The process of the sample preparation and the properties of the liquid environment, especially ultrapure water, seems to effect the long-range interaction much more than the degree of hydrophobicity or presence of different types of gases.

7. The contact angles measured on plates differ from those measured on fine particles. Nanometer scale surface roughness plays an important role in the formation of hydrophilic and hydrophobic surface sites during the silanizing process of the silica particles and plates.

8. Adhesion between particle and air bubble can occur even if the macroscopic contact angle is 0.

9. Nanometer sized roughness on the particle surface significantly effects the adhesion to air bubbles.

10. The increased applied load and increased contact time enhance the adhesion of the particle to the air bubble when no TPC formation occurs.

11. The effect of approach velocity in the 1.8-48 μm/sec range is not significant.

12. The particle-bubble interaction process is time dependent, dynamic phenomena. The jump-in force and adhesion decrease with time. This has to be taken into consideration in new flotation models.

13. The measured adhesion values between particles and air bubbles were higher than predicted from the maximum capillary force calculations.

14. The use of silica as model substrate in the force measurement studies has to be reassessed since silica surface slowly change with time when in contact with water.

15. The main source of errors in force measurements was analysed. It has been found that the spring constant of the AFM cantilevers changes considerably with time, and therefore in measurements performed over an extended period of time, repeated calibration is necessary.

11.2 RECOMMENDATIONS FOR FURTHER TESTS

This research work focused on providing an experimental solution for particle-bubble interaction studies. The obtained experimental results show several new aspects of these interactions. The following issues should be studied:

1. A more exact control of the hydrophobicity degree of silica particles should be worked out.

2. Adhesion force should be studied in more details by combining the force measurement technique with image processing and analysis. This could provide direct experimental evidence to validate the equation describing the capillary forces

stabilizing the particle-bubble aggregate and the tenacity of the particle-bubble attachment (NGUYEN AND SCHULZE 2003).

3. The effect of microscopic heterogeneities has to be taken into consideration and studied in more details.

4. More precise flotation models could be developed, that should include the dynamic phenomena, taking place on particle and bubble surfaces.

5. Means for measuring the bubble deformation should be found, and the meaning of the deformation in flotation models has to be cleared.

References chapter 11

Nguyen, A.V., Schulze, H.J., 2003. Colloidal Science of Flotation, *Marcel Dekker, Inc.,* New York (in press)